JOHANNES KEPLER
UNIVERSITY LINZ

Author
**Hathaichanok Seelajaroen**

Submission
**Linz Institute for Organic Solar Cells (LIOS) / Institute of Physical Chemistry**

Supervisor and first examiner
**o.Univ. Prof. Mag. Dr. DDr. h.c. Niyazi Serdar Sariciftci**

Second examiner
**Univ.-Prof$^{in}$. Dr$^{in}$. Sabine Hild**

February 2020

# BIO-ELECTROCATALYSIS USING IMMOBILIZED ENZYMES AND MICROORGANISMS

Doctoral Thesis

to confer the academic degree of

Doktorin der Naturwissenschaften

in the Doctoral Program

Naturwissenschaften

**JOHANNES KEPLER UNIVERSITY LINZ**
Altenberger Straße 69
4040 Linz, Austria
jku.at
DVR 0093696

JOHANNES KEPLER
UNIVERSITY LINZ

# SWORN DECLARATION

I hereby declare under oath that the submitted Doctoral Thesis has been written solely by me without any third-party assistance, information other than provided sources or aids have not been used and those used have been fully documented. Sources for literal, paraphrased and cited quotes have been accurately credited.

The submitted document here present is identical to the electronically submitted text document.

Place, Date

Signature

# ABSTRACT

Regarding to the increase in population and industry development, global energy demand tends to increase continuously. However, our main source of energy, the fossil fuels, like coal, oil and natural gas, are limited and start running out. Moreover, the combustion of such fossil-based energy carriers gives carbon dioxide ($CO_2$) back to the atmosphere which is considered as the major cause of the rising of global temperature. Therefore, renewable, cleaner and more sustainable energy sources are urgently needed. Converting inexhaustible energy (such as solar and wind energy) into chemicals or artificial fuels offers transportable fuels which are independent from place and time. One promising approach is to convert exhausted $CO_2$ into fuels, for example, formate, methane and methanol using renewable energies like solar and wind.

Developed from such idea, this study is aimed to investigate electrochemical systems for the conversion of $CO_2$ to value-added chemicals products by using bio-origin catalysts such as microorganisms and enzymes. Herein, microbial electrolysis cells containing *Methylobacterium extorquens*, acetogenic bacteria, were developed and their catalytic activities towards the conversion of $CO_2$ to formate were monitored under applying of a constant potential. In this part, direct electron injection and mediator-assisted approaches were investigated. Neutral red, a biocompatible dye, was introduced into the systems as redox mediator in two ways: homogeneous (dissolved in the solution) and heterogeneous (electropolymerized onto the electrode). Electrochemical characterization of such systems was carried out by means of cyclic voltammetry and electrolysis showing electrocatalytic activities towards the $CO_2$ reduction to formate. The performance was found to be enhanced with the aid of mediator in both systems.

Further investigation was performed by combining two bioelectrodes, bioanode and biocathode, which were developed from sewage sludge containing mixed culture microorganism, together in bio-electrochemical systems. The systems were developed serving as a wastewater treatment system where organic substances were oxidized at bioanode and $CO_2$ was reduced to methane ($CH_4$) at biocathode. Such system was successfully built up and system performance was investigated by monitoring chemical oxygen demand values and $CH_4$ amount. Additionally, electrode modifications for both electrodes using poly(neutral red) and chitosan approaches were carried out. The results revealed improved overall performance in both organics degradation and $CH_4$ production.

In addition, dehydrogenase enzymes were investigated as electrocatalysts in electrochemical catalytic system. The dehydrogenases are redox enzymes that catalyze redox reactions and require sacrificial electron donor such as nicotinamide adenine dinucleotide, reduced form (NADH). Avoiding using such costly cofactor, electrochemical injection of electrons from electrode directly into enzymes' active sites is suggested. Efficient immobilization of enzymes onto the electrode was presented by chemical grafting of conjugated dehydrogenases directly onto graphene (as a conductive nanoplatform). Using an alginate hydrogel matrix, we subsequently coated this bio-nano-electrocatalyst onto the electrode. This immobilization technique was employed for single dehydrogenase for the reduction of acetaldehyde to ethanol and furthermore, of three dehydrogenases for the cascade reduction of $CO_2$ all the way to methanol. The enzyme-graphene bio-nano-electrocatalysts show enhanced reductive current delivered into the system, leading to higher production rate.

# KURZFASSUNG

Der weltweite Bevölkerungsanstieg sowie die globale Industrialisierung führen zu einem stetigen Anstieg des weltweiten Energiebedarfs. Bis dato wird dieser Energiebedarf überwiegend durch nicht-regenerative fossile Brennstoffe wie Kohle, Erdöl und Erdgas gedeckt, aber diese Ressourcen werden mehr und mehr erschöpft. Überdies wird bei der Verwertung dieser fossilen Brennstoffe Kohlendioxid ($CO_2$) in die Erdatmosphäre freigesetzt, welches als Hauptverursacher für die globale Erderwärmung gilt. Um diesen beiden Problemen entgegenzutreten, werden „saubere“, erneuerbare und nachhaltige Energiequellen dringend benötigt. Eine Idee dafür ist, erneuerbare Energiequellen (wie Sonnen- oder Windenergie) in Brennstoffe oder Chemikalien umzuwandeln, sodass diese leicht transportiert und gespeichert werden können. Ein vielversprechender Ansatz dafür ist, das in Abluft enthaltene $CO_2$ in Brennstoffe wie Ameisensäure, Methan oder Methanol umzuwandeln.

Daher beschäftigt sich diese Arbeit mit elektrochemischen Systemen, welche biologische Katalysatoren wie Mikroorganismen und Enzymen nutzen, um $CO_2$ in wertvolle Chemikalien umzuwandeln. Dafür wurden *mikrobielle elektrochemische Zellen* mit dem *acetogenen* Bakterienstamm *Methylobacterium extorquens* für die Umwandlung von $CO_2$ in Ameisensäure untersucht. In diesem Ansatz wurde die direkte mit der indirekten Elektronenübertragung verglichen. Hierfür wurde der biologisch verträgliche Farbstoff Neutralrot in zwei verschiedenen Varianten als *Redoxmediator* verwendet: einmal homogen gelöst in der Elektrolytlösung und einmal heterogen auf die Elektrode polymerisiert. Die elektrochemische Charakterisierung erfolgte mit zyklischer Voltammetrie und *es wurde* die elektrokatalytische Aktivität für die $CO_2$ Reduktion zu Ameisensäure untersucht. In beiden Fällen konnte diese Aktivität durch die Zugabe von Neutralrot gesteigert werden.

In einem weiteren Ansatz wurde ein *mikrobielles elektrochemisches System* mit einer Bioanode und einer Biokathode untersucht. Hier war das Ziel Abwasser an der Bioanode zu oxidieren und gleichzeitig $CO_2$ an der Biokathode zu Methan zu reduzieren. Dieses System konnte erfolgreich etabliert werden und dessen Performance mit Hilfe des chemischen Sauerstoffbedarfs sowie der produzierten Menge an Methan überprüft werden. Zusätzlich wurde an beiden Elektroden der Einfluss von chemischer Modifikation mit Neutralrot und Chitosan untersucht, wobei in beiden Fällen eine verbesserte Performance erzielt werden konnte.

Als dritter Ansatz wurden Dehydrogenase Enzyme als Biokatalysatoren in elektrochemischen Systemen untersucht. *Dehydrogenasen* stellen eine Enzymklasse dar, welche natürliche Redoxreaktionen unter Verwendung von Elektronencarrier wie *Nicotinamidadenindinukleotid* (NAD) katalysieren. Um die Verwendung solch teurer *Coenzyme* vermeiden zu können, wird das direkte Adressieren des aktiven Zentrums des Enzyms forciert. Die effektive Immobilisierung der Enzyme auf Elektrodenoberflächen konnte durch kovalente Bindung der Enzyme auf *Graphen-Nanoplattformen* mit anschließender Fixierung mittels *Alginat-Hydrogel* auf Elektroden erreicht werden. Diese Immobilisierungsmethode konnte einmal für eine einzelne Dehydrogenase für die Reduktion von Acetaldehyd zu Ethanol und einmal durch die Kombination von drei Dehydrogenasen für die kaskadenartige Reduktion von $CO_2$ zu Methanol als effektiv demonstriert werden. *Diese Enzym-Graphenhybride* ermöglichen durch höhere reduktive Stromflüsse eine verbesserte *Umwandlungsrate*.

# ACKNOWLEDGEMENTS

First of all, I would like to sincerely thank to my supervisor, o. Univ. Prof. Mag. Dr.DDr. h.c. Niyazi Serdar Sariciftci for giving me the opportunities to pursue my PhD degree at LIOS, for the full supports in both scientific and non-scientific ways and all the advices which shape me to this direction.

I am grateful for the financial support from the Austrian Climate and Energy Fund within the project CO2TRANSFER (848862) and MELOS (861392) and the European Regional Development Fund (EFRE) within ENZYMBIOKAT project (GZ2018-98279-2) during my study.

Furthermore, I would like to thank Dr. Liviu Mihai Dumitru for introducing me to the “bio” field, very supportive guiding, ideas, kind and patience training as well as fruitful discussions and assisting through all the problems.

A big thank goes to Dr. Dogukan Hazar Apaydin, my big brother, for always answering me all questions, giving me training through many scientific stuffs and your patience to all my requests.

I would also love to thank Prof. Dr. Patchanita Thamyongkit for the supports that brought me here and general suggestions for living and working in this different place.

I want to also thank my “microorganisms” specialist: Marianne Haberbauer, Sabine Spiess and Sophie Thallner for all guidance and supports.

This study and laboratory work would be very difficult and boring without my great friends: Dominik Wielend, Wittawatt Keawsongsaeng and Nikolas Heitzmann for supportive discussions and sharing painful experiences. Not only about working, all general assists from all of you saved my life a lot! Special thank does to Dr. Bekele Teklemariam and Dr. Christoph Ulbricht for the big supports as always!

I want to also thank Assoc. Prof. DI Dr. Markus Clark Scharber, Dr. Cigdem Yumusak, Dr. Dong Ryeol Whang, Dr. Halime Coskun Aljabour, Dr. Stefanie Schlager, DI Dr. Philipp Stadler, Dr. Mateusz Bednorz, Dr. Abdalaziz Aljabour, Dr.-Ing. Serpil Tekoglu, Zeynep Bozkurt and also every LIOS members who contribute parts of my experiences and such a nice working environment. I also thank to my students: Melissa Hassel and Aylin Paktan for all the curiosities and bringing me to the fruitful discussions. Without these people, my study would be almost impossible: Gabriele Hinterberger, Gerda Kalab, Patrick Denk, Birgit Paulik, Sara Gusner and Isolde Wandling, for all technical supports and helpful advices together with helping me dealing with tons of documents.

Finally, only one thing leaded me deciding this direction is a promise to my dad. Dad, I know you are watching me from the place that is far away. All is dedicated to you and thank you for always being positive even in my mind. Also for the greatest person in my life, mom, I finally did it! You are always the great supports for the whole of my life. Without my personal “mental” support, I could not able to come this far without, thank you for always listening to my non-sense stories and being patient to all unpredictable but wonderful journeys.

## Table of Contents

## List of Abbreviations

| | |
|---|---|
| ADH | alcohol dehydrogenase |
| ATR | attenuated total reflection |
| BES | bio-electrochemical system |
| BCA | bicinchoninic acid |
| BSA | bovine serum albumin |
| CCS | carbon capture and sequestration |
| CCU | carbon capture and utilization |
| CE | chemical conversion efficiency |
| CoA | acetyl coenzyme A |
| COD | chemical oxygen demand |
| CV | cyclic voltammogram |
| DH | dehydrogenase |
| DIC | diisopropylcarbodiimide |
| DMF | dimethylformamide |
| DSMZ | Deutsche Sammlung Mikroorganismenund Zellkulturen |
| $E^0$ | standard reduction potential |
| $E^{0'}$ | formal reduction potential |
| EC | enzyme code |
| $E_p$ | peak potential |
| F | Faraday constant |
| FAD | flavin adenine dinucleotide |
| $FADH_2$ | flavin adenine dinucleotide, hydroquinone form |
| $F_{ald}DH$ | formaldehyde dehydrogenase |
| $F_{ate}DH$ | formate dehydrogenase |
| FE | faradaic efficiency |
| FG | fluorographene |
| FID | flame ionized detector |
| FTIR | Fourier transform infrared spectroscopy |
| $\Delta G_f$ | Gibbs free energy of formation |
| G-ADH | alcohol dehydrogenase modified graphene |
| GC | gas chromatography |
| G-CN | cyanographene |
| G-COOH | carboxylic acid graphene |
| G-DH | dehydrogenase modified graphene |
| $G\text{-}F_{ald}DH$ | formaldehyde dehydrogenase modified graphene |
| $G\text{-}F_{ate}DH$ | formate dehydrogenase modified graphene |
| GO | graphene oxide |
| IC | ion chromatography |
| ICP-MS | inductively coupled plasma mass spectrometry |
| $I_p$ | peak current |

| | |
|---|---|
| MCT | Mercury Cadmium Telluride |
| MEC | microbial electrolysis cell |
| MFC | microbial fuel cell |
| $NAD^+$ | β-Nicotinamide adenine dinucleotide hydrate |
| NADH | β-Nicotinamide adenine dinucleotide, reduced form |
| $NADP^+$ | β-Nicotinamide adenine dinucleotide phosphate |
| NADPH | β-Nicotinamide adenine dinucleotide phosphate, reduced form |
| oxyma | ethyl cyano(hydroxyimino)acetate |
| RHE | reversible hydrogen electrode |
| SEM | scanning electron microscopy |
| SHE | standard hydrogen electrode |
| TCD | thermal conductivity detector |
| TRIS | tris(hydroxymethyl)aminomethane |

## List of Figures

## List of Tables

## List of Schemes

# 1. Introduction

## 1.1. Greenhouse gases

The solar energy is the energy source for all life in the planet. It radiates to the Earth and either is reflected back to space by the atmospheric particles or the surface of the Earth or, more than half of the radiation passes through the atmosphere and is absorbed by Earth's systems and surfaces. After heating up, infrared thermal radiation is released from Earth and passed through the atmosphere and then to the space. Some of the radiation is absorbed by gas molecules in the atmosphere which are then re-emitted the radiation in all directions. The radiation absorption and re-emission process is called greenhouse effect and such gas molecules are called greenhouse gases.[1] This greenhouse effect is the most important process balancing the radiation and therefore, maintains temperature to be warm enough for ecological and biological systems. Without the greenhouse gases that prevent heat leaving, the global temperature would be much lower. The greenhouse gases are from both natural processes and human activities. The major greenhouse gases are listed below:[2]

- Carbon dioxide ($CO_2$)
- Methane ($CH_4$)
- Nitrous oxide ($N_2O$)
- Halogens
- Ozone ($O_3$)
- Water vapor ($H_2O$)

Although greenhouse gases assisted on warming the Earth's surface, continuous and dramatic increase in those gases have recently observed which links to the rising of the global temperature. The study entitled "On the influence of carbonic acid in the air upon the temperature of the ground" was published by Svante Arrhenius, a Swedish chemist and Nobel laureate, in 1896.[3] This work has been recognized as a great pioneering contribution to the climate change research field. According to the report, the calculation on the correlation of atmospheric $CO_2$ content (referred in the paper as carbonic acid) to the global temperature was presented, sparkling scientists the importance of the topic. Among abovementioned greenhouse gases, the thought of $CO_2$ is usually been evoked due to the huge change of $CO_2$ content which perfectly linked to increased temperature. Although $CH_4$ and $N_2O$ adsorbed more heat per molecules relative to $CO_2$, $CO_2$ is more abundant and stay much longer. Therefore, it is considered as the most impact greenhouse gas.

The global $CO_2$ concentration averaged monthly over marine surfaces is presented in **Figure 1**.[4] The information suggested continuous increase in atmospheric $CO_2$ content from 340 ppm in 1980 to 407.65 ppm in September 2019, without any signs of dropping. This increase in $CO_2$ leads directly to warmer global temperature, so called global warming. Not only the global warming, it relates to many other environmental issues such as climate change, ozone depletion and rise in sea level. Furthermore, the progressive rate tends to be increased over time. The main reason of this large $CO_2$ emission is strongly related to human activities especially fossil fuels combustion and deforestation in order to serve the population and economic growth.

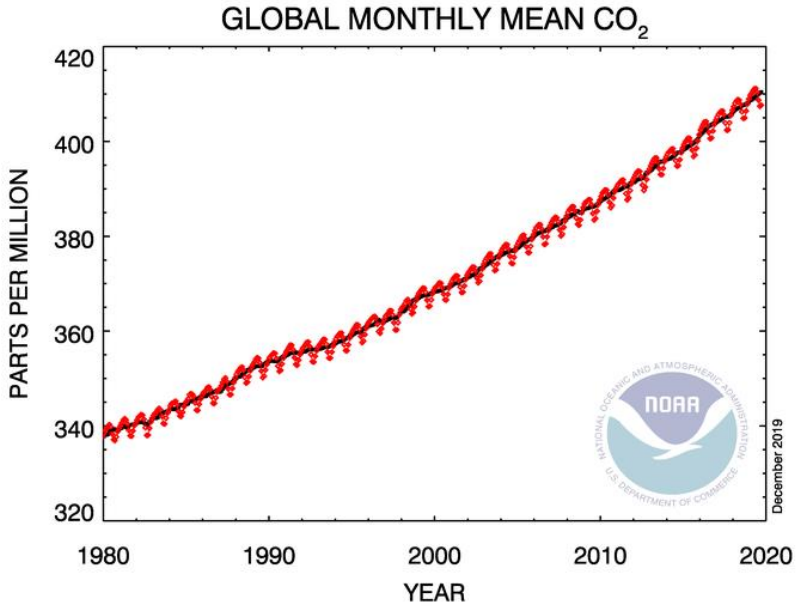


**Figure 1.** The graphs show monthly average $CO_2$ concentration above marine surface sites.[4]

Nevertheless, one could argue that the increase in $CO_2$ content observed currently is the natural phenomena. The information of historical changes of temperature and atmospheric $CO_2$ concentration over 400,000 years was reported previously.[5] The superposition of the two graphs are depicted together in **Figure 2**. In a cycle of around 100,000 year, the temperature change pattern was fluctuated within the range of 10-12°C of which the pattern is related to the relation between the Sun and the Earth. Additionally, the superposition curves clearly show that the atmospheric $CO_2$ content in the range of 180 and 280 ppm, is strongly synchronized with the temperature change, suggesting interrelation of temperature change and atmospheric $CO_2$ content. In a cycle, there are two periods; glacial and interglacial periods. The glacial period is a long cold period, where, the interglacial period is a short warm period. Although we are now in the interglacial period, this value range is far lower than that of the current level over 400 ppm. This information strongly supports that anthropogenic $CO_2$ affects significantly to the global warming issue.

To overcome the global warming issue, lowering atmospheric $CO_2$ content is crucial. An approach is to reduce $CO_2$ emission to the air and in the meanwhile utilize the existing $CO_2$. Therefore, the development of renewable energy, a cleaner and sustainable energy technology, is prerequisite for preventing/avoiding emission of such greenhouse gases.[1,3,6] Although the existing renewable energies, especially solar and wind energies, are practically inexhaustible and widely accessible,[7] such energy sources are currently limited due to lack of large energy storage and transportation from the place of production to end users for later use (**Figure 3**). A promising and feasible solution is to transferred such energy into a transportable form like chemicals and fuels which can be utilized later and somewhere else.[8–13]

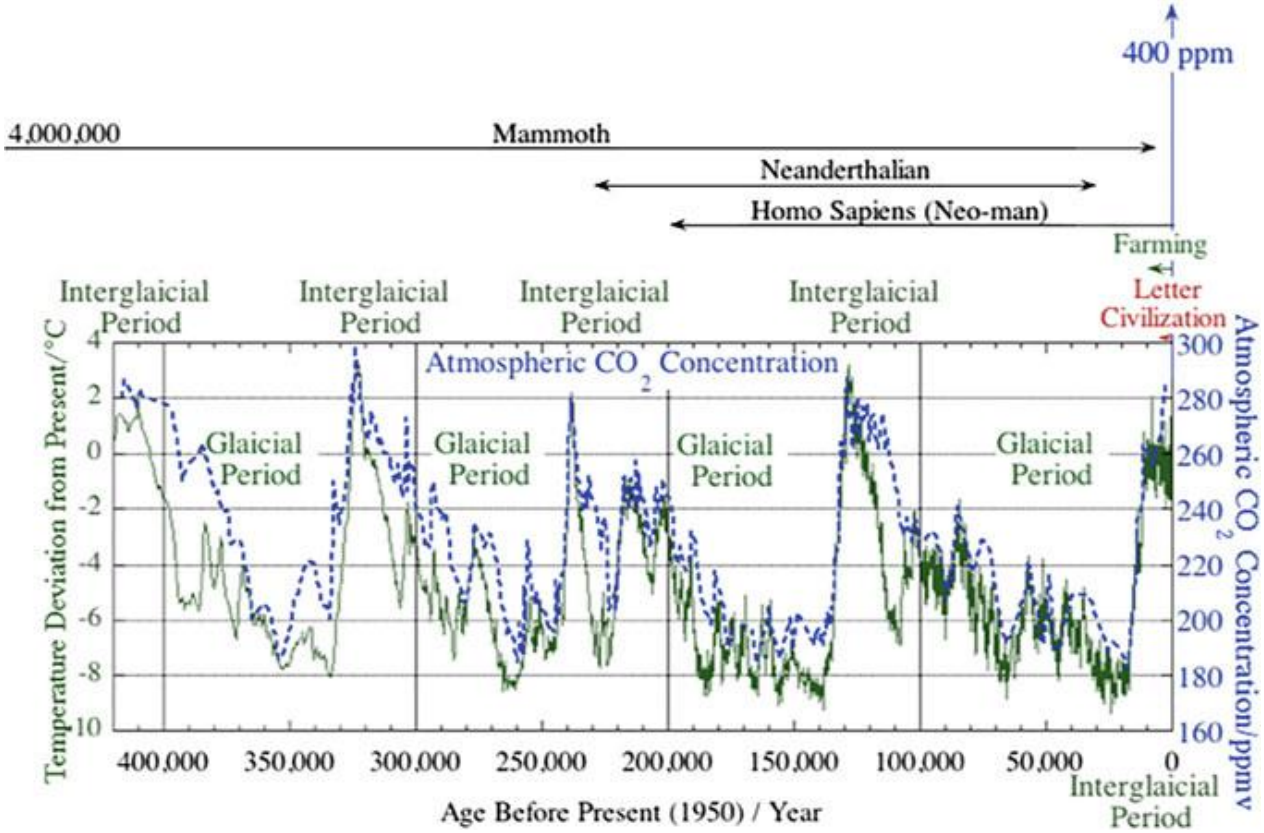


**Figure 2.** Superposition of historical temperature (green solid line) and atmospheric carbon dioxide (blue dashed line) recorded in Vostok ice core on Antarctica. (Reproduced from reference 5 with a permission from Springer Nature, © 2019.)

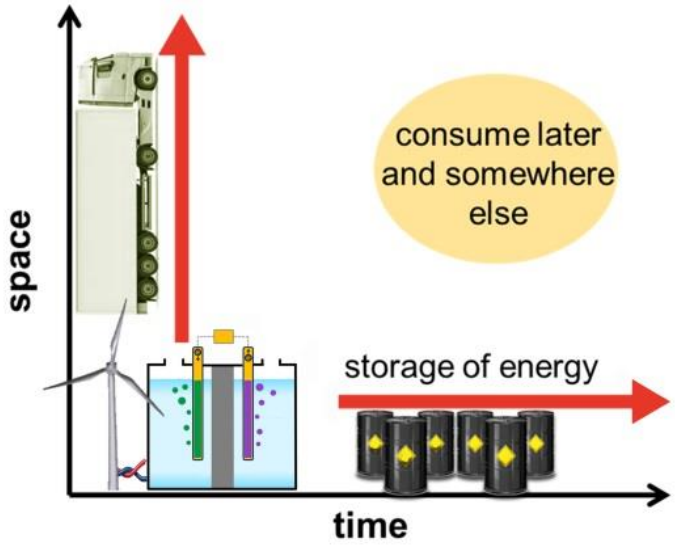


**Figure 3.** Correlation of time and space in production and utilization of renewable energies. Since it is seldom that the supply and demand of renewable energies are at the same location and at the same time, the necessity of a transportable storage medium is obvious. A chemical fuel synthesized by using renewable energy is a chemical storage medium, fulfilling the transportability as well.

## 1.2. $CO_2$ Reduction

The reduction of atmospheric $CO_2$ is of an urgent quest to deal with the current global warming situation. Currently, there are two technologies: carbon capture and sequestration (CCS) and carbon capture and utilization (CCU).[14] In both technologies, $CO_2$ is firstly captured from high-concentration $CO_2$ sources such as exhausted gas from power plants and biofuel refineries. In the CCS, the captured $CO_2$ is then transferred to a storage site, normally an empty underground field.

This technology is, in principle, for preventing the produced $CO_2$ from contribution to the atmosphere. However, during storing $CO_2$ in the geological place, high energy is consumed to convert $CO_2$ into its supercritical fluid. Also one should be concerned about storage leaks and environmental impacts of such sudden outburst of $CO_2$ as it happened during the catastrophe of Lake Nyos in Cameroon in 1986.[15]

On the other hand, the other method, CCU, is promising since the captured $CO_2$ is further utilized to make some useful out of it.[11] Some of the utilization possibilities are demonstrated in **Figure 4**.[16] The utilization can be divided into two ways: non-conversion and conversion. The non-conversion approach is, for example, the use of $CO_2$ as it is in order to enhance oil recovery. While, the conversion of captured $CO_2$ allowed us to be able to convert waste $CO_2$ into value-added products such as fuels, chemicals, plastics or for mineralization process.[8]

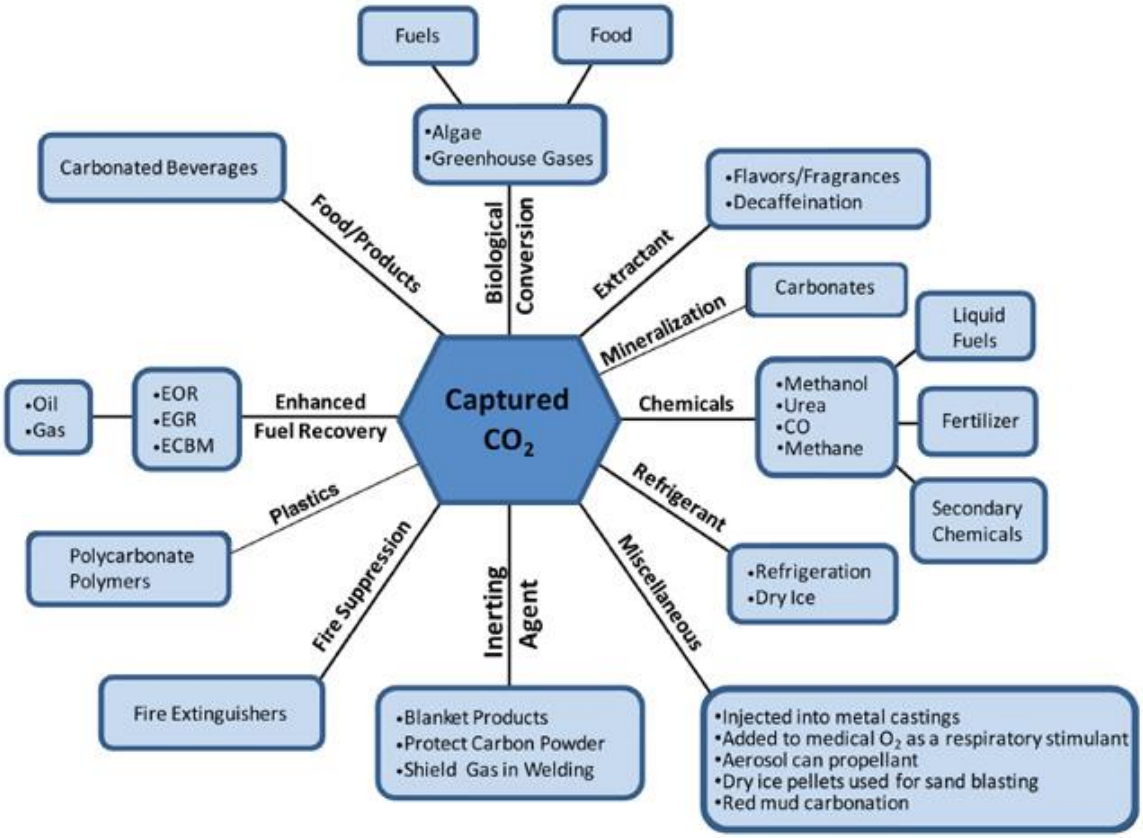


**Figure 4.** Utilization of captured $CO_2$.[16]

The conversion of $CO_2$ to fuels is of outmost interest. Firstly, $CO_2$ amount is being reduced which affect positively to environmental situation. Secondly, $CO_2$ is able to be converted into various

chemicals and fuels contains higher energy density for example carbon monoxide (CO), formate ($HCOO^-$), $CH_4$, methanol ($CH_3OH$), ethanol ($C_2H_5OH$) and ethane ($C_2H_4$).[8,12,13] These fuels could give back the energy through combustion, resulting $CO_2$ which can be used as a substrate (the carbon neutral cycle). This technology offers a great advantage of independence of place and time. This is the perfect method to make a cyclic use of carbon in our global energy systems without changing the energy vectors (*i.e.* carbon-based fuels) of the human civilization today.

Regarding a Gibbs free energy of formation ($\Delta G°_f$), $\Delta G°_f$ of $CO_2$ is of -394.4 $kJ \cdot mol^{-1}$ suggesting $CO_2$ as highly stable molecule.[17] Some possibilities of $CO_2$ reduction and their half-reduction potentials are summarized in **Table 1**.[18] To convert $CO_2$, the first step involves $CO_2$ activation transforming linear to bent molecular structure. This energetic activation is reflected in the very negative potential of the one-electron reduction of $CO_2$ which rearranges from the linear structure of $CO_2$ molecule to bent structure of its radical ($CO_2^{\cdot-}$). However, the multi-proton reductions coupled with protons take place at relatively low potentials because the bent form prefers to react with a nucleophile and later with an electrophile as observed in biological systems. According to the equations, the reductions depend largely on pH of the solution of which lower pH is preferable.

| Equation | $E^{0'}$ / V vs SHE | E / V vs RHE |
|---|---|---|
| $CO_2 + e^- \rightarrow CO_2^{\cdot-}$ | -1.90 | -1.49 |
| $CO_2 + 2H^+ + 2e^- \rightarrow CO + H_2O$ | -0.52 | -0.11 |
| $CO_2 + H^+ + 2e^- \rightarrow HCOO^-$ | -0.43 | -0.02 |
| $CO_2 + 4H^+ + 4e^- \rightarrow HCHO + H_2O$ | -0.51 | -0.10 |
| $CO_2 + 6H^+ + 6e^- \rightarrow CH_3OH + H_2O$ | -0.38 | 0.03 |
| $CO_2 + 8H^+ + 8e^- \rightarrow CH_4 + H_2O$ | -0.24 | 0.17 |

**Table 1.** Formal reduction potentials adjusted for pH 7 ($E^{0'}$ vs standard hydrogen electrode (SHE)) and standard reduction potential (E vs reversible hydrogen electrode (RHE) for the $CO_2$ reductions.

To drive these reactions, energy, electrons and protons is required. Therefore, source of input energy is of concern. The electrochemical[19–22] and photo(electro)chemical[23–27] $CO_2$ reduction approaches are examples where energy could be supplied from renewable source such as solar and wind energy, achieving sustainable and green technology. Due to high-energy barrier of the reaction as well as overpotentials, large amount of energy is needed. Therefore, catalysts are introduced into the system to lower the activation energy.[28–36] Several catalysts have been investigated and designed for $CO_2$ conversion applications, for example:

- Metal-based materials[20,22,37]
- Synthetic molecules and systems[25–27,38]
- Biological-origin materials.[39,40]

Among those catalysts, the biological ones have attracted special interests due to their large accessibility and availability from the biosphere, as compared to synthetic materials and rare metals. Moreover, these bio-catalysts provide remarkable high selectivity towards desired reactants and products. Further, they are often operated under particularly neutral and ambient conditions.[18,41,42] In this thesis, the main focus is put on the investigation of the biological-origin materials including microorganisms and enzymes for the reduction of $CO_2$ through the electrochemical approach. Details of both materials will be discussed later.

### 1.2.1. Microorganisms as catalysts

Employing microorganisms as electrocatalysts in electrochemical systems provides a great advantage in terms of system sustainability due to their abilities of self-regeneration and adaptation of the catalyst quantity over the support materials.[43,44] Moreover, microbial systems are relatively flexible to substrates (reactants), resulting tunable product formations. By definition of the catalyst, microorganisms are not true catalyst since parts of consumed energy is used for their growth. But they were found to be able to improve the system performance by reducing overpotential of the reaction.[45,46] Therefore, whole microorganism cells play an electrocatalyst role in the microbial electrochemical system. The microbial electrocatalytic systems are carried out in the electrochemical cell which is so-called "bio-electrochemical system" (BES).[44] A simplified overview of BES is shown in **Figure 5**. The BES is an electrochemical system where cathodic and/or anodic compartments consist of microbially assisted processes. The BESs can be operated in several modes including galvanic mode (power production and short circuit) in which power is delivered from the cell, and electrolysis mode (power supply from electricity or renewable energy sources) in which power is invested in order to drive unfavourable reactions.[47]

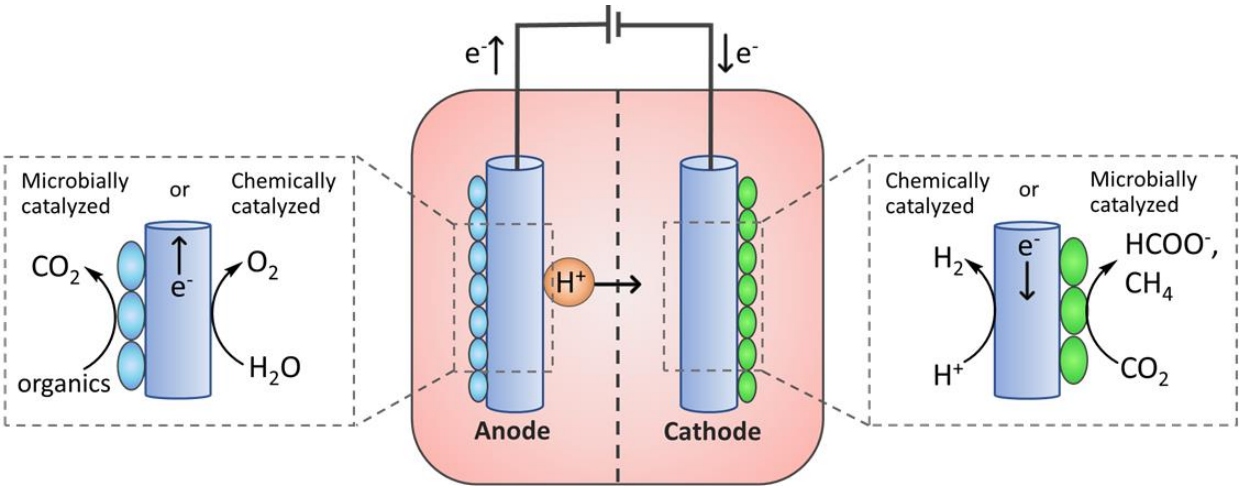


**Figure 5.** Overview of bio-electrochemical system (BES), simplified from reference 44.

The BESs where cathodic chamber containing microorganisms were exhibited in several applications, which are named as microbial electrolysis cells (MECs). One example is the bioremediations where input energy used for driving the respiration pathways, so-called electro-respiration, such as perchlorate reduction,[47,48] denitrification,[49,50] reductive dechlorination[51–53] and uranium recovery.[54] Another example is the electro-fermentation, where input cathodic current influences on existing fermentation pathways. For example, the electrochemical reduction of oxidized nicotinamide adenine dinucleotide ($NAD^+$) to reduced nicotinamide adenine dinucleotide (NADH) improved microbial production of butanol.[55,56]

The electron transport between electrode and microorganisms are, in general, called extracellular electron transport. Overview of extracellular electron transfer mechanisms from cathode to microorganisms in biotic cathodic environment, is demonstrated in **Figure 6**.[44] One of the extracellular electron transport pathways involves microbial metabolism driven by hydrogen ($H_2$) as electron donor in the production of $CH_4$.[57–59] This $H_2$ could be produced from either electrochemical or microbially assisted approaches. However, the use of $H_2$ has two limitations: low concentration in aqueous solution under ambient conditions due to low solubility and requirement of a costly platinum (Pt) electrode or other catalysts to achieve enough $H_2$ amount.[44]

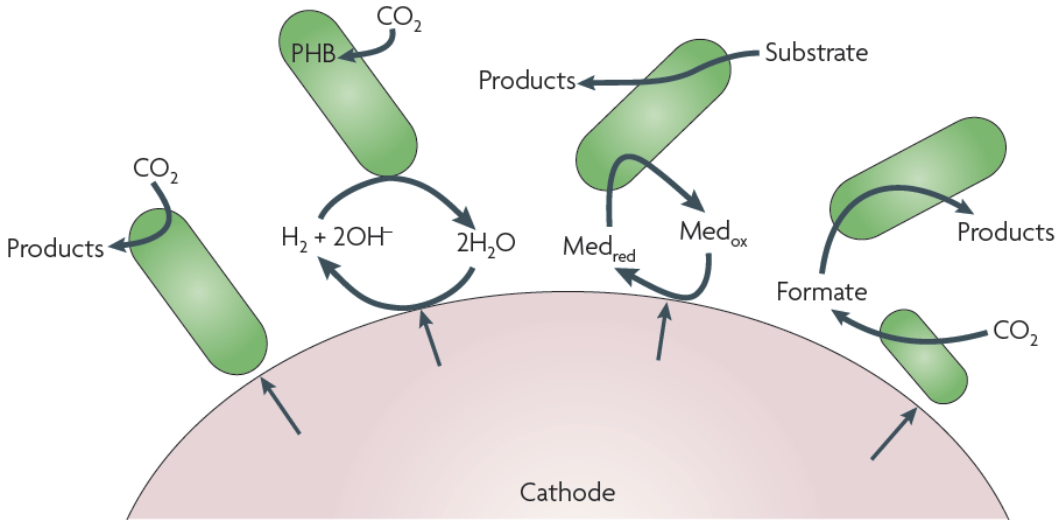


**Figure 6.** Overview of extracellular electron transfer mechanisms from cathode to microorganisms. (Reproduced from reference 44 with a permission from Springer Nature, © 2010.)

The extracellular electron transfer could be achieved electrochemically through the introduction of suitable redox molecules which act as redox mediators.

***The redox mediators are reduced/oxidized electrochemically at the electrode and then the reduced/oxidized mediators go through cell membrane, give/take electrons to/from microbial cells, become oxidized/reduced form and swim back to bulk solution and to the electrode.***

Therefore, only small amount of mediator is needed. As the mediators are dissolved in the solution, higher concentration could be achieved, suggesting effective electron shuttling. Several choices of materials, for example, 3-amino-7-dimethylamino-2-methylphenazine (neutral red), thionin, 1,1'-dimethyl-4,4'-bipyridinium (methyl viologen or paraquat), methylene blue and anthraquinone-2,6-disulfonate, can be chosen regarding to specific potential that matches to cofactor/metabolite required for the specific reaction.[46,60,61] However, these organic molecules have some drawbacks such as low stability, possible toxicity effects to microorganisms and/or environments, and contamination through processes. In an early study, Kim *et al.* showed enhanced microbial fermentation in the presence of methyl viologen and further demonstrated direct effect of mediator to the reduction $NAD(P)^+$, suggesting the role of the mediator.[56] Furthermore, Hongo *et al.* reported on using neutral red as a redox mediator (electron carrier) which enhanced microbial fermentation of L-glutamic acid to L-glutamine.[62] Later, in 1999, Park *et al.* demonstrated that microorganisms were able to grow on electrical-assisted neutral red instead of using $H_2$ like in the conventional approach.[63,64] The results suggested the neutral red can be used for enhancing product formation and microbial growth,[65] whereas methyl viologen was found to be toxic to microorganisms in some cases.[66] Additionally, inorganic mediators, such as ferric chloride ($FeCl_3$), could improve microbial electrochemical reduction of oxygen ($O_2$) through ferric (Fe(III)) reduction.

Another approach where no further $H_2$ or redox mediators are added, is extremely attractive since above-mentioned limitations of both cases will be eliminated. As an early evidence, microorganism growth as well as methane production rate were found to be improved when iron ($Fe^0$) that generated from corrosion was presence in the medium, as compared to conventional approach of

using $H_2$ and $CO_2$.[67,68] This suggested that microorganisms could accept electrons from solid iron without the need $H_2$. In 2004, the first observation was demonstrated on using *Geobacter metallireducens* directly attached on the electrode for electrochemical denitrification[49] and later, applied for other electron acceptors.[54] After that, other strains/microorganisms were also been reported on their direct electron transfer capabillities.[48,57,69,70] These microorganisms were called as electro-active microorganisms.

Several microorganisms have been investigated and reported for their capabilities of capturing and/or converting $CO_2$ to valuable products (like formate, acetate and $CH_4$) by using electrons supplied from electron carriers, such as $H_2$.[71–73] In the 1930s, the first acetogenic bacteria, *Clostridium aceticum,* was investigated showing that $CO_2$ and $H_2$ could convert to acetate through several intermediates *i.e.* formate and CO. This mechanism was further investigated and described later as the reductive acetyl-CoA or the Wood-Ljungdahl pathway while $H_2$ represented two-electron and two-proton source, as shown in **Scheme 1**.[74–77] On the other hand, methanogens produce methane from $CO_2$ and $H_2$ through C1 cycle of methanogenesis process.[78] The variation of product depends largely on microbe strain, growth condition and substrates.

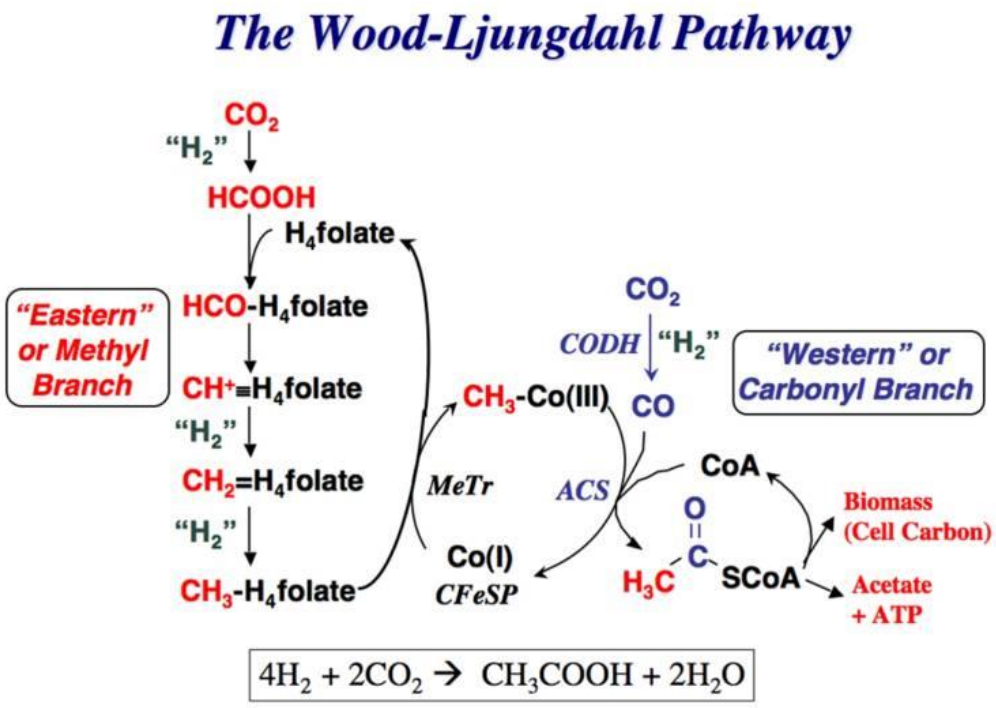


**Scheme 1.** Schematic of the reductive acetyl-CoA or the Wood-Ljungdahl pathway found in acetogens. (Reproduced from reference 77 with a permission from Elsevier, © 2008.)

Evidences of direct electron transfer mechanism of acetogens and methanogens for $CO_2$ conversion were reported. In 2008, Clauwaert *et al.* revealed enhanced microbial $CH_4$ production while applying voltage.[79] The observation was further supported by Cheng *et al.* showing that $CH_4$ was produced by methanogens coated on the carbon-based electrodes. The production was from applied voltage (applied electrons), not from $H_2$, suggesting an electromethanogenic process.[71] The study was carried out using mixed culture biocathode containing mainly archaea. This study has encouraged many scientists, leading to significant development in the field of microbial electrochemistry. Further investigation of hydrogenophilic methanogenic culture suggested their abilities to take electrons directly from the cathode through extracellular electron transfer.[73]

Moreover, Schlager *et al.* reported the generation of $CH_4$ *via* microbial assisted electrochemical reduction where gaseous $CO_2$ was the sole carbon source.[80] The simplified reduction equation is shown in **Equation 1**. Although several attempts were employed for fundamental investigations, information on direct electron transfer mechanism was still on debated. Some observations suggested extracellular electron transfer through proteins (like cytochromes) located at the outer microbial cell membrane.[44]

$$CO_2 + 8H^+ + 8e^- \rightarrow CH_4 + 2H_2O \qquad \textbf{(Equation 1)}$$

Apart from methanogens, methylotroph bacteria like *Methylobacterium extorquens* is also known to be able to grow by reducing C1 compounds like $CH_3OH$ or $CO_2$. [81,82] Recently, Hwang *et al.* firstly reported the capability of *M. extorquens* for the reduction of $CO_2$ to formate by using electrons supplied from a cathode through reduced methyl viologen.[83]

In case of microbial assisted oxidation, the electro-reducing microorganisms or so-called electrogens are the microorganisms that are capable of oxidizing organic compounds to $CO_2$ and the resulting electrons were transferred to electrodes as terminal electron acceptor.[84–86] As an example, 24 electrons could be extracted from 1 molecule of glucose, as summarized in **Equation 2**.

$$C_6H_{12}O_6 + 6H_2O \rightarrow 6CO_2 + 24H^+ + 24e^- \qquad \textbf{(Equation 2)}$$

This idea is called later as microbial fuel cell (MFC), a device that can generate electric current coupled to oxidation of organic substrates by microorganisms under anaerobic condition. The MFC could be employed for wastewater treatment technologies. The electrogens include diverse microorganisms including gram-positive and gram-negative organisms. Only the gram-negative microorganisms were known to be involved in extracellular electron transfer. To completely oxidize complex organic compounds, mixed culture microorganisms are preferred, as shown in **Figure 7**.[87] Among those, two most often studied microorganisms are *Geobacter sulfurreducens* and *Shewanella oneidensis* str. MR-1 of which their direct electron transfer mechanisms were reported through periplasmic and outer membrane complexes (like membrane-bound cytochromes)[84] and/or pili or pilus-like appendages (called as nanowires).[44]

Most attractive idea is to combine the two applications together, resulting a bio-electrochemical system equipped with a bioanode for wastewater oxidation/degradation and a biocathode for the conversion of $CO_2$ to $CH_4$, a value-added fuel. Two compartments are often separated by a proton-exchange membrane, allowing proton passing through. This technology has advantages over the conventional anaerobic digestion used for wastewater treatment units.[88] Since the two chambers are separated, generated $CH_4$ is not further oxidized back to $CO_2$ and methanogenic consortia is also protected from the inhibitors or by-products from wastewater treatment process. Further advantage is the feasibility of using diluted wastewater including municipal wastewater. However, using membrane could limit the delivered current and subsequent overall performance of the system.

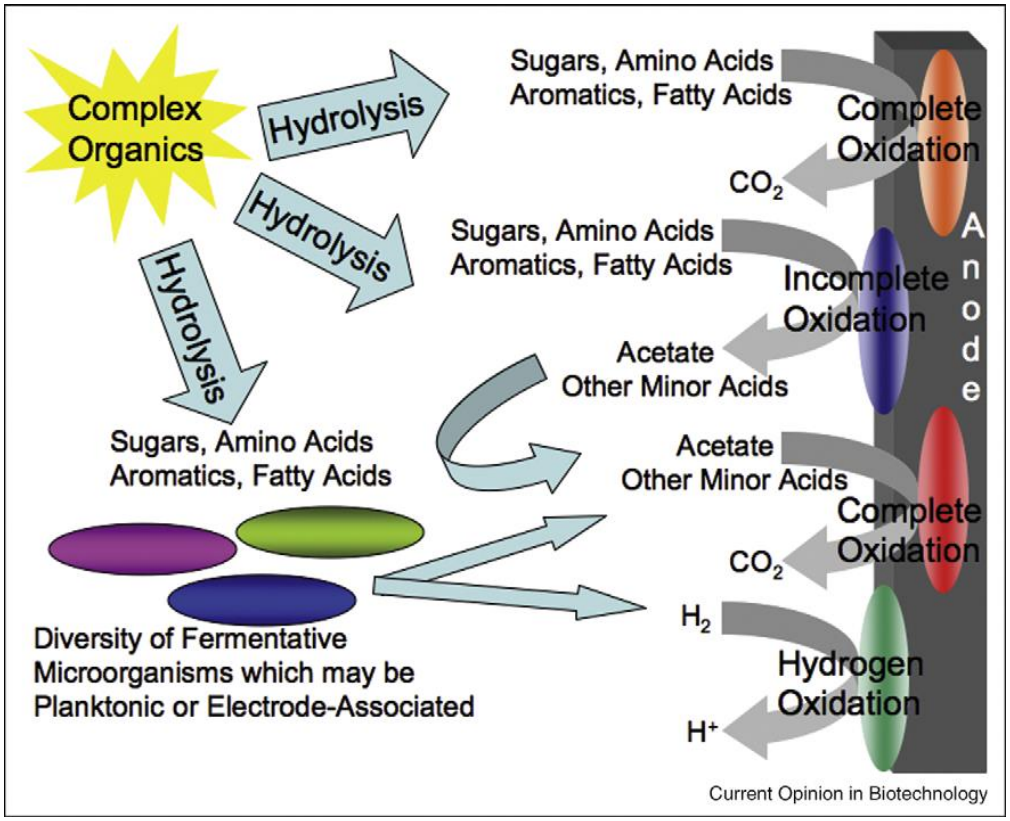


**Figure 7.** Simplified organic compounds oxidations occurred at mixed culture bioanode. (Reproduced from reference 87 with a permission from Elsevier, © 2008.)

However, higher $CH_4$ production rates is required for practical and industrial scale application. One approach is to improve the quality of electroactive biofilm coated onto electrodes leading to efficient electron transfer process which subsequently enhances $CH_4$ generation.[89,90] Different electrode materials and electrode modifications were proposed.[91] Common electrode materials are high surface area carbon-based (*i.e.* carbon cloth, carbon mesh and carbon felt) or inert metals like stainless steel.[60,89,92] It was further reported that modified carbon electrode could improve bacterial colonization and enhanced electron transfer, which further improved overall performance of MFCs and MECs.[93] Furthermore, the positively charge modified electrodes, for example, ammonia treatment,[94] chitosan (an amino- and hydroxyl-group contained polysaccharide),[95] and polyaniline,[96] can improve microbe-electrode interaction. The investigation of the decoration with thin layer metals (like Au, Pd and Ni) showed the potential of reducing the activation energy threshold of electron transfer.[93]

### 1.2.2. Enzymes for $CO_2$ reduction catalysis

Comparing to microbial technologies, using separated enzymes provides advantages of simple and well-defined system. Since enzymes are non-living proteins, they do not need growth and specific growth conditions. An efficient enzymatic system has been established in which the system selectively generates desired product with high production yield at mild conditions (ambient pressure and room temperature). The enzymatic systems could be performed as a single enzyme reaction or multi-enzyme cascade reaction, representing a remarkable diversity of substrate and reaction specifications.[18,41,97,98] Due to high selectivity towards substrate conversion, enzymes have been used in electrochemical biosensors for broad range of analytes *i.e.* cholesterol, polyphenols and glucose,[97,99] and in enzymatic biofuel cells.[100] Several

oxidoreductases (EC 1), enzymes that catalyze the electron transfer between the reductant (an electron donor) and the oxidant (an electron acceptor) were employed in such systems, such as glucose oxidase and horseradish peroxidase. These enzymes are also called as redox enzymes and usually extracted from microorganisms for example bacteria, archaea, fungi and yeast. Although some enzymes catalyzed the same reaction, different cofactors might be needed according to their mechanisms and different active sites or components (like different metal clusters or metal-containing active sites). The redox enzymes usually require natural cofactors including $NAD^+$/NADH, nicotinamide adenine dinucleotide phosphate ($NADP^+$/NADPH) and flavin adenine dinucleotide (FAD/$FADH_2$), but some enzymes like glucose oxidase do not require any cofactors and directly use oxygen as electron carrier. List of examples of redox enzymes and their reactions reported for electrochemical applications were summarized in **Table 1**.[97,99–101]

| Enzyme (EC number) | Reaction | cofactor |
|---|---|---|
| Glucose oxidase (1.1.3.4) | glucose + $O_2$ → glucono-1,5-lactone + $H_2O_2$ | - |
| Alcohol oxidase (1.1.3.13) | primary alcohol + $O_2$ → aldehyde + $H_2O_2$ | - |
| Glutamate oxidase (1.4.3.11) | L-glutamate + $O_2$ + $H_2O$ → 2-oxoglutarate + $NH_3$ + $H_2O_2$ | FAD |
| Alcohol dehydrogenase (1.1.1.1) | primary alcohol + $NAD^+$ ⇌ aldehyde + NADH + $H^+$<br>secondary alcohol + $NAD^+$ ⇌ ketone + NADH + $H^+$ | $NAD^+$/ NADH |
| Glucose dehydrogenase (1.1.1.47) | glucose + $NAD^+$ → glucono-1,5-lactone + NADH | $NAD^+$ |
| Lactate dehydrogenase (1.1.1.27) | lactate+ $NAD^+$ ⇌ pyruvate + NADH + $H^+$ | $NAD^+$/ NADH |
| Formate dehydrogenase (1.2.1.2) | formate + $NAD^+$ ⇌ $CO_2$ + NADH + $H^+$ | $NAD^+$/ NADH |
| Formaldehyde dehydrogenase (1.2.1.46) | formaldehyde + $NAD^+$ ⇌ formate + NADH + $H^+$ | $NAD^+$/ NADH |
| Carbon monoxide dehydrogenase (1.2.7.4) | $CO_2$ + $H_2O$ + 2 oxidized ferredoxin ⇌ $CO_2$ + $2H^+$ + 2 reduced ferredoxin | Ni-Fe cluster |
| Fumarate reductase (1.3.1.6) | succinate + $NAD^+$ ⇌ fumarate + NADH | $NAD^+$/ NADH |
| Glutamate dehydrogenase (1.4.1.2) | L-glutamate + $H_2O$ + $NAD^+$⇌ 2-oxoglutarate + $NH_3$ + NADH + $H^+$ | $NAD^+$/ NADH |
| Laccase (1.10.3.2) | 4 benzenediol + $O_2$ → 4 benzosemiquinone + $2H_2O$ | - |
| Peroxidase (1.11.1.7) | 2 phenolic compounds+ $H_2O_2$ → 2 phenoxyl radical + $2H_2O$ | - |
| Hydrogenase (1.12.7.2) | $H_2$ + 2 oxidized ferredoxin ⇌ $2H^+$ + 2 reduced ferredoxin | Fe-S cluster |

**Table 2.** Examples of redox enzymes and their reactions.

$CO_2$ is known as the sole carbon source of organic materials in all biological cycles and evolutions. There are six major metabolism pathways related to $CO_2$ fixation and related-metabolic processes including the Calvin cycle, the reductive citric acid cycle, the reductive acetyl-CoA route, the

3-hydroxypropionate cycle, the 3-hydroxypropionate/4-hydroxybutyrate cycle and the dicarboxylate/4-hydroxybutyrate cycle.[102] In these pathways, the reactions are catalyzed by several enzymes including synthases, lyases and oxidoreductases. Synthases involve in CoA-containing derivatives which are unsuitable for *in vitro* applications. While lyases are often used for catalyzing the interconversion of $CO_2$ and $HCO_3^-$ (catalyzed by carbonic anhydrase) and the carboxylation of raw materials (*i.e.* epoxides, aromatics and pyrroles) with $CO_2$. For a quest of renewable energy generation, dehydrogenases have been investigated since they are able to reduce $CO_2$ to carbon-based fuels.[103,104] As shown in the carbonyl branch of the reductive acetyl-CoA pathway (**Scheme 1**), carbon monoxide dehydrogenase (CODH) catalyzes the conversion of $CO_2$ to CO with the need of cofactor like ferredoxin, an iron-sulfur cluster, of which the equation is described in **Equation 3**. While the equation is simplified as two proton-assisted two-electron reduction (**Equation 4**).

$$CO_2 + \text{reduced ferredoxin} \rightarrow CO + \text{oxidized ferredoxin} \qquad (\textbf{Equation 3})$$

$$CO_2 + 2e^- + 2H^+ \rightarrow CO + H_2O \qquad (\textbf{Equation 4})$$

Additionally, $CO_2$ could be transformed to formate of which the reduction is catalyzed by formate dehydrogenase ($F_{ate}DH$, as shown in the Methyl branch of **Scheme 1**). The discovery of $F_{ate}DH$ in *Clostridium thermoaceticum*, an acetogen, was reported by Wood and Ljundahl in 1966.[105] Later, the reaction was demonstrated with the requirement of NADH served as electron and proton source, as shown in **Equation 5**.[106]

$$CO_2 + NADH \rightarrow HCOO^- + NAD^+ \qquad (\textbf{Equation 5})$$

To achieve higher hydrocarbon production, multienzyme system of three dehydrogenases including $F_{ate}DH$, formaldehyde dehydrogenase ($F_{ald}DH$) and alcohol dehydrogenase (ADH) is proposed for the conversion of $CO_2$ to methanol. The three reductions are shown in **Scheme 2** including the reduction of $CO_2$ to formate catalyzed by $F_{ate}DH$, the reduction of formate to formaldehyde (HCHO) catalyzed by $F_{ald}DH$ and lastly the reduction of formaldehyde to methanol ($CH_3OH$) catalyzed by ADH. Each reduction step requires one molecule of NADH as electrons and proton source. In 1999, Obert and Dave firstly demonstrated the enzymatic cascade reduction of $CO_2$ to $CH_3OH$ by using three dehydrogenases and NADH as a cofactor,[107] opening the doors for the bio-catalytic production of high energy content fuels.

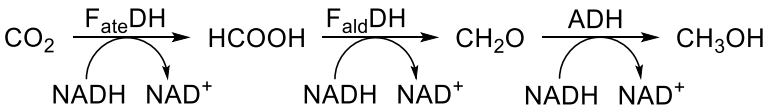


**Scheme 2.** Schematic cascade reductions of $CO_2$ to methanol catalyzed by $F_{ate}DH$, $F_{ald}DH$ and ADH through a chemical approach using NADH as a cofactor.

Although NADH is a very efficient proton and electron donor for the above-mentioned reductions,[108] it is oxidized to $NAD^+$ (*i.e.* is sacrificial), limiting large-scale application potential due to its cost and additional separation step from the reaction.[109,110] One approach is to regenerate active NADH needed for reactions. The *in situ* regeneration could be carried out through different approaches, for example, electrochemical approach using modified electrode such as poly(neutral red),[111] coupling approach with other enzymes (like glutamate dehydrogenase)[112] and photochemical approach.[113,114] To avoid using costly NADH, electrons required for $CO_2$ to $CH_3OH$ conversion, could be supplied from photogeneration or added electron shuttles.[103,104] An

alternative and very attractive non-NADH method is the electrochemical approach addressing electrons directly from the electrode to enzymes' active sites. This heterogeneous bio-electrocatalysis is not only bypass the need for NADH, but it offers advantages of simple catalyst recycling, product/catalyst separation and minimizing diffusion overpotentials.[44]

The electrocatalytic activity towards the reduction of $CO_2$ of $F_{ate}DH$ adsorbed on pyrolytic graphite edge electrode was demonstrated by Reda *et al.*, without additional shuttle or cofactor adding.[115] The authors proposed that two electrons are transferred from the electrode to enzyme active sites through iron-sulfur clusters as electron relay units, as shown in **Figure 8**. Furthermore, in 2014, Amao and Shuto depicted non-covalent immobilization of $F_{ate}DH$ onto methyl viologen modified indium tin oxide electrodes for electrochemical $CO_2$ conversion to formate.[116] The direct electron transfer behavior was also reported for ADH, showing the potential for electrochemical addressing of dehydrogenases.[117] Recently, Schlager *et al.* reported the successful direct electron injection of immobilized enzyme(s) using alginate silicate matrix onto carbon felt electrodes. ADH was used in single-enzyme electrochemical system for the conversion of butyraldehyde to butanol,[110] while three dehydrogenases were employed for conversion of $CO_2$ to $CH_3OH$, as depicted in **Scheme 3**.[109] In each reduction step requires two electrons and two protons supplied from electrodes and electrolyte solution, respectively.

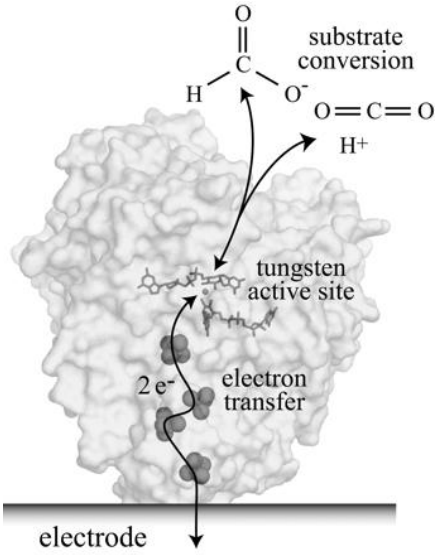


**Figure 8.** Proposed electrocatalytic interconversion of $CO_2$ and formate by a $F_{ate}DH$ adsorbed on pyrolytic graphite edge electrode surface.[115]

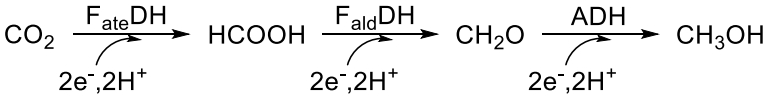


**Scheme 3.** Schematic cascade reductions of $CO_2$ to methanol catalyzed by $F_{ate}DH$, $F_{ald}DH$ and ADH through an electrochemical approach.

In order to achieve efficient electron transfer, proper integration of enzyme onto electrode is required. The ideal effective immobilization technique should preserve enzymatic activity from random distribution and poor orientation and improve electrode stability due to denaturation. Several strategies have been employed, for example, adsorption, sol-gel process, covalent binding, immobilization in polymeric films.[118] Immobilization on board range of support materials such as chitosan biopolymers,[97,119–121] ZnO nanowires[122,123] carbon nanotubes and sol-gel matrices[124–127] have been investigated. The sol-gel approach is an easy and practical approach

where enzyme activity is well-preserved, while covalent binding offers great electrode stability.[118] However, the use of sol-gel matrix (like alginate matrix) alone hinders diffusion of reactants to active sites as well as products from active sites. Consequently, electrochemical reactions slow down, so higher overpotentials are required. A new support that having higher ion and electrical conductivities is needed.

Graphene as a two-dimensional carbon-based nanomaterial is of promise as enzyme immobilization platform due to its extremely large surface, high electronic conductivity, biocompatibility and high chemical stability.[128,129] Due to the fact that graphene lacks of suitable functionalities for protein conjugation (*i.e.* hydroxyl and carboxylic acid group), therefore, it displays very low reactivity for functionalization.[130,131] On the other hand, graphene oxide (GO), a graphene derivative containing various functional groups such as epoxy, hydroxyl and carboxylic groups, is suggested as a versatile platform for conjugation of enzymes and other biological molecules, as shown in **Figure 9**. The adsorption of enzymes through electrostatic interaction[128] and chemically crosslinked protein/enzyme networks[132] on graphene surfaces were reported. However, such non-covalent immobilization often has low stability as a main drawback. Stability of enzyme/graphene hybrid material can be enhanced by direct covalent conjugation of enzymes through their primary amine groups onto graphene sheets.[133] The enzyme-graphene conjugated materials were employed for many bio-electrochemical applications such as biosensors[134–136] and biofuel cells.[132,137]

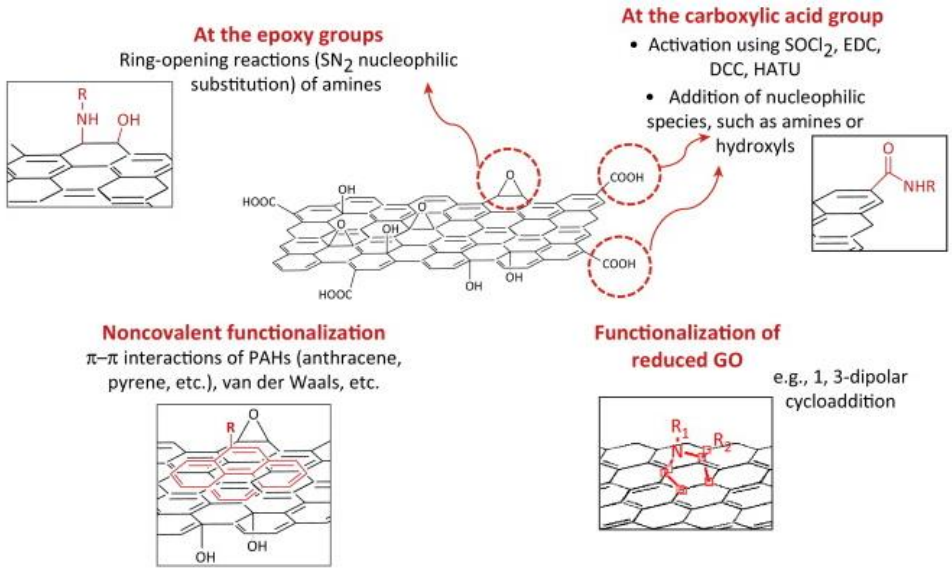


**Figure 9.** Overview of possible functionalization on graphene oxide. (Reproduced from reference 138 with a permission from Elsevier, © 2014.)

The conventional graphene oxide contains dense but uncontrolled/random functional groups,[139–141] making it an insulator as well as limiting covalent conjugation yield. Suffering from such conjugation, densely and selectively functionalized carboxylic acid graphene (**G-COOH**) was reported recently by Bakandritsos *et al.* The **G-COOH** was synthesized through two-step process (**Scheme 4**): nucleophilic substitution of fluorographene (**G-F**) with cyanide into cyanographene (**G-CN**) and subsequent oxidation of the resulting **G-CN** to **G-COOH** by $HNO_3$.[142]

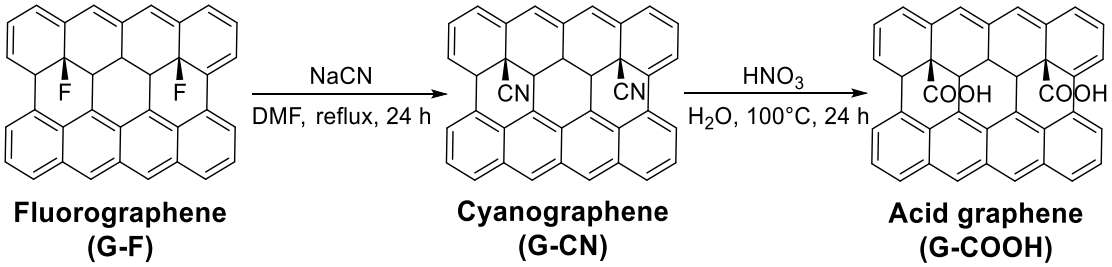


**Scheme 4.** Schematic synthesis of **G-COOH**.

This selective **G-COOH** offers opportunities for controllable graphene functionalization *via* amide bond formation with various primary amine derivatives such as cysteamine, 2-(2-aminoethoxy)ethanol and diamine ethylenedioxy-bis-(ethylamine), as shown in **Figure 10**.

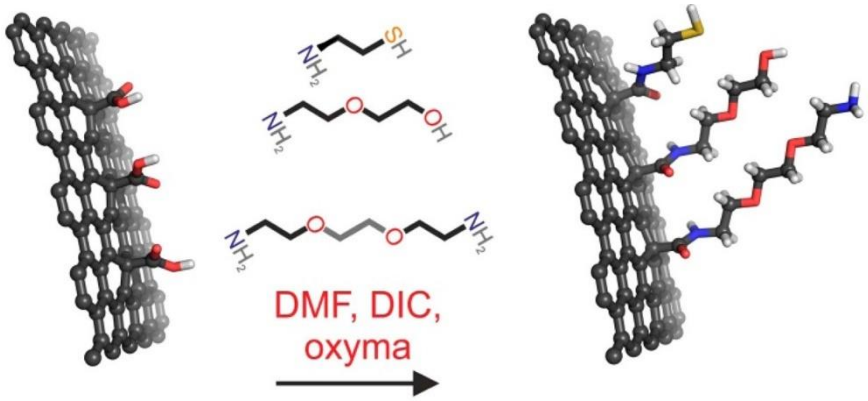


**Figure 10.** Preparation of conjugated **G-COOH** with cysteamine, 2-(2-aminoethoxy)ethanol and diamine ethylenedioxy-bis-(ethylamine) in dimemethylformamide using diisopropylcarbodiimide (DIC) and ethyl cyano(hydroxyimino)acetate (oxyma) as coupling reagents.[142] © 2017 American Chemical Society

In this thesis, we have used the carboxylic acid graphene as a nanoplatform for enzyme immobilization which will be discussed in section 3.2.1.

# 2. Experimental

## 2.1. Materials

All chemicals were used as received and are listed in **Table 3**. Ultrapure deionized water used in this work was prepared by using a Sartorius arium mini water systems.

| Chemicals | Supplier | Purity/Grade/Units | Abbreviation |
|---|---|---|---|
| *N*-(3-Dimethylaminopropyl)-*N'*-ethylcarbodiimide hydrochloride | Sigma-Aldrich | - | EDC-HCl |
| 1-(3-Dimethylthylaminopropyl)-3-ethylcarbodiimide | Alfa Aesar | 98% | EDC |
| Acetaldehyde anhydrous | Sigma-Aldrich | ≥99.5% | $CH_3CHO$ |
| Acetic acid, glacial anhydrous | Merck | 100% | $CH_3COOH$ |
| Acetone | VWR Chemicals | technical | - |
| Alcohol dehydrogenase (EC 1.1.1.1) from *Saccharomyces cerevisiae* | Sigma-Aldrich | ≥300 unit/mg protein | ADH |
| Ammonium chloride | Sigma-Aldrich | ≥99.5%, Bioultra | $NH_4Cl$ |
| Bovine Serum Albumin | Sigma-Aldrich | ≥96% | BSA |
| Calcium chloride | Carl Roth | ≥98% | $CaCl_2$ |
| Carbon dioxide | Linde | 99.999% | $CO_2$ |
| Chitosan, low molecular weight | Aldrich | - | chitosan |
| Copper sulfate pentahydrate | Sigma-Aldrich | ≥99.0% | $CuSO_4 \cdot 5H_2O$ |
| Ethanol, absolute for analysis | Merck | A.C.S. reagent | EtOH |
| Formaldehyde solution | Sigma-Aldrich | stabilized with methanol, ~37 wt. % in $H_2O$ | HCHO |
| Formaldehyde dehydrogenase (EC 1.2.1.46) from *Pseudomonas sp.* | Sigma-Aldrich | 1-6 unit/mg solid | $F_{ald}DH$ |
| Formate dehydrogenase (EC 1.2.1.2) from *Candida boidinii* | Sigma-Aldrich | 5-15 unit/mg protein | $F_{ate}DH$ |
| Glucose anhydrous | Sigma-Aldrich | ≥99.5% | $C_6H_{12}O_6$ |
| Helium | Linde | 99.999% | He |
| Hellmanex solution | Hellma-Analytics | - | - |
| Hydrogen | Linde | 99.999% | $H_2$ |
| Hydrochloric acid, fuming | Merck | 37% (7.7 M) | HCl |
| Hydrogen peroxide | Merck | 29-31% | $H_2O_2$ |
| *N*-Hydroxysuccinimide | Aldrich | 98% | NHS |
| *N*-Hydroxysulfosuccinimide sodium salt | Aldrich | ≥98% | sulfo-NHS |
| Magnesium sulfate heptahydrate | Sigma-Aldrich | ≥98%, A.C.S. reagent | $MgSO_4 \cdot 7H_2O$ |

| | | | |
|---|---|---|---|
| Methanol | VWR | ≥99.9%, HPLC grade | MeOH |
| Neutral red | Sigma-Aldrich | Bioreagent | - |
| β-Nicotinamide adenine dinucleotide hydrate | Sigma-Aldrich | ≥96.5% | $NAD^+$ |
| β-Nicotinamide adenine dinucleotide, reduced disodium salt | Sigma-Aldrich | ≥95% | NADH |
| Nitric acid | VWR | 65% | $HNO_3$ |
| Nitrogen | Linde | 99.999% | $N_2$ |
| Polypeptone | Carl Roth | - | - |
| Potassium nitrate | Alfa Aesar | ≥99.0% | $KNO_3$ |
| Potassium phosphate dibasic | Sigma-Aldrich | ≥98.0%, reagent | $K_2HPO_4$ |
| Potassium phosphate monobasic | Sigma-Aldrich | 99.5-100.5%, reagent | $KH_2PO_4$ |
| 2-Propanol | VWR | ≥99.7% | IPA |
| Sodium acetate | Sigma-Aldrich | ≥99.0% | $NaCH_3COO$ |
| Sodium alginate, from brown algae | Sigma-Aldrich | - | - |
| Sodium bicinchoninate | Alfa Aesar | - | - |
| Sodium carbonate anhydrous | Fluka Analytical | ≥99.5% | $Na_2CO_3$ |
| Sodium chloride | ACM | 99.97% | NaCl |
| Sodium formate anhydrous | Sigma-Aldrich | ≥99.0% | HCOONa |
| Sodium hydrogen carbonate | Alfa Aesar | 99.7-100.3% | $NaHCO_3$ |
| Sodium hydroxide | Merck | 99-100% | NaOH |
| Sodium tartrate dihydrate | Alfa Aesar | 99% | - |
| Sodium tungstate dihydrate | Fluka | 99% | $Na_2WO_4$ |
| Synthetic air | Linde | - | - |
| Tris(hydroxymethyl)aminomethane | Sigma-aldrich | ≥99.9%, primary standard and buffer | TRIS |
| Tryptone/Peptone from casein | Carl Roth | - | - |
| Yeast extract | Carl Roth | - | - |

**Table 3.** List of chemicals used in this thesis.

### 2.1.1. Electrode preparation

To prepare chromium/gold (Cr/Au) coated glass substrates, glass slides were cleaned by sonicating for 15 mins each in acetone, 2% Hellmanex solution, deionized water and 2-propanol at the last step. Then, the glass slides were treated in an evaporation chamber for thermal evaporation of 5 nm chromium followed by 80 nm gold as being the Cr/Au substrate for Fourier transform infrared spectroscopy (FTIR) measurement. A transparent Cr/Au coated glass electrode was prepared in a similar manner with thickness of 3 nm Cr and 15 nm Au for UV/Vis measurement.

## 2.2. Methods

### 2.2.1. Electrochemical measurements

#### 2.2.1.1. Electrochemistry

In conventional electrochemical experiments, diffusion is generally the most considered mass transport of *i.e.* ions and redox species from bulk solution to electrode surface. The diffusion is a random movement of species from higher concentration region to lower concentration region. The diffusion of particular species (flux, *J*) is dependant to concentration gradient ($\partial c/\partial x$) and diffusion coefficient (D), as described in the Fick's first law (**Equation 6**).

$$J = -D\frac{\partial c}{\partial x} \qquad \textbf{(Equation 6)}$$

While diffusion rate ($\partial c/\partial t$), which is defined as change of concentration over time, is proportional to second derivative of concentration gradient, as given in the Fick's second law (**Equation 7**).

$$\frac{\partial c}{\partial t} = D\frac{\partial^2 c}{\partial x^2} \qquad \textbf{(Equation 7)}$$

Taken together with Faraday's law, variation of current (flux of electrons at electrode surface) controlled by diffusion process ($i_d$) as a function of time ($t^{1/2}$) could be derived for a planar electrode, as given in the Cottrell equation (**Equation 8**).

$$i_d = \frac{nFAD^{1/2}c_0^*}{\pi^{1/2}t^{1/2}} \qquad \textbf{(Equation 8)}$$

Where n is number of electrons, F is Faraday's constant, A is electrode area and $c_0^*$ is bulk concentration of electroactive species. It simply shows that longer the experiment, lower current at a certain distance (referred to electrode) is observed, resulting larger diffusion layer. Once diffusion layer reaches the maximum thickness of stagnant layer, the concentration gradient does not decrease further, therefore current will remain constant and no longer time dependent. This relation is considered, for example, in chronoamperometry, where the potential is stepped from t=0 where no electroactive species reaction to a value where those species reach the electrode. The recorded current decreases and then remains constant.

For electrochemical investigation of redox molecules, electrodes and electrocatalysis, cyclic voltammetry is widely employed. The experiments are usually carried out in a three-electrode set-up consisting of working (WE), reference (RE) and counter (CE) electrodes. The sweep potential is imposed as a cyclic potential waveform, as shown in **Figure 11a**, to a working electrode relative to a reference electrode which maintains a constant potential. The waveform is often described by initial, first switching and second switching/final potentials where the sweeping starts, switches from forward to reversed direction and switches back to the forward direction again or is at the final potential.

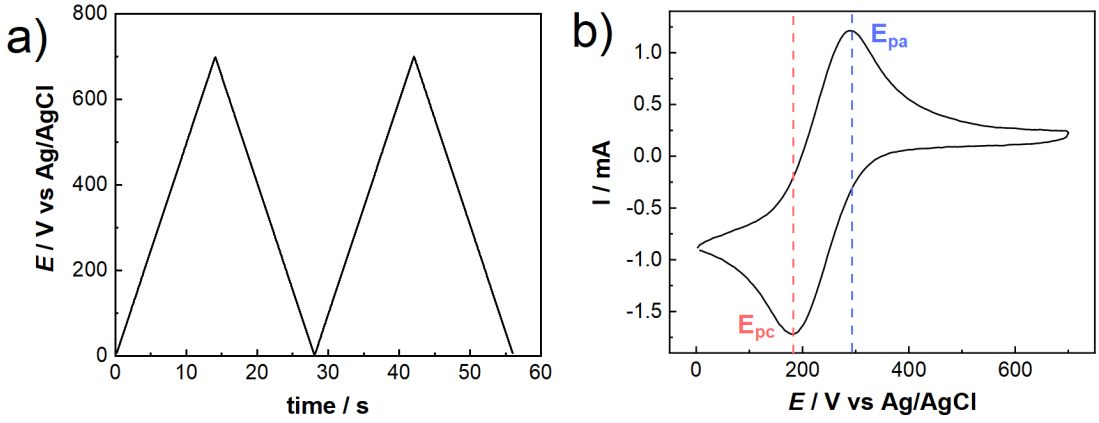


**Figure 11.** a) Cyclic potential waveform and b) cyclic voltammogram of Fe(III)/Fe(II) in aqueous solution.

The response current-potential curve is called cyclic voltammetry. The cyclic voltammogram (CV) of Fe(III)/Fe(II) redox couple is depicted in **Figure 11b**, where $E_{pc}$ and $E_{pa}$ are defined as cathodic and anodic peak potentials, respectively. In the reversible system, the separation of peak potentials ($\Delta E_p$) at 25°C should be close to 59/n mV where n is number of electrons transferred in electrochemical reaction (**Equation 9**).

$$\left|\Delta E_p\right| = \left|E_{pa} - E_{pc}\right| = \frac{59}{n} \qquad \textbf{(Equation 9)}$$

Additionally, peak current in a reversible redox system ($i_p$) is proportional to square root of scan rate ($v^{1/2}$), as described in the Randles-Sevcik equation (**Equation 10**).

$$i_p = (2.69 \times 10^5) n^{3/2} A c D^{1/2} v^{1/2} \qquad \textbf{(Equation 10)}$$

Where A is electrode area and c is concentration of redox species. According to the equation, linear relation between $i_p$ and $v^{1/2}$ provide information on reversible electrochemical process which is controlled by diffusion process and the related diffusion coefficient can be determined.

#### 2.2.1.2. Experiment

The electrochemical experiments including cyclic voltammetry and constant potential electrolysis were carried out in a three-electrode system consisting of working, reference and counter electrodes. The electrochemical cell configuration is described in detail in next sections. The experiments were performed, and the data were recorded using a potentiostat which can be considered as a current-to-voltage converter, together with a data acquisition system. The potentionstats used in this study, a Jaissle Potentiostat-Galvanostat (Germany) and an IVIUM CompactStat (the Netherlands), are shown in **Figure 12**.

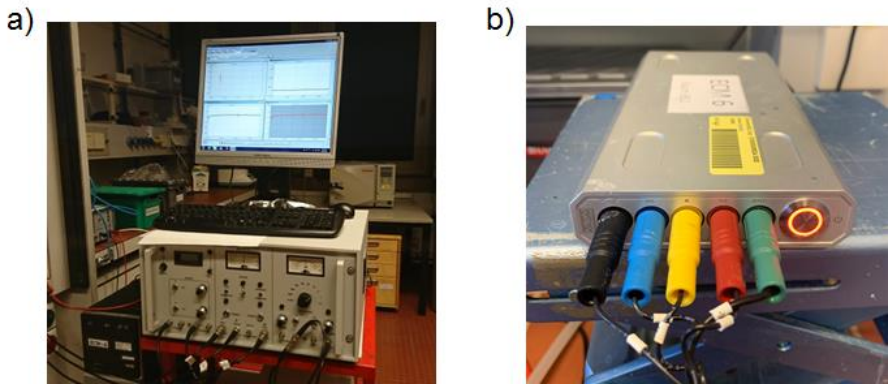


**Figure 12.** Photos of potentiostats used in this study a) a Jaissle Potentiostat-Galvanostat and b) an IVIUM CompactStat.

In this study, the reported electrochemical potentials were of Ag/AgCl (3 M KCl), otherwise mentioned separately. The conversion of potentials between different references was calculated using the following chart:

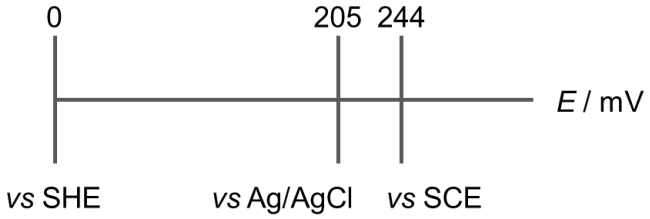


### 2.2.2. Attenuated total reflection Fourier transform infrared spectroscopy (ATR-FTIR)

Attenuated total reflection Fourier transform infrared spectroscopy (ATR-FTIR) is an important non-invasive technique to identify functionality of the materials. In the measurement, the sample is firstly placed on an internal reflection element (sometimes is called an ATR crystal). The infrared beam is directed onto the crystal at an angle which is greater than the critical angle, allowing internal reflection at least one point. At every reflection point, evanescence wave is generated which can be absorbed by the sample coated on the crystal. After existing the crystal, the beam is then collected by detector. To avoid the loss of signals and/or provide total reflection, materials with high refractive index are used as ATR crystals such as germanium, zinc selenide (ZnSe) and diamond. Depending on choice of crystal, the incident angle is varied. By increasing number of reflection points, signal-to-noise ratio of signals can be enhanced. A schematic representation of ATR-FTIR measurement where internal reflections in an ATR crystal are presented is shown in **Figure 13**.

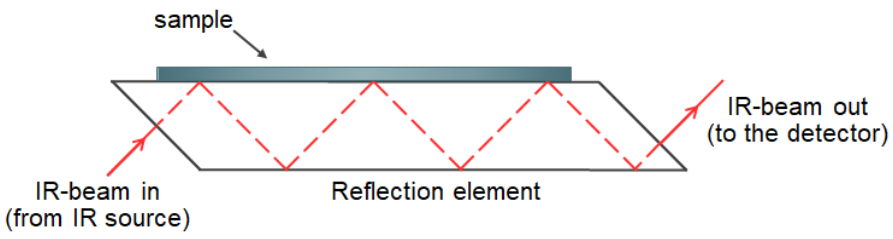


**Figure 13.** Schematic representation of ATR-FTIR measurement, showing internal reflections (dashed line).

In this thesis, FTIR spectra were recorded under $N_2$ atmosphere using a Bruker IFS-66/S and a Bruker Vertex 80 equipped with a Platinum ATR module (**Figure 14**) over 32 and 128 scans, respectively. Both machines consist of Mercury Cadmium Telluride (MCT) detector. In case of using a Bruker IFS/66S machine, the samples were prepared by drop-casting sample solution onto a ZnSe crystal which was polished by using diamond paste (1 µm size, Struers, Denmark) followed by cleaning with acetone using Soxhlet method for 16 h, prior to use. The absorbance spectra reported herein was obtained from **Equation 11**.

$$absorbance = -\frac{T_{sample} - T_{ZnSe}}{T_{ZnSe}} \quad \text{(Equation 11)}$$

Where $T_{sample}$ refers to transmission of sample coated on a ZnSe crystal and $T_{ZnSe}$ refers to transmission of a bare ZnSe crystal.

Since the IFS/66S machine is equipped with ATR module where the diamond reflection element is placed below, therefore the samples including powder and thin film coated on Cr/Au coated glass substrate were placed face to the diamond.

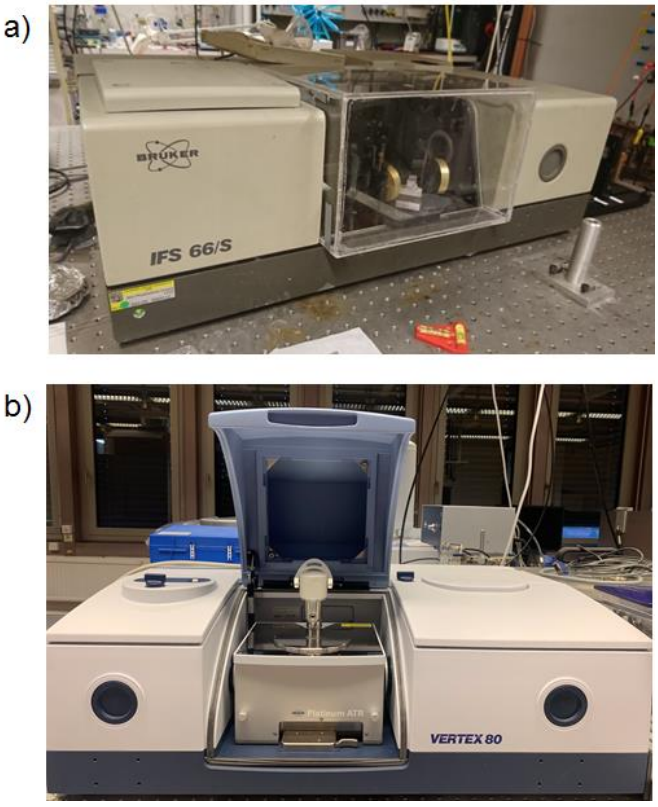


**Figure 14.** Photos of ATR-FTIR instruments: a) a Bruker IFS-66/S and b) a Bruker Vertex 80.

### 2.2.3. Microscopy

For the scanning electron microscopy (SEM) measurements, the SEM images were taken using a JEOL JSM-6360 LV scanning electron microscope (**Figure 15**) at the accelerating voltage of electron beam of 7.0 kV with a working distance of 15 mm. While Nikon Eclipse LV100ND microscope was used to take a picture of carbon felt samples using incident light.

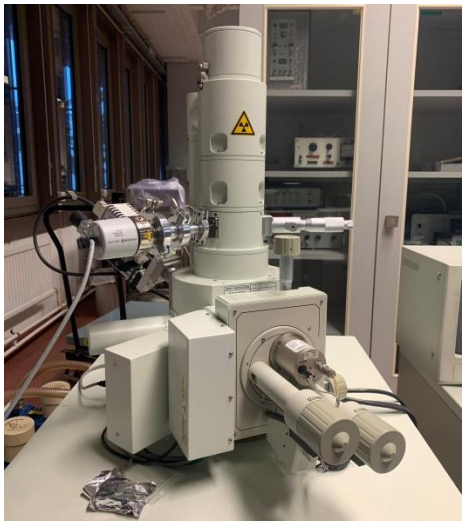

**Figure 15.** A photo of a scanning electron microscope.

### 2.2.4. UV/Vis spectroscopy

The absorbance spectra of thin film or monomers were recorded using a Perkin Elmer Lambda 1050 UV-Vis-NIR spectrophotometer. Baseline correction was carried out prior the measurements. For thin film or drop-casted film coated on a Cr/Au transparent electrode, the measurements were done by using a bare electrode as reference. While the monomer solution was prepared in a quartz cuvette for measurements. The absorbance measurement in enzymatic assay and protein determination was performed in 96-well microplates using a Thermo Scientific Multiskan FC microplate photometer at room temperature (**Figure 16**).

**Figure 16.** A photo of microplate reader.

## 2.3. Product analysis

### 2.3.1. Gas injection gas chromatography

To analyze gas product(s) in headspace above electrolyte solution, 2 mL of headspace gas was taken using a gas-tight syringe and injected to gas injection chromatograph (GC, Thermo Scientific Trace GC Ultra). The GC machine was equipped with two columns using two different carrier gases namely $N_2$ and He in order to broaden the range of analytes. Both channels were connected with a thermal conductivity detector (TCD) and operated with the same temperature program as

shown in **Table 4**. The $N_2$ channel was used for qualification analysis of $H_2$, $CH_4$ and $CO_2$ while CO and be quantified in He channel. **Figure 17** shows chromatograms of standard gases including $H_2$, $CH_4$ and $CO_2$ which were detected in $N_2$ channel at the retention time of 0.23, 0.50 and 1.0 min, respectively.

| Temperature | Time/Rate |
|---|---|
| 30°C | Hold for 2 min |
| 30-130°C | 10°C·min$^{-1}$ |
| 130°C | Hold for 8 min |

**Table 4.** Temperature program operated in gas injection GC.

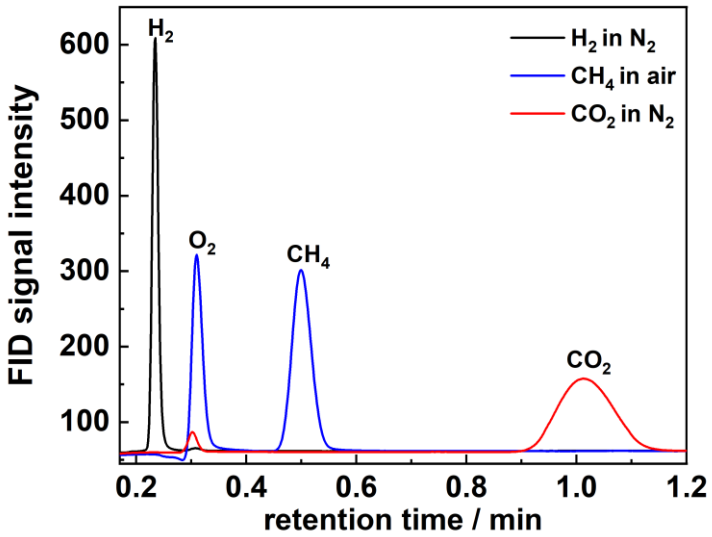


**Figure 17.** Gas injection gas chromatograms of 2 mL standard gas consisting of 20 µL $H_2$ gas (black), 46 µL $CH_4$ (blue) and 43 µL $CO_2$ (red).

### 2.3.2. Liquid injection gas chromatography

Liquid injection gas chromatograph (liquid-GC) was used to detect and quantify low molecular weight alcohols in the liquid samples. The analysis was performed on Thermo Fisher Trace 1310 gas chromatograph equipped with a TR-V1 column (30 m×0.25 mm diameter×1.4 µm film thickness) and a flame ionized detector (FID). The measurements were split mode with the split flow of 10 mL·min$^{-1}$ and He was used as a carrier gas with the constant flow of 1.5 mL·min$^{-1}$. The temperature program for detection of methanol, ethanol and 2-propanol was shown in **Table 5**. The chromatogram of standard alcohol solutions containing methanol (49 ppm), ethanol (42 ppm) and 2-propanol (41 ppm) were observed at the retention time of 4.1, 5.2 and 6.1 min, respectively (**Figure 18**).

| Temperature | Time/Rate |
|---|---|
| 40°C | Hold for 2 min |
| 40-80°C | 5°C·min$^{-1}$ |
| 80-250°C | 15°C·min$^{-1}$ |
| 250°C | Hold for 4 min |

**Table 5.** Temperature program operated in liquid injection GC.

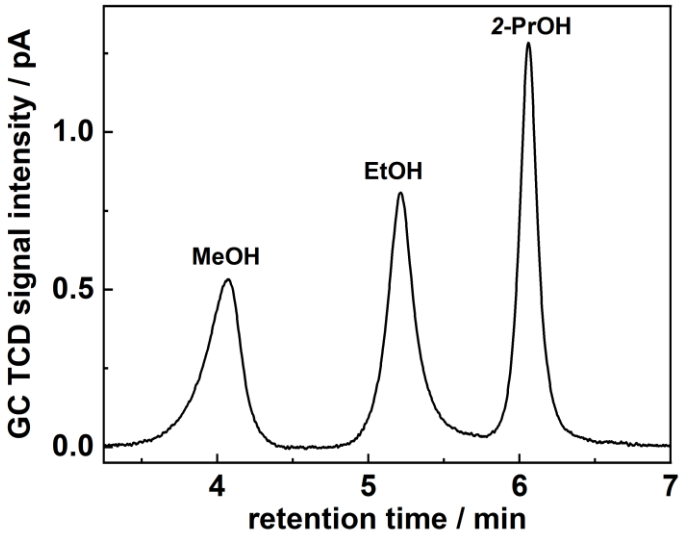


**Figure 18.** Liquid injection gas chromatogram of standard alcohol solution containing methanol (49 ppm), ethanol (42 ppm) and 2-propanol (41 ppm).

### 2.3.3. Ion chromatography

Ions analysis was carried out using Thermo Scientific Dionex ICS-5000 ion chromatograph (IC) equipped with IonPac AG19 guard column (2×50 mm), an IonPac AS19 column (2×250 mm) and a Dionex suppressor-conductivity detector. The samples were diluted with ultrapure deionized water (with the ration of 1:50) and the measurements were carried out using an autosampler at a constant temperature of 25°C. KOH was used as eluent with the flow rate of 0.25 $mL \cdot min^{-1}$ at different concentrations shown in**Table 6**. A chromatogram of interested ions, formate ($HCOO^-$, 10 ppm) and acetate ($CH_3COO^-$, 10 ppm), is shown in **Figure 19** of which the ions are detected at the retention of 6.67 and 5.92 min, respectively.

| KOH concentration | Time |
|---|---|
| 10 mM | 0-7 min |
| 100 mM | 7-12 min |
| 10 mM | 12-25 min |

**Table 6.** Concentration of KOH eluent used in IC measurements.

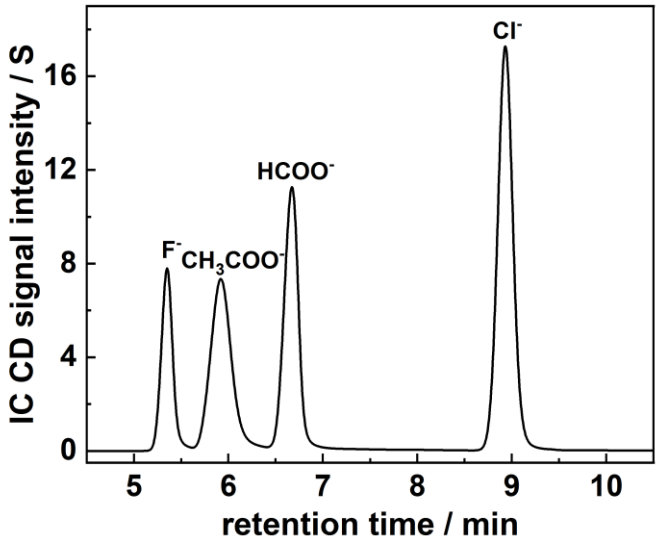


**Figure 19.** Ion chromatogram of standard solution containing fluoride (2 ppm), acetate (10 ppm), formate (10 ppm) and chloride (6 ppm).

## 2.4. Microbial electrolysis for $CO_2$ reduction

### 2.4.1. Microbial electrochemical system configurations

#### 2.4.1.1. Electrochemical setup for microbial electrochemical reduction of $CO_2$ to formate and $CH_4$

The adaptation of *Methylobacterium extorquens* and its microbial electrolysis experiments were carried out in a two-compartment electrochemical cell of which anode and cathode compartments were separated by a pre-treated Nafion membrane, a proton exchange membrane (PEM), allowing proton transport between the two chambers (**Figure 20**). Two types of Nafion membranes were used namely Nafion 324 and Nafion 117. The Nafion 324 membrane was received from Sigma-Aldrich and was used for microbial electrochemical reduction of $CO_2$ to formate. The Nafion 324 membrane was pre-treated by soaking in 3 M HCl aqueous solution for 2 h, subsequently rinsing and then boiling in deionized water for additional 30 min. While Nafion 117 sheet, purchased from Chemours, was equipped in microbial electrochemical cells for the conversion of $CO_2$ to $CH_4$. The Nafion 117 was boiling in $H_2O_2$, deionized water, 0.5 M $H_2SO_4$ and deionized water, sequentially. Each step was carried out for 1 h.

A three-electrode system consists of a spongy-like carbon electrode (carbon felt, 2.5×6.5×0.6 $cm^3$, SGL Carbon GmbH) or modified carbon felt electrode with a platinum wire as electrical contact, a Ag/AgCl (3 M KCl; Basi) and a platinum plate (1.4×4.1 $cm^2$) as working, reference and counter electrodes, respectively. As shown in **Figure 20b**, the working and reference electrodes are in a cathode chamber while a counter electrode is in an anode chamber.

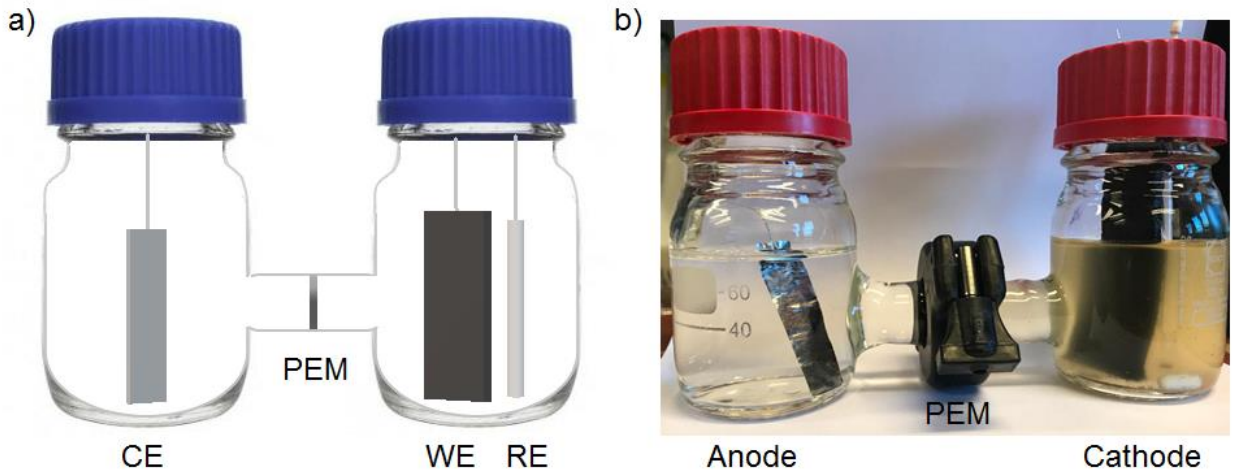


**Figure 20.** a) Schematic and b) a photograph of two-compartment microbial electrolysis cell having biocatode.

#### 2.4.1.2. Electrochemical setup for microbial electrolysis containing two bioelectrodes

The microbial electrochemical experiments for the reduction of $CO_2$ to $CH_4$ in the cathode chamber assisted with the oxidation of organic substances in an anode chamber were performed in the two-compartment three-electrode configuration as shown in **Figure 21**. The cell contained two carbon felt electrodes (or modified carbon felt electrodes) as working and counter electrodes. These two electrodes were in anode and cathode compartments which were separated by a pre-treated Nafion 117 membrane. A Ag/AgCl (3 M NaCl) reference electrode was placed next to a working electrode in the anode chamber.


**Figure 21.** A photograph of two-compartment microbial electrolysis cell containing a bioanode and a biocathode.

### 2.4.2. Electrode modification for microbial electrolysis system

#### 2.4.2.1. Preparation of poly(neutral red) modified carbon felt

A poly(neutral red) modified carbon felt was prepared electrochemically in one-compartment electrochemical cell equipped with a carbon felt working electrode, a Ag/AgCl (3 M KCl) reference electrode and a platinum plate counter electrode. Following the previous report,[143] a carbon felt electrode was pre-treated prior to use. The pre-treatment step was carried in 0.1 M $KNO_3$ aqueous solution by sweeping potential between 0 to 1.00 V vs Ag/AgCl (3 M KCl) with the scan rate of

50 mV·s$^{-1}$ over 20 cycles. After that, the pre-treated carbon electrode was placed in 0.1 M phosphate buffer solution pH 6.0 containing 1 mM neutral red (chemical structure of neutral red is shown in **Figure 22**) and 0.1 M $KNO_3$. The electropolymerization was performed at potentials between -1.00 and 1.00 V with the scan rate of 50 mV·s$^{-1}$ over 20 cycles.

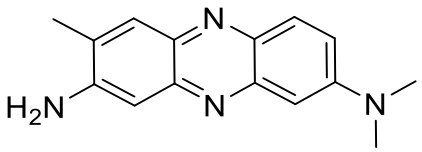

**Figure 22.** Structure of neutral red monomer.

#### 2.4.2.2. Preparation of chitosan modified carbon felt

According to previous report,[93] the preparation of chitosan modified carbon felt contained the oxidation of a carbon-based electrode, the activation of carboxylic group through carbodiimide chemistry and the reaction with chitosan. A general chemical structure of chitosan was shown in **Figure 23**. With slight modification,[93] a carbon felt electrode was soaked in concentrated $HNO_3$ at room temperature for 14 h and then was rinsed thoroughly with deionized water until the resulting water became neutral. After that, the oxidized carbon felt was dried under vacuum for 14 h. Then, the electrode was placed in the mixture ethanol and water (4:1 v/v) containing 50 mM EDC and 50 mM of NHS and was soaked at room temperature for 2 h. Then, the electrode was transferred and left in 2% acetic acid solution containing chitosan (1% w/v) at pH 6.5 (adjusted with 1 M NaOH solution) at room temperature for 14 h. Finally, the chitosan modified electrode was rinsed carefully with deionized water and allowed to dry under vacuum.

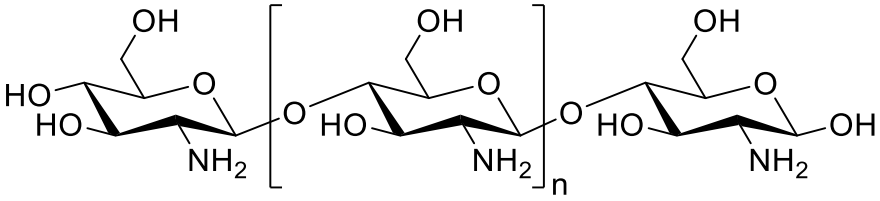

**Figure 23.** Structute of chitosan.

### 2.4.3. Experimental procedures

#### 2.4.3.1. Microbial electrolysis cell for the reduction of $CO_2$ to formate

##### 2.4.3.1.a Microbial electrode preparation

According to abovementioned procedure (section 2.4.1.1. , the setup was built in a laminar air flow cabinet (Alpina, Poland) using sterilized components including glassware, cap and septa (sterilized at 121°C in an autoclave). After that, nutrient medium (components are listed in **Table 7**) containing *M. extorquens* inoculum (10% v/v) was used as cathodic electrolyte solution.[82] The *M. extorquens* pure culture (DSM-1337, Deutsche Sammlung Mikroorganismenund Zellkulturen (DSMZ)) was provided by acib GmbH. While anodic solution was sterilized 0.2 M phosphate buffer solution pH 7.0. To provide anaerobic condition for microorganisms, the cathode compartment was saturated with $CO_2$. The biofilm formation was taken place by applying constant potential of -0.75 V vs Ag/AgCl (3 M KCl) for one month with gentle stirring at room temperature. The cathodic chamber was purged with $CO_2$ once a week. During this period, 2 mL of cathodic headspace gas samples were taken daily and analyzed using a gas chromatography

| Chemicals | Amount/concentration (per L) |
|---|---|
| Polypeptone | 10 g |
| Yeast extract | 2 g |
| $MgSO_4 \cdot 7H_2O$ | 2 g |
| MeOH | 0.5% (w/v) |
| $Na_2WO_4$ | 0.3 µM |

**Table 7.** Composition of nutrient medium *for M. extorquens*.[82]

#### 2.4.3.1.b Microbial electrolysis

After the one-month adaptation, the cathodic and anodic solutions were replaced with 0.2 M phosphate buffer solution pH 7.0. In this section, three different microbial electrolysis cells were investigated namely **MEC 1**, **2** and **3**. The biocathodes in all three MECs were prepared with the same procedure. **MEC 1** is defined as a microbial electrolysis system equipped with biofilm coated carbon felt as a biocathode. In **MEC 2**, neutral red (50 µM) was added into cathodic solution as a redox mediator. While **MEC 3** is referred to the system where carbon felt electrode was firstly modified with poly(neutral red) and this modified electrode was then inoculated with *M. extorquens*. For all MECs, the long-term electrolysis was performed continuously at applied potential of -0.75 V vs Ag/AgCl (3 M KCl) under $CO_2$-saturated condition with gentle stirring at room temperature. Every 1 or 2 day, the liquid sample was taken from cathodic solution for formate analysis using an ion chromatograph. As a batch operation, the cathodic chambers were purged weekly with $CO_2$ for 2 h in order to keep the systems saturated with $CO_2$, and the electrolyte solutions, both anodic and cathodic ones, were replaced with freshly prepared buffer solutions every 3-4 weeks, assigned as running cycles. In case of the **MEC 2**, neutral red was added into catholyte every replacement of electrolyte. The experiments were continuously performed for around 12 weeks.

### 2.4.3.2. Microbial electrolysis cell for the reduction of $CO_2$ to $CH_4$

#### 2.4.3.2.a Microbial electrode preparation

As mentioned in section 2.4.1.1. the establishment of the autoclaved setup was done under sterilized condition in a laminar air flow cabinet. At the beginning, the cathodic chamber was filled with 80 mL of nutrient medium containing 10% (v/v) inoculum of mix cultured microorganisms. The inoculum was prepared by centrifugation (4000 rpm for 10 min) of sewage sludge collected from a communal wastewater treatment plant (Linz AG, Austria), provided by acib GmbH The compositions in nutrient medium, as listed in **Table 8**, were prepared according to the reported study,[71] which was called as Cheng's medium. The medium also contained electrolyte salts, trace minerals and vitamins which are necessary for the growth of microorganisms. The lists of components in trace element and vitamin solutions are summarized in **Table 9** and **Table 10**, respectively. The trace mineral and vitamin solutions were prepared, sterilized and provided by acib GmbH. While the anodic chamber was filled with 80 mL of 0.1 M phosphate buffer solution pH 7.0. This phase was performed by applying a constant potential of -0.8 V vs Ag/AgCl (3 M NaCl) for 4 weeks at room temperature with gentle stirring. In this first 2 weeks, glucose (0.22 g) was added into cathodic solution which was then purged with $CO_2$ every week. The other 2 weeks, the cathode chamber was only purged with $CO_2$ once a week.

| Chemicals | Amount (per L) |
|---|---|
| $KH_2PO_4$ | 3 g |
| $K_2HPO_4$ | 2.5 g |
| NaCl | 0.13 g |
| $NH_4Cl$ | 0.31 g |
| $NaHCO_3$ | 6 g |
| $MgSO_4 \cdot 7H_2O$ | 0.04 g |
| Trace element solution | 12.5 mL |
| Vitamin solution | 5 mL |

**Table 8.** Composition of Cheng's medium.

| Chemicals | Amount (per L) |
|---|---|
| Hydrochloric acid | 10 mL |
| $FeCl_2 \cdot 4H_2O$ | 1.50 g |
| $ZnCl_2$ | 70 mg |
| $MnCl_2 \cdot 4H_2O$ | 100 g |
| $H_3BO_3$ | 6 mg |
| $CoCl_2 \cdot 6H_2O$ | 19 g |
| $CuCl_2 \cdot 2H_2O$ | 2 mg |
| $NiCl_2 \cdot 6H_2O$ | 24 mg |
| $Na_2MoO_4 \cdot 2H_2O$ | 36 mg |

**Table 9.** Composition of trace element solution according to DSMZ medium 320, provided by acib GmbH.

| Chemicals | Amount (per L) |
|---|---|
| Biotin | 2 mg |
| Folic acid | 2 mg |
| Pyridoxine-HCl | 10 mg |
| Thiamine-HCl | 5 mg |
| Riboflavin | 5 mg |
| Nicotinic acid | 5 mg |
| Calcium D-pantothenate | 5 mg |
| Vitamin B12 | 0.1 mg |
| *p*-aminobenzoic acid | 5 mg |
| Lipoic acid | 5 mg |

**Table 10.** Composition of vitamin solution according to DSMZ medium 140, provided by acib GmbH.

#### 2.4.3.2.b Microbial electrolysis

After 4 weeks, the biofilm was formed on the electrode. The cathodic and anodic solutions were replaced with Cheng's medium and 0.1 M phosphate buffer solution (pH 7.0), respectively. This microbial electrolysis set-up is defined in this study as **MEC 4**. The experiment was carried out by applying a constant potential of -0.80 V vs Ag/AgCl (3 M NaCl) at room temperature under $CO_2$-saturated condition with gentle stirring. To monitor the $CH_4$ generation, headspace samples were taken twice a week for headspace analysis using a gas chromatograph. After headspace

sampling, the cathodic chamber was flushed with $CO_2$ and the electrolytes were refreshed every 3-4 weeks, labelled as running cycles.

#### 2.4.3.3. Bio-electrochemical system for wastewater treatment

##### 2.4.3.3.a Microbial electrode preparation

The bio-electrochemical systems for both organic substances oxidation and $CO_2$ reduction were built in the sterilized condition, as mentioned in section 2.4.1.2. Both bioanode and biocathode were developed from the same inoculum. The inoculum was prepared by the centrifugation (4000 rpm for 10 min) of sewage sludge obtained from a communal wastewater treatment plant (Linz AG, Austria), provided by acib GmbH. After establishment of the setup, the cathode chamber was filled with 20 mL of inoculum and 200 mL of Cheng's medium containing glucose (0.22 g), while the anode compartment was filled with 20 mL of inoculum and 200 mL of Cheng's medium containing additional carbon sources to simulate a communal wastewater.[144] The synthetic wastewater components are listed in **Table 11**. The adaptation was performed by applying a constant potential of 0.40 V vs Ag/AgCl (3 M NaCl) under $CO_2$-saturated condition at room temperature with gentle stirring. To ensure enough biomass, glucose (0.22 g) was added to cathodic solution, followed by purging with $CO_2$ once a week, in the meanwhile, half of anodic solution was replaced with freshly prepared Cheng's medium containing synthetic wastewater, followed by purging with $CO_2$. Further investigations were done on electrode modifications with poly(neutral red) and chitosan. The bioelectrodes of these modified electrodes were prepared in a similar way to the bare carbon felt electrode system.

| Chemicals | Amount (per L) |
|---|---|
| Tryptone | 69 mg |
| Yeast extract | 37.5 mg |
| Sodium acetate | 44 mg |
| Glucose | 168 mg |

**Table 11.** Composition of components added to 1 L of Cheng's medium, obtaining Cheng's medium containing synthetic wastewater.

##### 2.4.3.3.b Microbial electrolysis

After the 4-week adaptation phase, 200 mL of cathodic solution was replaced with freshly prepared Cheng's medium without glucose addition. The microbial electrolysis was carried out by controlling potential at 0.40 V vs Ag/AgCl (3 M NaCl) at room temperature with gentle stirring under anaerobic conditions ($N_2$-saturated condition for anode compartment and $CO_2$-saturated condition for cathode compartment). The headspace samples from the cathode chamber and liquid samples from the anode chamber were taken twice a week for headspace analysis and chemical oxygen demand (COD) measurement, respectively. After sampling, the cathode chambers were purged with $CO_2$ to keep the condition saturated, while, in anode chamber, half of anodic solution was replaced with freshly prepared Cheng's medium containing synthetic wastewater and the chamber was flushed with $N_2$ to achieve anaerobic condition. In every 4-week, 200 mL of cathodic solution was replaced with fresh medium to provide microorganisms with sufficient trace elements and vitamins, assigned as different running cycles. The system consisting of the bioelectrodes using bare carbon felt electrodes was defined as **BES 1**, while the poly(neutral red) and chitosan modified systems were defined as **BES 2** and **3**, respectively.

#### 2.4.4. Determication of efficiencies

##### 2.4.4.1. Faradaic efficiency

Faradaic efficiency (FE) is an important parameter determination performance and selectivity of the system. The Faradaic efficiency can be calculated by dividing moles of product observed in the experiment ($mol_{product}$) by moles of electrons consumed during the reaction ($mol_{electron}$) which were corrected with number of electrons needed for such reduction (n). The moles of product were obtained from gas or ion chromatography. While the moles of consumed electrons were calculated from consumed charges during controlled-potential electrolysis. In all microbial electrolysis systems, the experiments were performed in a batch mode in which the electrolysis was stopped for feeding and then re-started. While applying a constant potential, the current was recording. By plotting recorded current (in ampere (A)) vs running time (in second (s)), the integrated area of such plots represented the charge (in coulomb (C)) passes through the electrochemical system. The consumed charges were then converted to the numbers of electron moles by dividing with Faraday constant (F) of 96485 $C \cdot mol^{-1}$. The calculation is shown in **Equation 12**.

$$FE = \frac{\mathrm{mol}_{\mathrm{product}}}{\frac{1}{\mathrm{n}} \times \mathrm{mol}_{\mathrm{electron}}} \qquad \text{(Equation 12)}$$

According to mentioned reductions, n is equal to 2 in the reduction of $CO_2$ to formate and $H_2$ formation, while n is equal to 8 in the reduction of $CO_2$ to $CH_4$.

##### 2.4.4.2. COD removal efficiency

COD values of liquid samples were analyzed photometrically by acib GmbH. The measurements were performed by mixing 2 mL of sample and COD reagent (Nanocolor COD 160 and 1500, Macherey-Nagel) and the tubes were then heated at 148°C for 2 h in a thermostat (Nanocolor Vario Mini, Macherey-Nagel). After cooling down to room temperature, COD values were measured using a LED photometer (Compact Photometer PG-3, Macherey-Nagel) at the wavelength of 620 nm. The COD removal was reported as the change of COD values (ΔCOD) from the beginning ($COD_{initial}$) at after certain electrolysis time. Accordingly, COD removal efficiency can be calculated by dividing ΔCOD with $COD_{initial}$, as shown in **Equation 13**.

$$\mathrm{COD\ removal\ efficiency} = \frac{\Delta \mathrm{COD}}{\mathrm{COD}_{\mathrm{initial}}} \qquad \text{(Equation 13)}$$

## 2.5. Enzymatic reductions

#### 2.5.1. Preparation of enzyme graphene bio-nano catalyst

The enzyme immobilization on carboxylic acid graphene was performed through amidation, which will be discussed later in section 3.2.1. The graphene was used as received which was provided by Dr. Aristides Bakandritsos (Regional Centre of Advanced Technologies and Materials, Olomouc, Czech Republic). With a slight modification of the reported procedure,[134] a solution of EDC-HCl (7.7 mg, 0.015 M) and **G-COOH** aqueous dispersion (0.2 mL of 10 $mg \cdot mL^{-1}$ solution) in 2.3 mL of 0.1 M phosphate buffer solution pH 7.4 was prepared. The mixture was then treated with sulfo-NHS (18 mg, 0.03 M) at room temperature for 2 h. The modified graphene acid was purified by centrifugal washing with 0.1 M phosphate buffer pH 7.4 for 4 times and the solid was collected, obtaining **G-NHS**.

For enzyme conjugation, the resulting **G-NHS** (2 mg) was re-dispersed in 0.1 M phosphate buffer pH 7.4 (1 mL). The enzyme was added as a solution into the **G-NHS** suspension and the reaction was incubated at room temperature for 14 h. The enzyme solution was prepared by gentle dissolving dehydrogenase in 0.5 mL of 0.1 M phosphate buffer pH 7.4. The added amount was 2.5 mg, 10 mg or 2.5 mg of ADH, $F_{ate}DH$ or $F_{ald}DH$, respectively. The coupling reaction was performed separately for each enzyme. After that, dehydrogenase functionalized graphene was collected and unbound enzyme was washed out by centrifugation with buffer solution for 4 times, resulting ~2 mg of **G-ADH** or **G-$F_{ate}$DH** or **G-$F_{ald}$DH**.

#### 2.5.1.1. Protein determination

Protein amounts attached on graphene could be determined using bicinchoninic acid (BCA) assay (**Scheme 5**).[145] The assays consist of two reactions: the reduction of $Cu^{2+}$ to $Cu^{+}$ by peptide bonds under basic condition and the chelation of $Cu^{+}$ with two BCA molecules, forming a purple complex of BCA-$Cu^{+}$. The resulting BCA-$Cu^{+}$ complex absorbs maximum light at a wavelength of 562 nm.

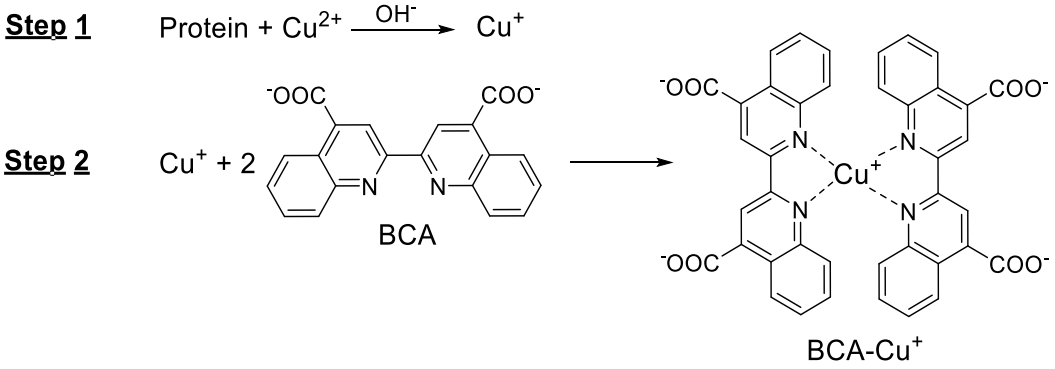


**Scheme 5.** Schematic BCA assay.

The amount of proteins can be quantified calorimetrically at the maximum absorbance. To prepare BCA's working reagent, two solutions (reagent A and B) were prepared separately. In 100 mL of reagent A consisted of sodium bicinchoninate (0.1 g), $Na_2CO_3 \cdot H_2O$ (2.0 g), sodium tartrate dihydrate (0.16 g), NaOH (0.42 g), $NaHCO_3$ (0.95 g) and deionized water. Reagent B consisted of $CuSO_4 \cdot 5H_2O$ (0.4 g) in 10 mL deionized water. The working reagent was prepared by mixing 100 mL of reagent A and 2 mL of reagent B. The protein determination of sample was performed by mixing 100 µL of sample with 2 mL of working reagent and incubation at 60°C for 30 min. After cooling down, absorbance at 562 nm of sample was recorded and compared with known protein standard, bovine serum albumin (BSA), for protein content determination. The absorbance spectra and the corresponding calibration curve of BSA solutions at various concentrations are shown in **Figure 24** and **Figure 25**, respectively.

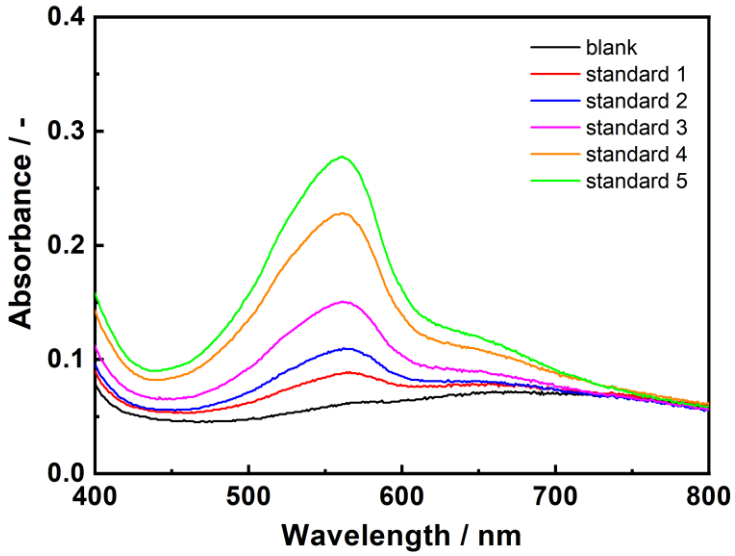


**Figure 24.** Absorbance spectra of resulting solutions from BCA assay of different BSA standard solutions (concentrations of 0.10, 0.19, 0.38, 0.75 and 1 mg·mL$^{-1}$).

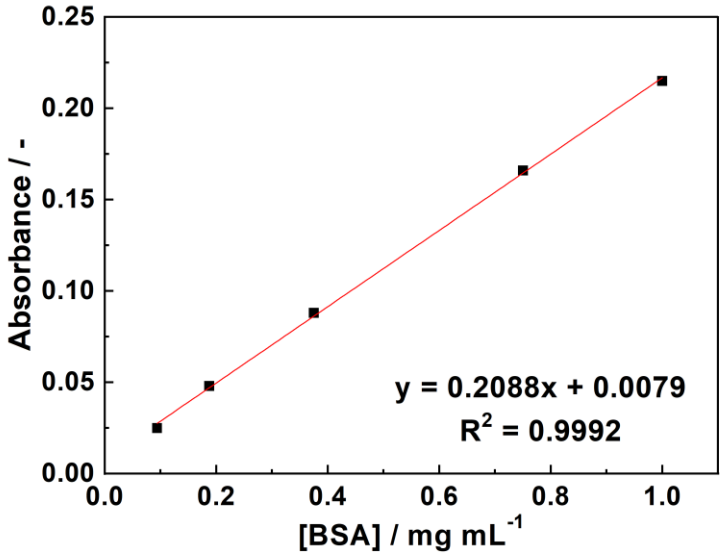


**Figure 25.** Calibration curve for optical absorbance at 562 nm for protein determination using BCA assay at various concentrations of BSA solutions.

#### 2.5.1.2. Enzymatic activity determination

##### 2.5.1.2.a ADH enzymatic activity assay

The enzymatic activity of ADH was determined by measuring the absorbance increase at 340 nm corresponding to the formation of NADH concomitant with ethanol oxidation using a microplate reader. The working solution contains ethanol aqueous solution (20 µL, 2.25 M), TRIS-HCl buffer solution pH 8.8 (200 µL, 0.1 M) and enzyme aqueous solution (20 µL). To initiate the reaction, $NAD^+$ aqueous solution (20 µL, 5 mM) was added into the mixture. While one unit of ADH enzyme activity is defined as the amount of ADH that converts 1 µmol of $NAD^+$ to NADH per minute at pH 8.8 at 25°C. The enzyme activity is determined by averaging the produced NADH per minute

for the first 5 min. Amount of NADH was determined by comparison the optical absorbance at 340 nm with various standard NADH solutions (**Figure 26**).

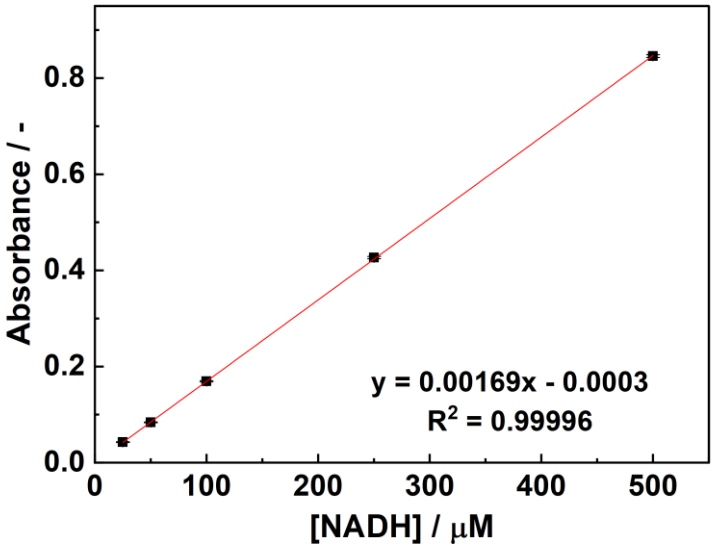


**Figure 26.** Calibration curve for optical absorbance at 340 nm of various NADH solutions.

#### 2.5.1.2.b $F_{ate}$DH enzymatic activity assay

The enzymatic activity of $F_{ate}$DH was determined by measuring the absorbance increase at 340 nm corresponding to the formation of NADH concomitant with formate oxidation using a microplate reader. The working solution contains formate aqueous solution (75 µL, 0.2 M), phosphate buffer solution pH 7.0 (150 µL, 0.1 M), deionized water (20 µL) and enzyme solution (25 µL). To initiate the reaction, $NAD^+$ aqueous solution (30 µL, 10.5 mM) was added into the mixture. While one unit of $F_{ate}$DH enzyme activity is defined as the amount of $F_{ate}$DH that converts 1 µmol of $NAD^+$ to NADH per minute at pH 7.0 at 25°C. The enzyme activity is determined by averaging the produced NADH per minute for the first 5 min using resulting NADH calibration curve (**Figure 26**).

#### 2.5.1.2.c $F_{ald}$DH enzymatic activity assay

The enzymatic activity of $F_{ald}$DH was determined by measuring the absorbance increase at 340 nm corresponding to the formation of NADH concomitant with formaldehyde oxidation using a microplate reader. The working solution contains formaldehyde solution (10 µL, 0.08%), phosphate buffer solution pH 7.5 (200 µL, 0.05 M), deionized water (15 µL) and enzyme aqueous solution (25 µL). To initiate the reaction, $NAD^+$ aqueous solution (50 µL, 5.7 mM) was added into the mixture. While one unit of $F_{ald}$DH enzyme activity is defined as the amount of $F_{ald}$DH that converts 1 µmol of $NAD^+$ to NADH per minute at pH 7.5 at 25°C. The enzyme activity is determined by averaging the produced NADH per minute for the first 5 min using resulting NADH calibration curve (**Figure 26**).

### 2.5.2. Enzyme immobilization using alginate matrix

#### 2.5.2.1. Preparation of alginate beads

As reported previously,[113] alginate hydrogel beads were prepared by crosslinking alginic acid with $Ca^{2+}$ (as shown in **Scheme 6**). Firstly, alginic acid sodium salt (0.05 g) was dissolved gently in 2 mL of 0.1 M TRIS-HCl buffer solution (pH 7.4). After that, enzyme-functionalized graphene

(**G-DH**) suspension was added into alginate solution. The modified graphene suspension was prepared by dispersed 2 mg of modified graphene in 1 mL of 0.1 M TRIS-HCl buffer solution pH 7.4. To prepare the beads, the mixture (alginate and **G-DH**) was added dropwise into 0.2 M $CaCl_2$ aqueous solution with gentle stirring. The gel formation was carried out for 20 min. Then, the beads were rinsed gently with deionized water, resulting alginate beads containing enzyme functionalized graphene. In case of three-dehydrogenase system, the beads were prepared by using a mixture of alginic acid sodium salt and **G-F$_{ate}$DH** (0.5 mL), **G-F$_{ald}$DH** (0.25 mL) and **G-ADH** (0.25 mL) solutions, resulting alginate beads containing **G-DHs**.

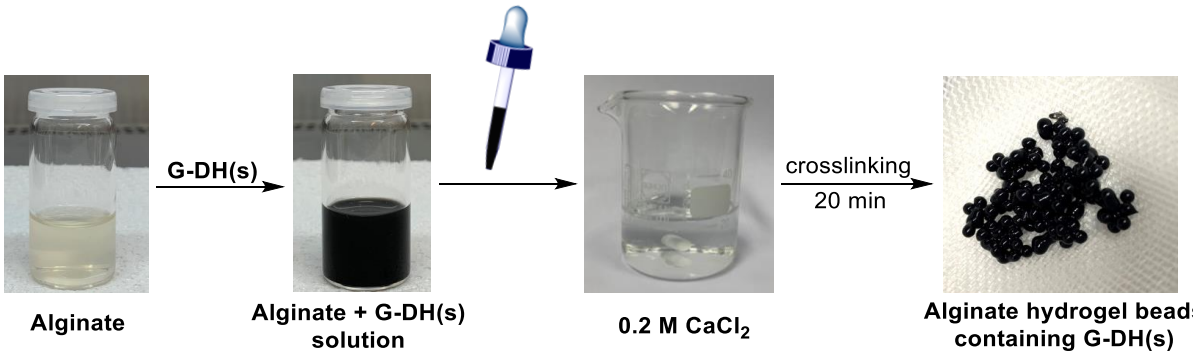


**Scheme 6.** Preparation of alginate beads containing enzyme(s)-functionalized graphene (**G-DH**(**s**)).

#### 2.5.2.2. Preparation of alginate coated carbon felt electrode

With the similar manner to alginate beads, the alginate solution in 0.1 M TRIS-HCl buffer solution (pH 7.4) was prepared by dissolving alginic acid sodium salt (0.05 g), subsequently adding 1 mL of enzyme functionalized graphene suspension (2 mg·mL$^{-1}$). As shown in **Scheme 7**, a carbon felt electrode (connecting with a platinum wire for electrical contact) was then soaked in prepared alginate solution and was transferred into 0.2 M $CaCl_2$ solution for crosslinking, resulting carbon felt electrode coated with alginate hydrogel containing enzyme functionalized graphene. In case of three-dehydrogenase system, the electrode was prepared by soaking a carbon felt in the mixture of alginic acid sodium salt and **G-F$_{ate}$DH** (0.5 mL), **G-F$_{ald}$DH** (0.25 mL) and **G-ADH** (0.25 mL) solutions, resulting carbon felt electrode coated with alginate matrix containing **G-DHs**.

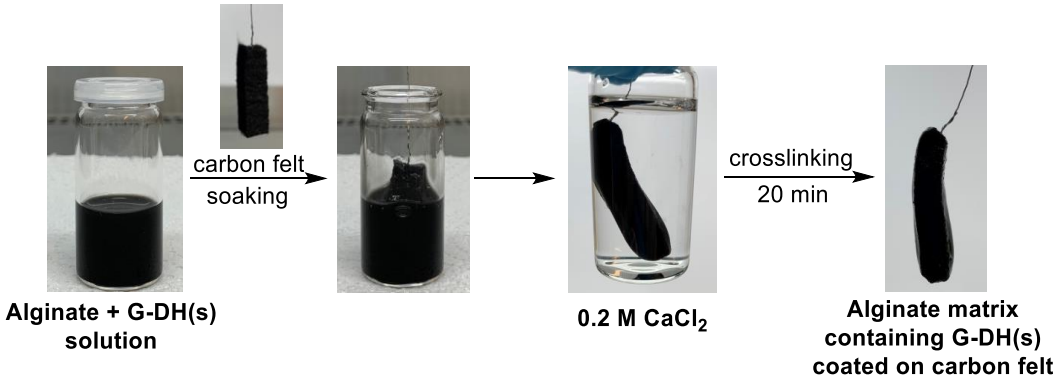


**Scheme 7.** Preparation of carbon felt electrode coated with alginate matrix containing **G-DH**(**s**).

### 2.5.3. Enzymatic activities

#### 2.5.3.1. Conversion of acetaldehyde to ethanol

To prove the activity of ADH covalently attached on graphene, a set of samples was prepared including bare **G-COOH**, **G-COOH** mixed with ADH, **G-ADH**, free ADH and **G-ADH** immobilized

in alginate matrix (**G-ADH** alginate beads). **G-COOH** mixed with ADH sample was prepared by incubation of **G-COOH** and ADH in 0.1 M phosphate buffer solution pH 7.4 at room temperature for 14 h and then centrifugal to remove non-adsorbed ADH.

A mixture of 0.3 M acetaldehyde aqueous solution (0.5 mL), 0.1 M TRIS-HCl buffer solution pH 7.4 (1.8 mL) and the aqueous sample solution (0.2 mL) or the prepared gel beads was treated with 2 mM NADH aqueous solution (0.5 mL) at room temperature for 2 h under $N_2$-saturated condition (the setup was shown in **Figure 27**). For product analysis, liquid samples were taken before and after 2-h reaction and were analyzed using a gas chromatograph. A blank experiment using deionized water as sample was done as a comparison.

**Figure 27.** A photo of setup for enzymatic chemical reduction.

#### 2.5.3.2. Conversion of $CO_2$ to methanol

The alginate beads containing **G-DHs** were transferred in 0.1 M TRIS-HCl buffer solution pH 7.0 (10 mL) containing NADH (9 mg, 0.13 mmol). The reaction was performed for 14 h under $CO_2$-saturated condition (using a setup shown in **Figure 27**). The liquid sample was collected and analyzed using liquid injection gas chromatograph.

### 2.5.4. Enzymatic electrolysis

#### 2.5.4.1. Electrochemical setup

Enzymatic electrochemical experiments were carried out in two-compartment electrochemical cell (H-cell type, 2×25 mL), as demonstrated in **Figure 28**. The two compartments were separated by a glass frit to avoid re-oxidation of the reduction product(s) at the anode. The carbon felt or alginate modified carbon felt electrode was equipped as a working electrode. A Ag/AgCl reference electrode (3 M NaCl) was placed next to working electrode, while a platinum plate was used as a counter electrode placed in another chamber. Further, caps together with septa were equipped offering gas purging and sampling availabilities.

**Figure 28.** A photo of a setup for enzymatic electrolysis experiments.

#### 2.5.4.2. Experimental procedures

##### 2.5.4.2.a Electrochemical reduction of acetaldehyde to ethanol catalyzed by G-ADH

The experiments were performed using a setup described in section 2.5.4.1. A modified carbon felt electrode coated with alginate matrix containing **G-ADH** which was mentioned in section 2.5.2.2. was used as a working electrode (a cathode). 20 mL of 0.1 M TRIS-HCl buffer solution pH 7.4 was filled to both compartments as electrolyte solutions. The cathode chamber was purged with $N_2$ for 1 h. Then the electrode was characterized by means of cyclic voltammetry. The cyclic voltammograms were recorded at potentials between 0 to -1.20 V vs Ag/Ag with the scan rate of 10 $mV \cdot s^{-1}$. After that, acetaldehyde was added to cathodic compartment at the final concentration of 1 M and the cathode chamber was purged again with $N_2$ for an additional hour. In the presence of acetaldehyde, another cyclic voltammogram was recorded. Afterwards, an electrolysis was carried out by applying a constant potential of -1.00 V vs Ag/AgCl continuously for 20 h in the presence of acetaldehyde under $N_2$-saturated condition. During electrolysis, 2 mL of cathodic solution was taken after 5 and 20 h of reaction for ethanol analysis using a liquid injection gas chromatograph.

##### 2.5.4.2.b Electrochemical reduction of $CO_2$ to methanol catalyzed by G-DHs

With the similar setup as the previous section, a carbon felt modified with alginate hydrogel containing **G-DHs** was used as a working electrode and 0.1 M TRIS-HCl buffer solution pH 7.0 was used as electrolyte solutions in both chambers. The cyclic voltammograms were recorded by sweeping the potentials between 0 and -1.20 V vs Ag/AgCl with the scan rate of 10 $mV \cdot s^{-1}$ under $N_2$- and $CO_2$-saturated conditions. Then, a controlled potential electrolysis was performed at a potential of -1.20 V vs Ag/AgCl for 20 h. During the electrolysis, cathodic solution was taken after 5 and 20 h of reaction for methanol analysis using a liquid injection gas chromatograph.

### 2.5.5. Determination of efficiencies

#### 2.5.5.1. Chemical conversion efficiency

The efficiencies of the reduction of acetaldehyde to ethanol and the reduction of $CO_2$ to methanol catalyzed by enzyme functionalized graphene in the presence of NADH as a cofactor, were defined as chemical conversion efficiency. As NADH served as an electron donor, this conversion efficiency was calculated by dividing moles of product ($mol_{product}$) by moles of added NADH

($mol_{NADH}$) corrected by the number of NADH required in certain reaction (m), as shown in **Equation 14**.

$$\text{chemical conversion efficiency} = \frac{\text{mol}_{\text{product}}}{\frac{1}{m} \times \text{mol}_{NADH}} \quad \textbf{(Equation 14)}$$

According to enzymatic reductions mentioned in the first chapter (**Scheme 2**), for each molecule of NADH, one molecule of acetaldehyde is converted to one molecule of ethanol (m=1), while the conversion of $CO_2$ to methanol required three molecules of NADH (m=3).

#### 2.5.5.2. Faradaic efficiency

As mentioned in section 2.4.4.1. (**Equation 6**), the Faradaic efficiencies of enzymatic electrochemical reductions were determined in a similar way in which number of electrons needed for reduction (n) are 2 for the reduction of acetaldehyde to ethanol and 6 for the reduction of $CO_2$ to methanol.

# 3. Results and Discussion

## 3.1. Microbial electrolysis

The results described in this section are published in: *ChemBioChem* **2019**, *20*, 1196.
DOI: 10.1002/cbic.201800784
Authors: Hathaichanok Seelajaroen, Marianne Haberbauer, Christine Hemmelmair, Abdalaziz Aljabour, Liviu Mihai Dumitru, Achim Walter Hassel and Niyazi Serdar Sariciftci

In this section, the microbial electrolysis systems having *Methylobacterium extorquens* were investigated their long-term electrocatalytic activities towards the conversion of $CO_2$ to formate in the absence of mediator and in the presence of neutral red as redox mediators (**MEC 1-3**). Apart from the pure strain acetogen, mixed culture from sewage sludge was also presented its activity toward the electromethanogenesis (**MEC 4**) and further combined with bioanodes, resulting dual-application bio-electrochemical systems. The effects of electrode modifications on long-term performance of organics degradation and $CH_4$ production were also examined (**BES 1-3**).

### 3.1.1. Electrode modification

As electrode modification could enhance the overall performance of the microbial electrochemical systems. Here, two modifications were employed including poly(neutral red) and chitosan coating. Neutral red was generally used as redox mediator since its redox potential ($E^{0'}$ = -525 mV vs Ag/AgCl for $NRH_2/NRH^+$) is similar to that of $NAD^+$/NADH redox couple ($E^{0'}$ = -515 mV vs Ag/AgCl for NADH/$NAD^+$), an important electron carrier in cellular respiration.[63,65,146] While chitosan biopolymer is a promising material due to cost-effectiveness and bio-compatibility.[95,147,148]

#### 3.1.1.1. Poly(neutral red) coated carbon felt

As reported previously,[143] poly(neutral red) was prepared by electropolymerization of neutral red monomer. Firstly, the carbon felt electrode was pre-treated electrochemically in 0.1 M $KNO_3$ aqueous solution by sweeping potentials between 0 to 1.00 V vs Ag/AgCl with the scan rate of 50 $mV \cdot s^{-1}$ over 20 cycles. **Figure 29** presents cyclic voltammograms recorded over scanning cycles. The graphs revealed a decrease in oxidative currents at around 1 V from 0.07 $mA \cdot cm^{-2}$ in the first cycle to 0.04 $mA \cdot cm^{-2}$ in the 6$^{th}$ cycle and remained stable afterwards.

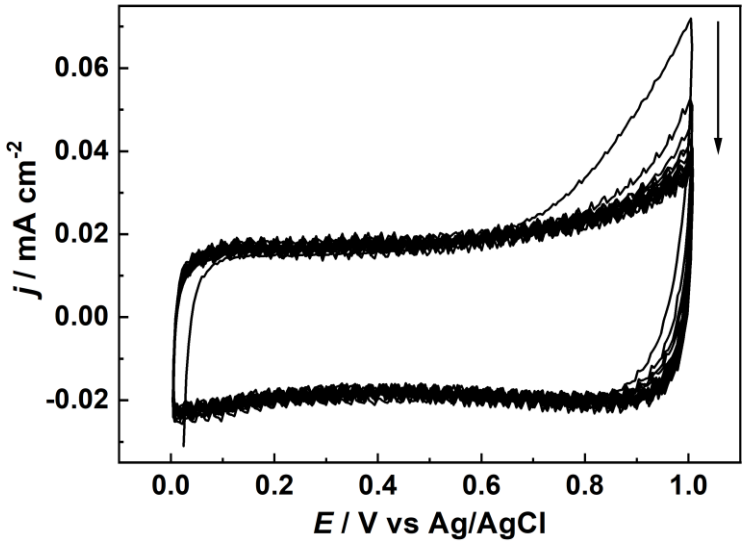


**Figure 29.** Cyclic voltammograms of the pre-treatment of a carbon felt electrode in 0.1 M $KNO_3$.

The pre-treated electrode was used as a working electrode for electrochemical preparation of poly(neutral red). The electropolymerization was done by sweeping potentials between -1.00 to 1.00 V vs Ag/AgCl at the scan rate of 50 $mV \cdot s^{-1}$ over 20 cycles in phosphate buffer solution (pH 6.0) containing 1 mM neutral red and 0.1 M $KNO_3$ (**Figure 30**). The observed broad peak at around 0.75 V vs Ag/AgCl is attributed to the monomer oxidation peak of which the peak potential was shifted towards the positive potential as the number of scanning cycles increased, indicating the changes of electrode surface according to polymer formation. Furthermore, the redox couples at around 0 and -0.50 V vs Ag/AgCl, corresponding to the doping/de-doping of the polymer and the reduction/re-oxidation of neutral red moiety, respectively, were observed. Upon the electropolymerization, peak currents increased as more polymer formed onto the electrode. The reductive peaks shifted negatively and became broader due to branching of formed poly(neutral red).

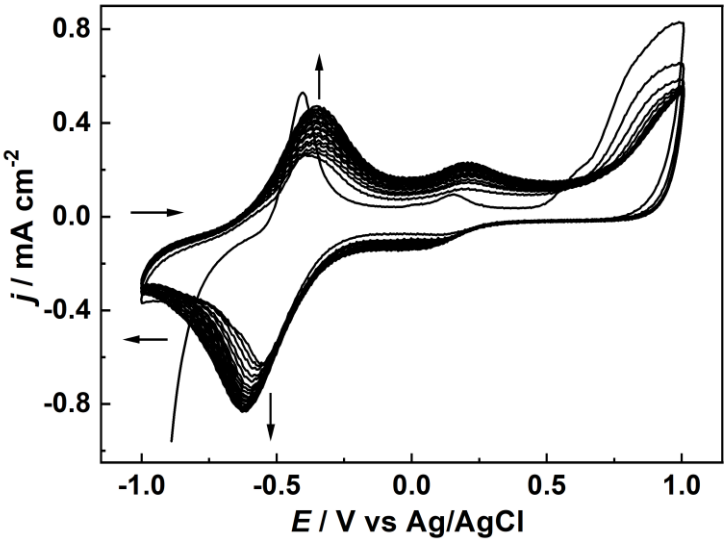


**Figure 30.** Cyclic voltammograms of electropolymerization of neutral red in 0.1 M phosphate buffer solution (pH 6.0) containing 1 mM neutral red and 0.1 M $KNO_3$.

The proposed mechanism of the oxidative electropolymerization of poly(neutral red) was suggested through its primary amine groups, as shown in **Scheme 8**.

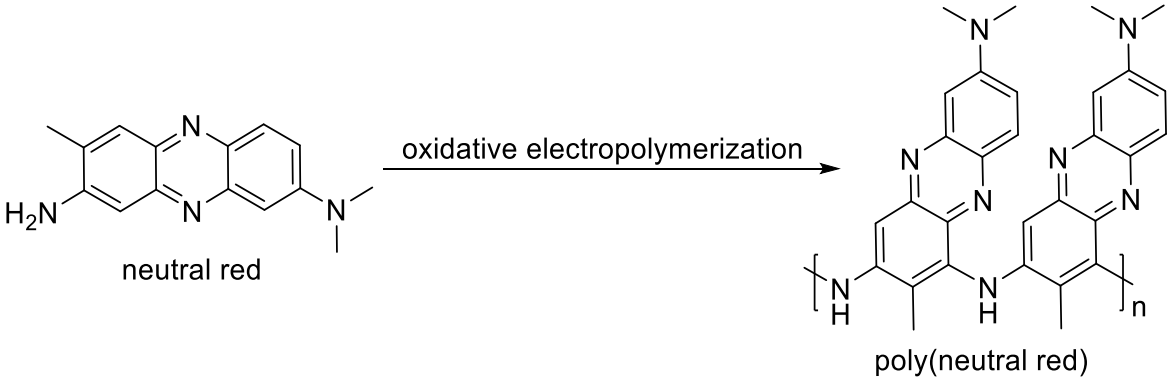


**Scheme 8.** Proposed electropolymerization of neutral red.

The electrochemical characterization of poly(neutral red) coated onto a carbon felt electrode were performed by means of cyclic voltammetry. The cyclic voltammograms were recorded in monomer-free phosphate buffer solution pH 6.0 at different scanning rates: 5, 10, 25, 50 and 100 $mV \cdot s^{-1}$, as shown in **Figure 31**. The shape and current of anodic and cathodic peaks were affected by a scanning rate (v). The plot of anodic and cathodic peak currents ($I_{pa}$ and $I_{pc}$) of oxidation/re-reduction of neutral red moiety and square root of scan rate ($v^{1/2}$) revealed linear relation over the studied range (**Figure 32**). The slopes of linear relations of anodic and cathodic peaks were found to be 0.71 and -0.79 $mA \cdot mV^{-1/2} \cdot s^{1/2}$, respectively. The results revealed that the electrochemical process of the poly(neutral red) modified carbon felt electrode is controlled by diffusion processes which is in accordance to the previous studies.[143,149]

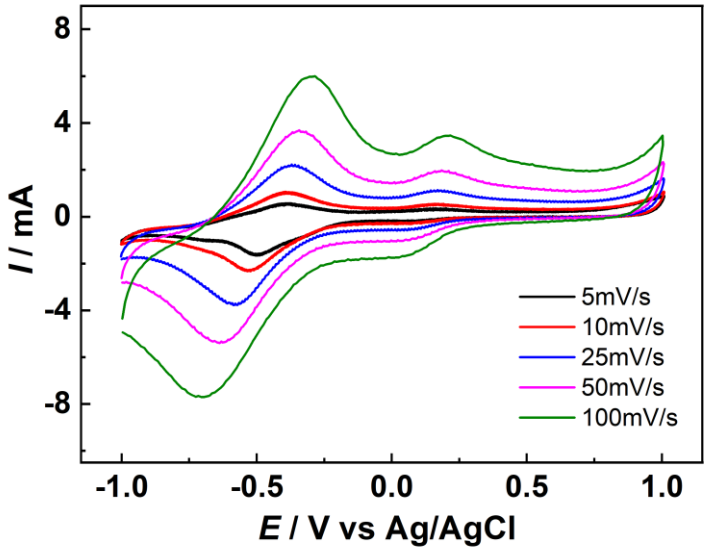


**Figure 31.** Cyclic voltammograms of poly(neutral red) coated onto a carbon felt electrode in 0.1 M phosphate buffer solution pH 6.0 at different scan rates (5, 10, 25, 50 and 100 $mV \cdot s^{-1}$).

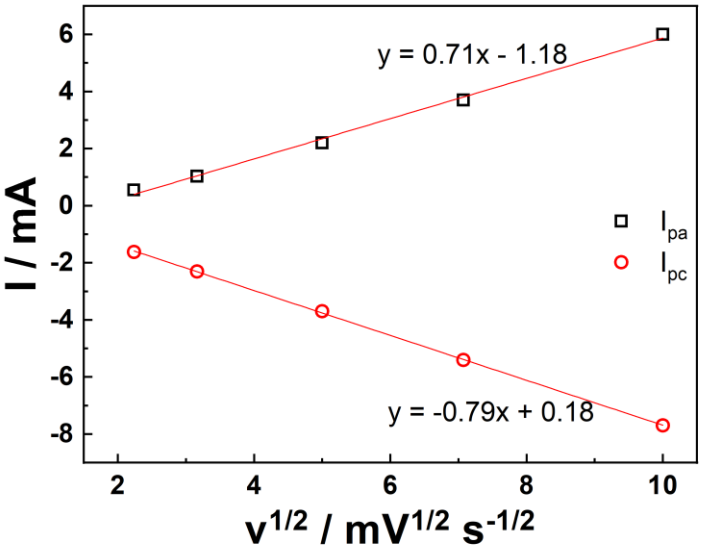


**Figure 32.** Dependence of anodic and cathodic peak currents ($I_{pa}$ and $I_{pc}$) on square root of scan rate ($v^{1/2}$).

The SEM images of bare carbon felt and poly(neutral red) modified carbon felt were taken, as shown in **Figure 33**. The images confirmed poly(neutral red) formation on the felt.

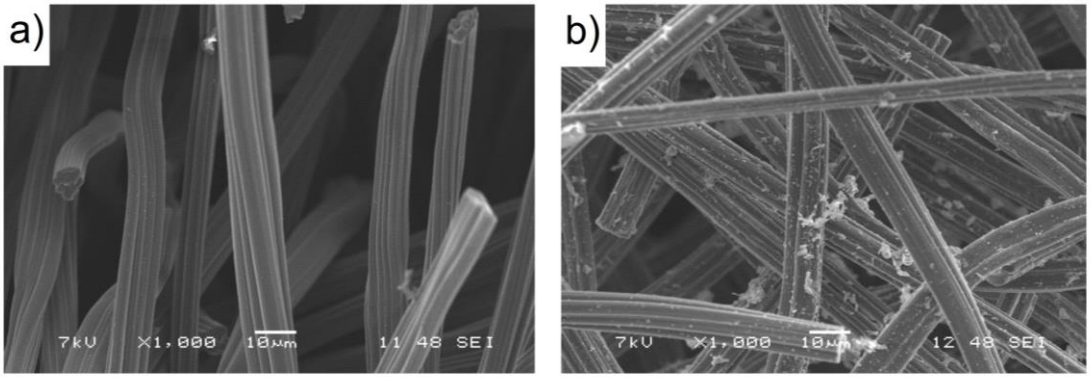


**Figure 33.** SEM images of a) bare carbon felt and b) poly(neutral red) coated on carbon felt. Scale bar is of 10 µm.

Further characterization of poly(neutral red) was carried out using infrared spectroscopy and absorption spectroscopy. According to the measurement limitations, poly(neutral red) coated on Cr/Au coated glass was prepared with the similar manner to carbon felt electrode one. The absorption spectra of neutral red monomer and poly(neutral red) were plotted, as shown in **Figure 34**. The spectrum of neutral red (red solid line) presented characteristic peaks at wavenumber of 1619, 1192 and 821 $cm^{-1}$, attributed to the vibrations of C=C or C=N bonds, in-plane bending of C-H bond and the deformation vibration of benzene ring, respectively. These peaks were preserved in the infrared spectrum of poly(neutral red) (blue solid line) and the wavenumber were shifted negatively by 10, 7 and 9 $cm^{-1}$ for C=C or C=N vibration, C-H vibration and benzene ring deformation vibration, respectively. These observations implied an increase in conjugation degree in polymeric form.

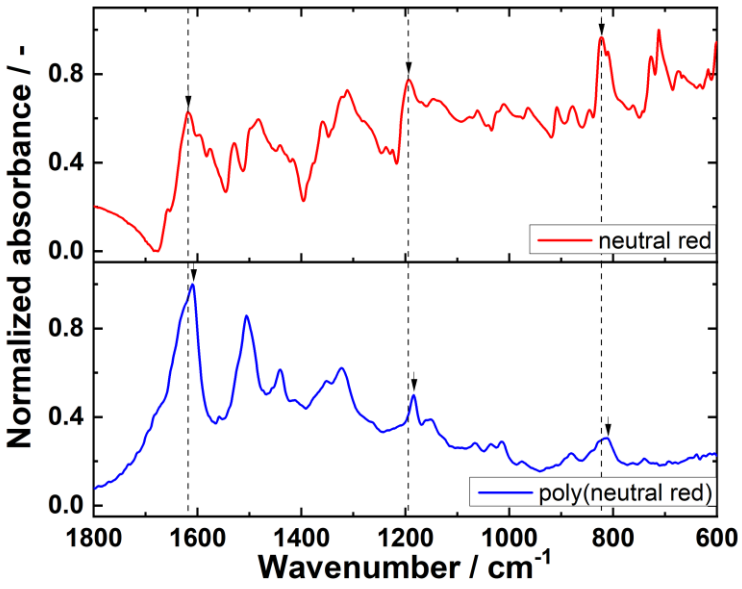


**Figure 34.** FTIR spectra of neutral red (red solid line) and poly(neutral red) coated on Cr/Au coated glass electrode (blue solid line).

**Figure 35** shows absorbance spectra of neutral red dissolved in water (black line), drop-casted neutral red on a transparent Cr/Au coated glass (blue solid line) and poly(neutral red) coated on a transparent Cr/Au coated glass (red solid line). The absorbance maxima of neutral red solution, drop-casted film and poly(neutral) were found to be 531, 500 and 455 nm, respectively. The broad feature was observed in both drop-casted and polymeric forms, suggesting the aggregation of phenazine core structure.

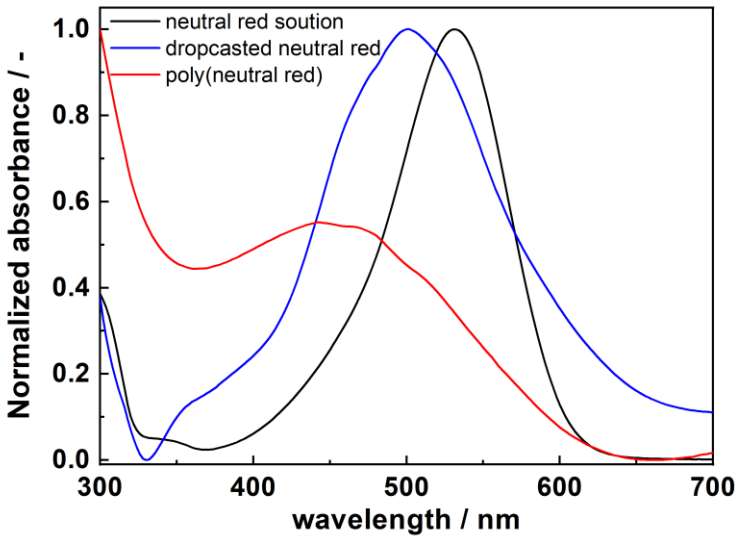


**Figure 35.** UV/Vis absorbance spectra of neutral red aqueous solution (black solid line), drop-casted neutral red on a transparent Cr/Au coated glass (blue solid line) and poly(neutral red) coated on a transparent Cr/Au coated glass (red solid line).

### 3.1.1.2. Chitosan coated carbon felt

The chitosan modified carbon felt electrode was prepared by covalently bound chitosan biopolymer onto carbon-based electrode surface (**Scheme 9**). Firstly, a carbon felt was oxidized under strong acid condition of concentrated $HNO_3$, yielding random oxygen-containing functional groups including hydroxyl and carboxylic acid groups, as shown in the first step. The obtained carboxylic acid groups were then activated using EDC and NHS as coupling reagents. This activation leads to *o*-acylisourea unstable intermediate (carbon felt-EDC intermediate) which couple with NHS, resulting amine-reactive ester (carbon felt-NHS). The resulting ester allows efficient conjugation to primary amine groups of chitosan, yielding chitosan modified carbon felt.

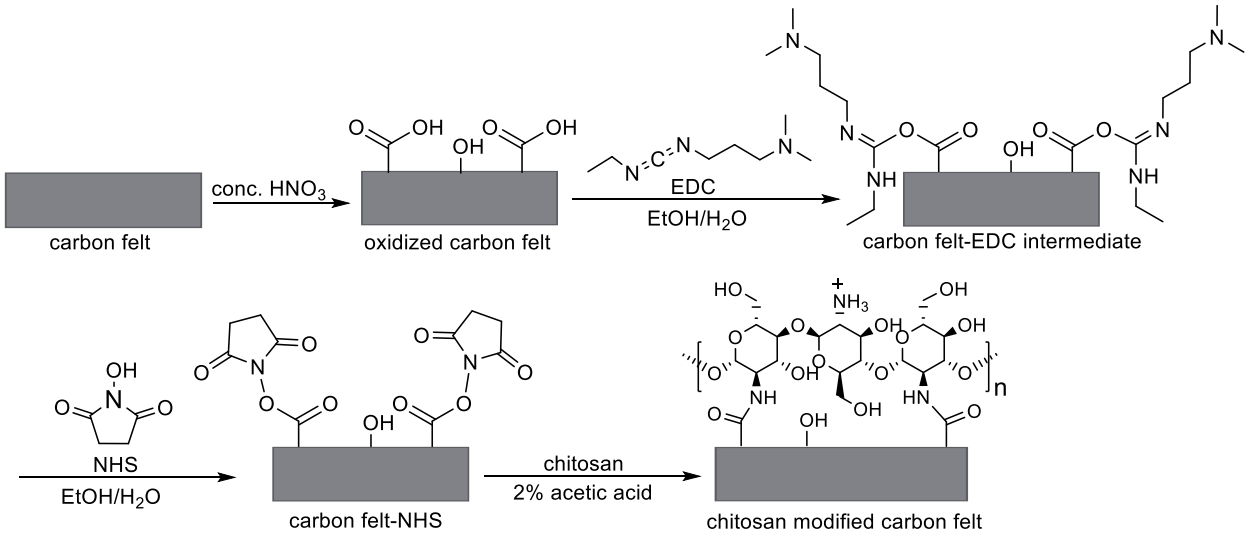


**Scheme 9.** Preparation of chitosan modified carbon felt electrode.

The chitosan modified carbon felt was allowed to dry at ambient temperature overnight. SEM images of dried sample were taken, as shown in **Figure 36**. The images reveal homogeneous-covered chitosan film coated onto the surface of carbon felt.

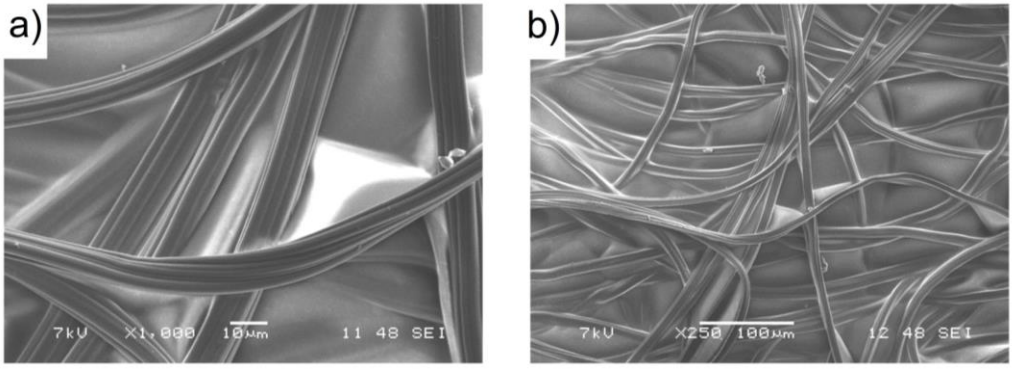


**Figure 36.** SEM images of chitosan modified carbon felt electrode with the scale bar of (a) 10 µm and (b) 100 µm.

### 3.1.2. Microbial electrochemical reduction of $CO_2$ to formate

*M. extorquens* biocathodes were prepared in two-compartment electrochemical cell having a carbon felt, a Ag/AgCl and a Pt plate as working, reference and counter electrodes, respectively. In the cathodic chamber, the electrolyte solution contained 10% of *M. extroquens* inoculum (**Figure 37a**) in medium which was suitable for microorganism growth. While the anodic solution was 0.2 M phosphate buffer solution pH 7.0. The cathodic compartment was kept under anaerobic condition by saturating with $CO_2$. The adaptation was carried out by controlling a potential of -0.75 V vs Ag/AgCl for 4 weeks. After that, the pinkish biofilm of *M. extorquens* was observed on the carbon felt electrode, as shown in **Figure 37b** and **c**.

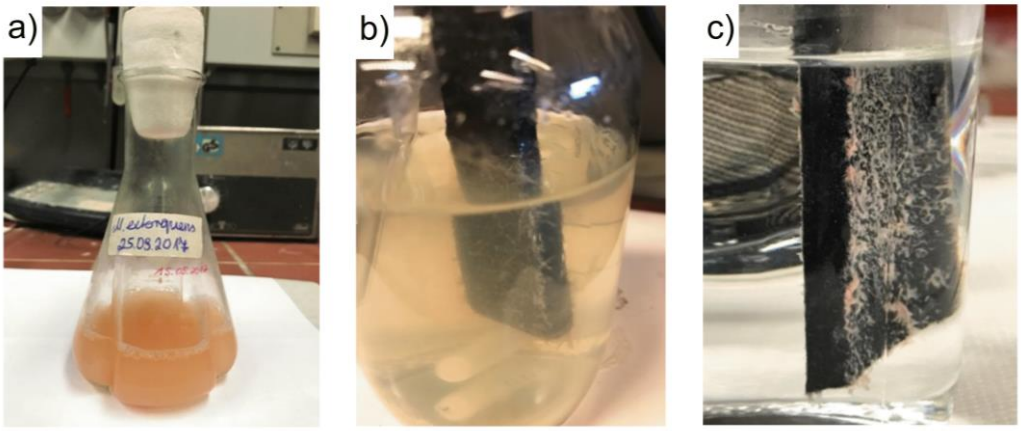


**Figure 37.** Photos of a) *M. extorquens* inoculum and biofilm formation after 4-week adaptation on b) a bare carbon felt electrode in the medium and c) the poly(neutral red) modified carbon felt electrode in phosphate buffer solution.

During the adaptation period, headspace samples were taken from the cathodic compartment and were analyzed using a gas injection gas chromatograph. The analytic results revealed $H_2$ formation as the only observed product. The accumulated amount of produced $H_2$ was plotted over the adaptation time (**Figure 38**). Since the chamber was purged once a week with $CO_2$ (marked with arrows), the accumulation of $H_2$ production was plotted accordingly. The plot revealed continuous $H_2$ production. The highest production rate of 0.9-1.0 $mmol \cdot day^{-1}$ was observed in the first day directly after flushing the chamber with $CO_2$. However, a decrease in the accumulated amount of $H_2$ after the third day of each purging cycle might be because the $H_2$ was

utilized by microorganisms themselves as their sole electron donor as described in the reductive acetyl-CoA pathway.[150] Furthermore, electrical charges (Q) consumed in the system were plotted over time. **Figure 38** shows constant electrons consumption over the period. Additionally, the linear fitting of accumulated charge data was introduced, and the fitting curves were presented as red dashed-lines. From the linear fitting, the slopes of the curve referred to charge consumption rates which were found of 170-420 $C \cdot day^{-1}$. Moreover, charge consumption was considerably lower after 14 days of adaptation while $H_2$ formation remained stable. These showed more efficient electrochemical-assisted $H_2$ production. Further, Faradaic efficiencies of $H_2$ production in the first day of the cycle were calculated and found to be in the range of 35-98%.

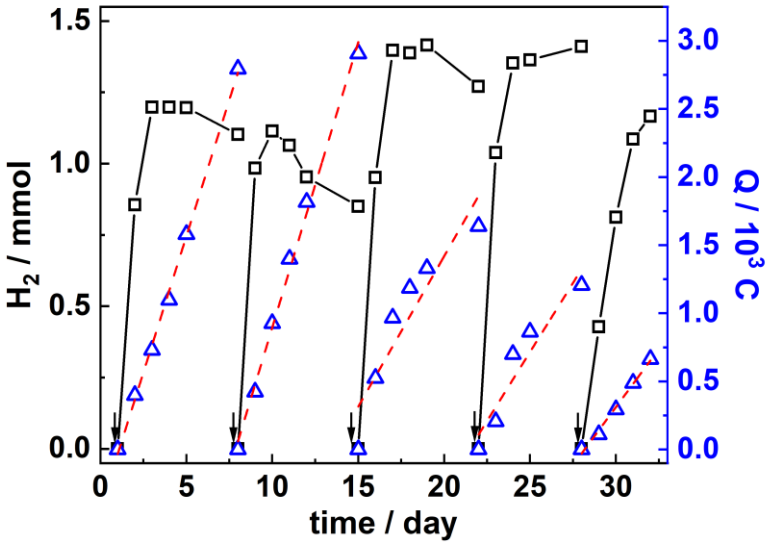


**Figure 38.** Plots of produced $H_2$ (black square) and consumed electrical charges (blue triangle) over adaptation time. Arrows indicate $CO_2$ purging in the cathodic chamber. Red dashed line shows linear fitting curves of accumulated charges.

Since the aim of this study is to investigate the effect of neutral red as a redox mediator in both homogeneous and heterogeneous approaches, the biocathodes equipped in all three MECs were prepared with the similar manner as mentioned previously. After one-month adaptation, the biofilm formation was observed on the electrodes (**Figure 37b** and **c**). The biocathodes were cut into small pieces and allowed to dry under ambient conditions. **Figure 39** shows a photo comparing two biocathodes prepared from a bare carbon felt (**Figure 39a**) and poly(neutral red) modified carbon felt (**Figure 39b**) electrodes. The closer looks were further examined using optical (**Figure 40**) and scanning electron microscope (**Figure 41**). The photo and optical microscopic images presented the pink-pigmented biofilm which is a physical character of methylobacterium. Additionally, SEM images showed that biofilms consisted of rod-shaped cells, confirming the formation of *M. extorquens* biofilm. Moreover, more pinkish biofilm was observed covered the modified electrode, suggesting that poly(neutral red) modified electrode enhanced biofilm growth.

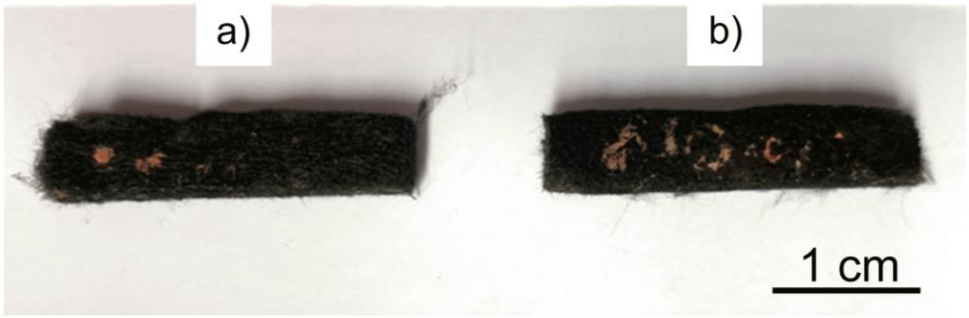


**Figure 39.** A photo of a) the dried bare carbon felt with the biofilm and b) the dried poly(neutral red) modified carbon felt with the biofilm.

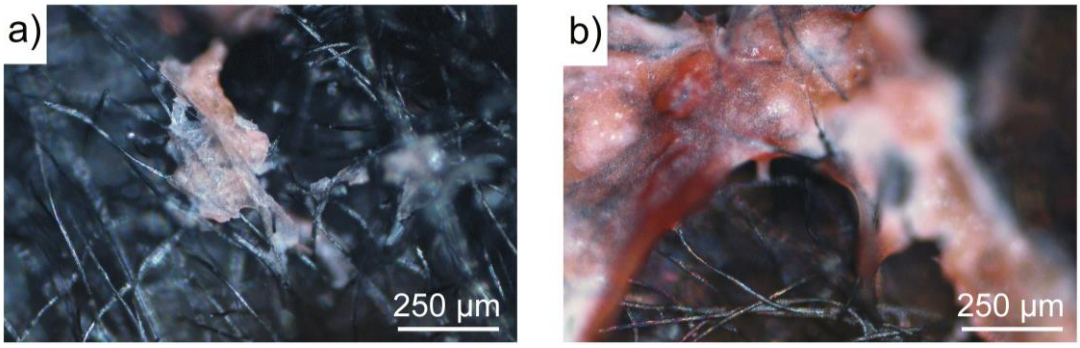


**Figure 40.** Optical microscopic images of a) the dried bare carbon felt with the biofilm and b) the dried poly(neutral red) modified carbon felt with the biofilm. Scale bar is of 250 µm.

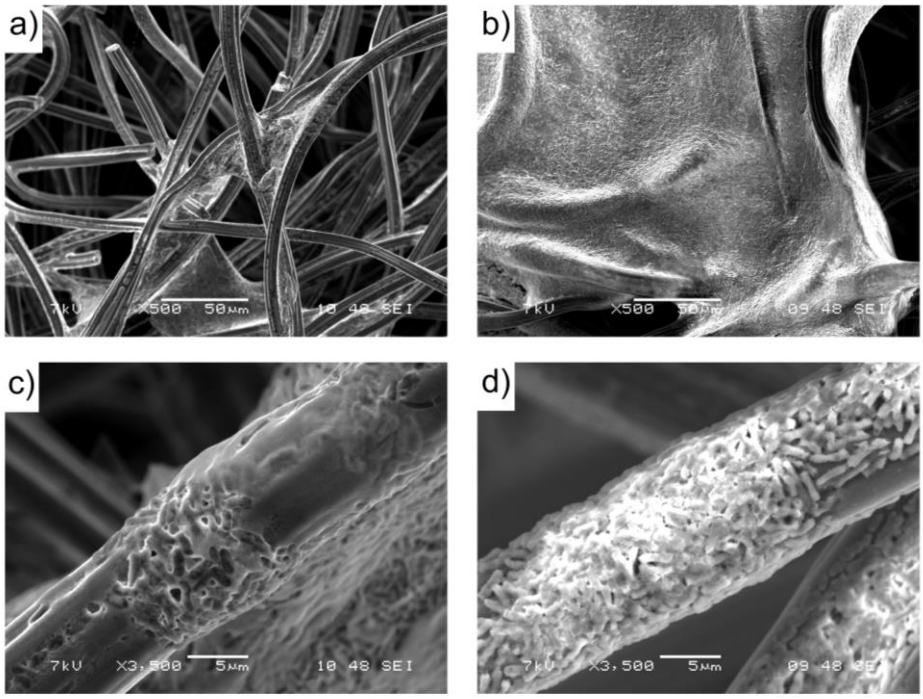


**Figure 41.** SEM images of a) and c) the bare carbon felt with the biofilm and b) and d) the poly(neutral red) modified carbon felt with the biofilm. Scale bars are of 50 µm (for a) and b)) and 5 µm (for c) and d).

Since the carbon felt is a sponge like electrode, the electrolyte was easily adsorbed inside the electrode. Therefore, after the adaptation period, the electrodes were placed in 0.2 M phosphate buffer solution pH 7.0 to remove the remaining medium. Then, the prepared biofilm coated carbon

felt electrodes were equipped in the two-compartment electrochemical systems where both cathodic and anodic electrolytes were freshly prepared 0.2 M phosphate buffer solution pH 7.0, while in **MEC 2**, the catholyte contained 50 µM neutral red, as shown in **Figure 42**. All MECs were characterized electrochemically by means of cyclic voltammetry. **Figure 43** presents cyclic voltammograms of all MECs recorded under $N_2$- (blue) and $CO_2$- (red) saturated conditions with a scan rate of 1 $mV \cdot s^{-1}$. The graphs revealed an increase in the reductive current in the present of $CO_2$, as compared to $N_2$-saturated condition, suggesting electrocatalytic activities toward $CO_2$ reduction. Additionally, reductive currents observed in **MEC 2** and **3**, were found to be higher than those of **MEC 1**, indicating enhanced electron transfer facilitated by neutral red and poly(neutral red), respectively. The reduction peaks observed around -0.3 V were corresponded to neutral red monomer.


**Figure 42.** A photo of **MEC 2** containing 50 µM neutral red in cathodic electrolyte solution

All three MECs were investigated their long-term catalytic performances towards $CO_2$ reduction by monitoring product formation while a potential of -0.75 V vs Ag/AgCl was applied constantly. The cathodic chambers were kept under $CO_2$-saturated condition by purging with $CO_2$ every 2 days and the electrolyte solutions in both chambers were refreshed every 3-4 weeks, labelled as running cycles. In case of **MEC 2**, the fresh catholyte contained dissolved neutral red with a concentration of 50 µM. The electrolysis was carried out for 82 days (three running cycles). During the electrolysis, headspace and liquid samples were taken from cathodic chambers and analyzed using ion and gas chromatographs, respectively. The analytic results revealed that formate was the only product observed in the systems.

The accumulated formate formation found in all MECs was plotted over the running time together with accumulated consumed charges, as shown in **Figure 43**. The data were fitted linearly (shown as dashed lines), revealing trends of production and consumption rates of each running cycles, while the rates of overall running period were calculated by dividing of overall production/consumption with overall running days (82 days). The data including total formate formation, consumed electrical charges, formation rates, charge consumption rates and average Faradaic efficiencies, were summarized in **Table 12**.

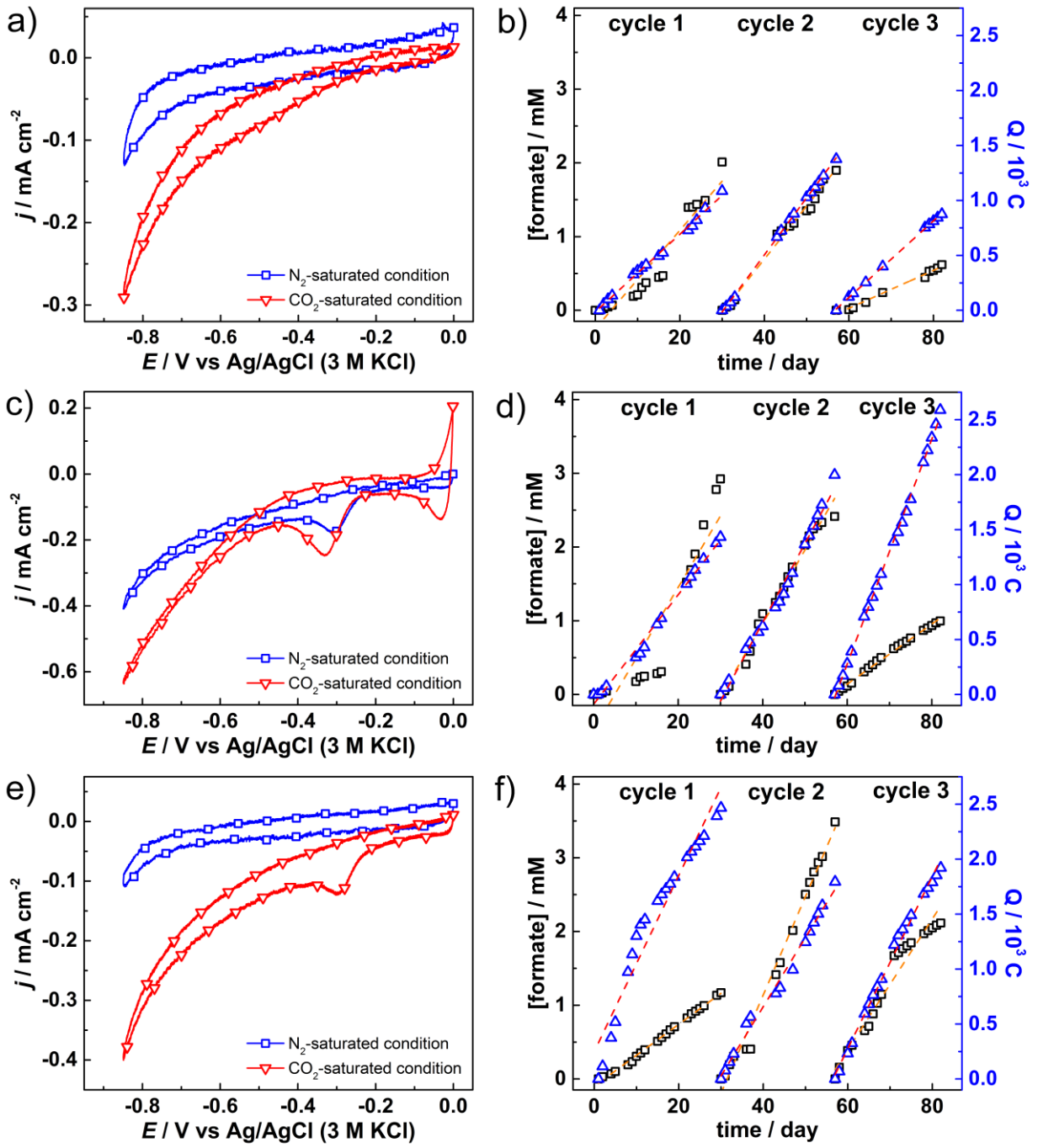


**Figure 43.** Cyclic voltammograms recorded at potentials between 0 to -0.85 V vs Ag/AgCl with a scan rate of 1 mV·s$^{-1}$ in 0.2 M phosphate buffer solution pH 7.0 under $N_2$- (blue solid line) and $CO_2$- (red solid line) saturated conditions (a, c and e) and plot of accumulated formate formation (black square) and consumed electrical charges (blue triangle) (b, d and f) for **MEC 1**, **2** and **3**, respectively.

Formate formation in **MEC 1** was found to be stable in the first two cycles with the production rate of 70 μM·day$^{-1}$ and the accumulated formate of 2.0 and 1.9 μM. The production rate decreased significantly to 30 μM·day$^{-1}$ in the third cycle. The Faradaic efficiencies decreased slowly as longer experiments running. In **MEC 2**, formate formation reached 2.9, 2.4 and 1.0 mM, corresponding to the production rates of 100, 100 and 40 μM·day$^{-1}$ in cycle 1, 2 and 3, respectively. While electrical charges tended to increase constantly over the running cycles with the rates of 50, 70 and 100 C·day$^{-1}$. The corresponding Faradaic efficiencies were found to be 8% in the first cycle and decreased to 5% and 1%, in the second and third cycles, respectively. The **MEC 3** showed an increase in formate formation rate from 40 in the first cycle to 130 μM·day$^{-1}$ in the second cycle but the formation rate was then decreased to 90 μM·day$^{-1}$ in the third cycle. The average Faradaic efficiencies were of 2, 8 and 4% in cycles 1, 2 and 3, respectively. For whole three running cycles, the average formation and consumption rates as well as corresponding Faradaic efficiencies of **MEC 2** and **3**, were higher as compared to **MEC 1**. The observations indicated that adding redox mediator could enhance electron transfer between electrode and microbes, resulting improved performance. Moreover, with the modified electrode, an increase in formate formation was detected. The microscopic results suggested that the poly(neutral red) modified electrode is a good support for *M. extorquens* as better biofilm coverage observed (**Figure 39Figure 41**). This might be attributed to to higher nitrogen to carbon ratio, from amine groups of poly(neutral red) coated onto the electrode, which promotes the adhesion of microorganisms to the electrode.[94,151,152]

However, the system degradation of all three MECs was observed after the second cycle especially in **MEC 2** and **3**. It could be because the media were changed therefore planktonic cells (swimming microorganism) might be gone or could be because of contamination from environment outside the MEC. However, in the real operation, the systems will be run in continuous mode where the medium were slowly circulated. This might lower chances of contamination and loss of bacteria.

The results suggested that the systems were stable in terms of formate formation upto 57 running days. Comparing to the reported study of methylobacterium, the experiment was performed in the presence of methyl viologen as redox mediator and reported only for 80 h electrolysis.[82] Concerning the toxicity of methyl viologen (known as paraquat, a herbicide) as well as instability issues, the introduction of neutral red as redox mediator is of promising. In addition, the introduction of heterogeneous poly(neutral red) offers more practical system where the product simplification is simplified.

| System | Parameter | Cycle 1 (30 days) | Cycle 2 (27 days) | Cycle 3 (25 days) | Overall (82 days) |
|---|---|---|---|---|---|
| **MEC 1** | [formate] / mM | 2.0 | 1.9 | 0.6 | 4.5 |
| | Q / C | 1090 | 1380 | 875 | 3345 |
| | formate production rate / $\mu M \cdot day^{-1}$ | 70 | 70 | 30 | 55 |
| | Q rate / $C \cdot day^{-1}$ | 35 | 50 | 30 | 40 |
| | average %FE | 3 | 2 | 1 | 2 |
| **MEC 2** | [formate] / mM | 2.9 | 2.4 | 1.0 | 6.3 |
| | Q / C | 1430 | 2000 | 2590 | 6020 |
| | formate production rate / $\mu M \cdot day^{-1}$ | 100 | 100 | 40 | 80 |
| | Q rate / $C \cdot day^{-1}$ | 50 | 70 | 100 | 70 |
| | average %FE | 8 | 5 | 1 | 4 |
| **MEC 3** | [formate] / mM | 1.2 | 3.5 | 2.1 | 6.8 |
| | Q / C | 2470 | 1790 | 1920 | 6180 |
| | formate production rate / $\mu M \cdot day^{-1}$ | 40 | 130 | 90 | 80 |
| | Q rate / $C \cdot day^{-1}$ | 80 | 60 | 80 | 75 |
| | average %FE | 2 | 8 | 4 | 4 |

**Table 12.** Comparison of total formate formation, accumulated consumed charges (Q), formate production rate, charge consumption rate and averaged Faradaic efficiencies of the **MEC 1**, **2**, and **3** in each running cycle.

As the results revealed that the performance of the systems was enhanced in the presence of neutral red. However, the mechanism of neutral red assisted electron transfer is not clear. One of the proposed mechanisms is shown in **Scheme 10**. In the neutral aqueous solution, neutral red is in its neutral form (NR). While applying a constant potential of -0.75 V, NR will be reduced electrochemically to its oxidized form ($NRH_2$) ($E^{0'}$ of $NRH_2/NRH^+$ is of -0.53 V vs Ag/AgCl).[63] The resulting $NRH_2$ can diffuse into a microbial cell and transfer electrons for the reduction of $NAD^+$ back to NADH ($E^{0'}$ of $NAD^+$/NADH is of -0.525 V vs Ag/AgCl) which is an important cofactor for $CO_2$ conversion to formate, catalyzed by formate dehydrogenase ($F_{ate}DH$) locating inside the cell.

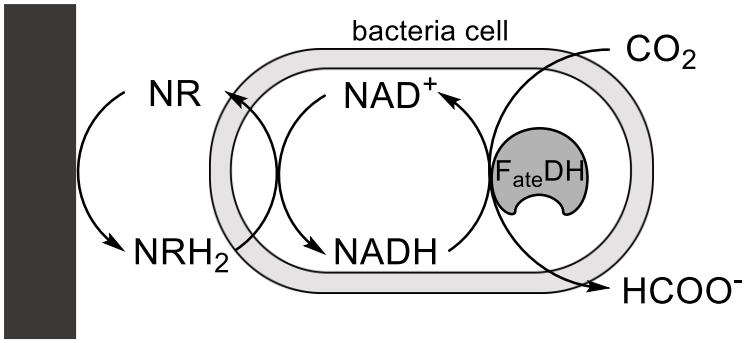


**Scheme 10.** Proposed mechanism of neutral red-assisted electron transfer to a microbial cell.

### 3.1.3. Microbial electrochemical reduction of $CO_2$ to $CH_4$

To investigate the microbial electrochemical conversion of $CO_2$ to $CH_4$ in **MEC 4**, the biocathode was prepared by adaptation in Cheng's medium[71] containing mixed culture inoculum (from sewage sludge) by applying a constant potential at -0.80 V vs Ag/AgCl under $CO_2$-satuared condition for 4 weeks. In the first 2 weeks, glucose was added into the cathodic solution to ensure enough biomass and the compartment was then purged with $CO_2$ once a week for 2 weeks. The other 2 weeks, only $CO_2$ purging was done once a week. During this adaptation period, headspace samples of cathode chamber were taken and analyzed using a gas chromatograph. **Figure 44** exhibits gas chromatograms of the headspace samples taken after 1 day, 3 weeks and after 4 weeks of the adaptation period. At the retention time around 5 min, a peak of $CH_4$ was observed after 3 weeks of microbial adaptation while $H_2$ amount decreased as more adaptation, suggesting adaptation of methanogens for electro-methanogenesis.

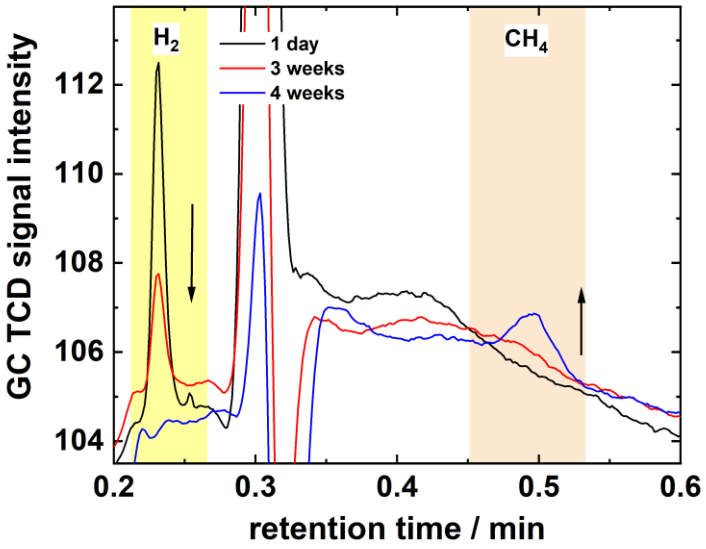


**Figure 44.** Headspace analysis of headspace samples taken from cathode chamber during adaptation period.

After 4 weeks of adaptation, the biofilm was observed on carbon felt electrodes. The electrolyte solutions were replaced with freshly prepared solutions. The long-term electrochemical reduction was performed under $CO_2$-saturated condition by applying a constant potential of -0.80 V vs Ag/AgCl. The electrolyte solutions were replaced every 4 weeks, defined as a running cycle. To monitor the reaction, headspace sample was taken twice a week and immediately after sampling, cathode chamber was flushed with $CO_2$. **Figure 45** reveals accumulated $CH_4$ production and accumulated consumed electrical charges over time. In this first cycle, most of the $CH_4$ production was observed in the first 14 day while the electrical charge was consumed linearly. In the second cycle, $CH_4$ production was more linear than the first cycle and went along with charge consumption. However, the $CH_4$ production was lower, as compared to that of cycle 1. The saturation of methane production might due to depletion of substrate. As summarized in **Table 13**, $CH_4$ production rates were of 4 and 3 $\mu mol \cdot day^{-1}$ in cycle 1 and 2, respectively, while charge consumption rates were of 50 and 20 $C \cdot day^{-1}$ in cycle 1 and 2, respectively. The corresponding Faradaic efficiencies for $CO_2$ reduction towards $CH_4$ production were found to be 7, 12 and 8%, in cycle 1, 2 and whole period, respectively.

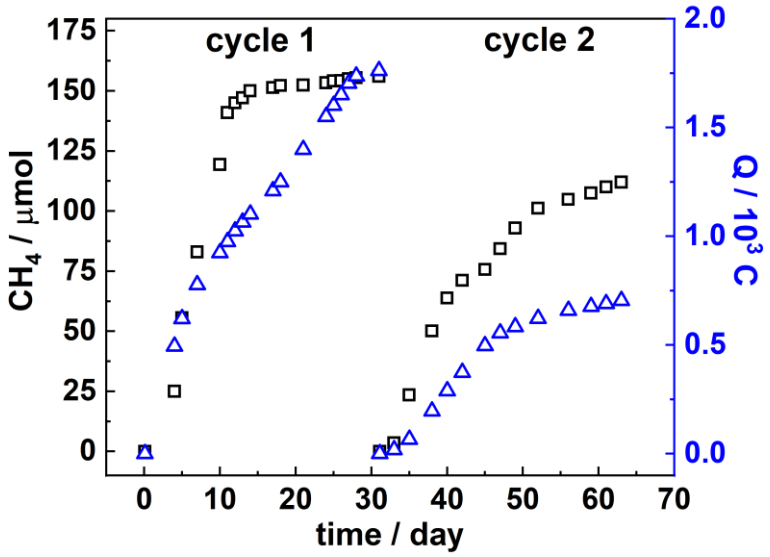


**Figure 45.** Plot of accumulated $CH_4$ production (black square) and consumed electrical charges (blue triangle) over time.

| Parameter | Cycle 1 (31 days) | Cycle 2 (32 days) | Overall (63 days) |
|---|---|---|---|
| $CH_4$ / µmol | 160 | 110 | 270 |
| Q / C | 1760 | 700 | 2460 |
| $CH_4$ production rate / µmol·day$^{-1}$ | 4 | 3 | 4 |
| Q rate / C·day$^{-1}$ | 50 | 20 | 40 |
| average %FE | 7 | 12 | 8 |

**Table 13.** Summarization of **MEC 4**.

### 3.1.4. Bio-electrochemical systems for dual applications

In this section, the microbial electrolysis systems where cathode and anode were bioelectrodes, were investigated their performances toward organic substances degradation and $CH_4$ production. In the anode chamber, organic compounds such as glucose and acetate, were degraded by exoelectrogens which then gave back electrons to the electrochemical system. The electrons and protons from oxidation were utilized by microorganisms at the biocathode to reduce $CO_2$ to $CH_4$. The microbial electrolysis systems were developed in a two-compartment electrochemical cell where the two chambers were separated by a proton exchange membrane, allowing proton transfer. Carbon felt electrodes were used as working and counter electrodes. Both bioanode and biocathode were prepared in Cheng's medium containing mix cultured inoculum from sewage sludge by controlling at a potential of 0.40 V vs Ag/AgCl under anaerobic conditions for 4 weeks. The anodic potential was chosen instead of cathode potential due to the system instability which was observed in **MEC 4**. This might be because high negative potential could affect membrane-bound proteins of microorganisms.

The anodic chamber was fed constantly with synthetic wastewater consisting of glucose, acetate, yeast extract and tryptone. While only glucose was used in the cathodic chamber to ensure

enough biomass in the first two weeks of adaptation and then only $CO_2$ was supplied to the compartment. In this period, the systems were fed once a week and the cathodic and anodic chambers were purged with $CO_2$ and $N_2$, respectively, in order to achieve suitable anaerobic condition.

As shown in the previous section, the enhanced microbial electrocatalytic performance was observed when the carbon felt electrode was modified. Further investigation on electrode modification was carried out in the mix cultured microbial systems. Two modifications were chosen including poly(neutral red) and chitosan modified carbon felt electrodes. The bioelectrodes of modified carbon felt were prepared with a same manner as bare carbon felt ones. The microbial systems equipped with the biofilms coated on bare carbon felts, poly(neutral red) modified carbon felts and chitosan modified carbon felts were defined later as **BES 1**, **2** and **3**, respectively.

Long-term experiments of all BESs were carried out in a batch mode by applying a constant potential of 0.40 V vs Ag/AgCl and the reactions was monitored by COD and headspace analysis. The systems were fed twice a week by refreshing half of andic solution with freshly prepared Cheng's medium containing synthetic wastewater (COD of around 600 $mg \cdot L^{-1}$) and flushing the anodic chamber with $N_2$, while flushing the cathodic chamber with $CO_2$. Further, 90% of cathodic solution was replaced with freshly prepared Cheng's medium every 4 weeks assigned as running cycles. The anodic liquid samplings and cathodic headspace samplings were done twice a week before feeding for COD and $CH_4$ quantification, respectively.

#### 3.1.4.1. BES 1

Long-term analysis of **BES 1** was shown in **Figure 46**. The plots present accumulated $CH_4$ production at the cathode and COD removal at the anode together with electrical charges passed through the system over time. The experiments were performed in three cycles (in total of 91 days). The dashed lines of linearly data fitting were also presented showing the consumption/production rates. The results were summarized in **Table 14**. The increased $CH_4$ production was observed from the rate of 25 $\mu mol \cdot day^{-1}$ in the first cycle to 40 and 60 $\mu mol \cdot day^{-1}$ in the second and third cycles, respectively. The average COD removal efficiencies were of 25, 52 and 55% in cycle 1, 2 and 3, respectively. The corresponding Faradaic efficiencies towards $CH_4$ production were found to be 39, 29 and 38% in cycle 1, 2 and 3, respectively. The results revealed gradual improvement in oxidation and reduction efficiencies over the cycles, suggesting gradual adaptation of microorganisms to the working conditions. Comparing to **MEC 4** system where negative potential was applied at biocathode and abiotic anode was employed, **BES 1** presented continuous $CH_4$ production in each cycle and increased production over cycles with relatively higher charge passing through. The results reflected higher stability of the systems and higher performance which might result from controlled positive potential at the anode and supplied electrons from oxidation.

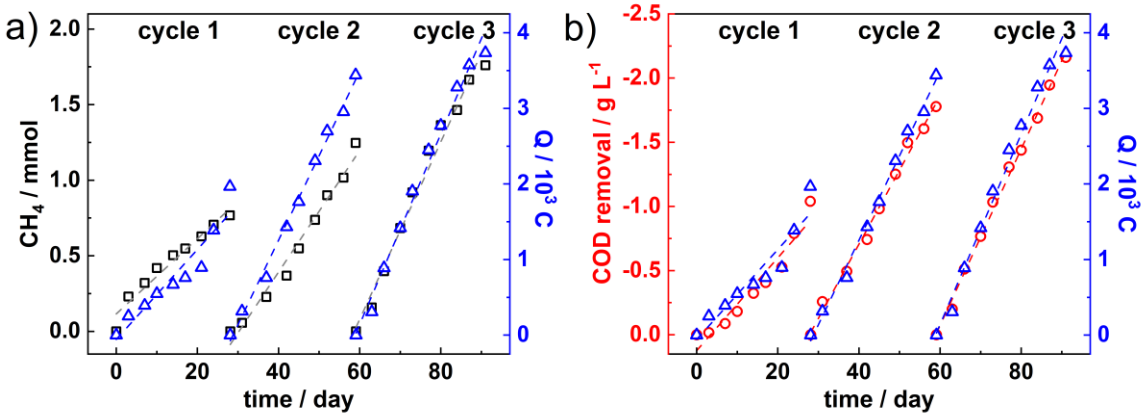


**Figure 46.** Plots of a) accumulated $CH_4$ production and b) accumulated COD removal together with accumulated charges passes through **BES 1** over running time.

| Parameter | Cycle 1 (28 days) | Cycle 2 (31 days) | Cycle 3 (32 days) | Overall (91 days) |
|---|---|---|---|---|
| $CH_4$ production / mmol | 0.8 | 1.2 | 1.8 | 3.8 |
| Q / C | 1970 | 3440 | 3735 | 9140 |
| COD removal / $g \cdot L^{-1}$ | 1.0 | 1.8 | 2.2 | 5.0 |
| $CH_4$ production rate / $\mu mol \cdot day^{-1}$ | 25 | 40 | 60 | 40 |
| Q rate / $C \cdot day^{-1}$ | 60 | 110 | 130 | 100 |
| COD removal rate / $mg \cdot L^{-1} \cdot day^{-1}$ | 40 | 60 | 70 | 55 |
| average %FE | 39% | 29% | 38% | 36% |
| Average %COD removal | 25% | 52% | 55% | 44% |

**Table 14.** Summarization of **BES 1**.

#### 3.1.4.2. BES 2

In the **BES 2**, the biofilms grew on the poly(neutral red) modified carbon felt electrodes. After the adaptation period, the long-term performance was investigated by monitoring the COD removal and $CH_4$ production at constant applied potential of 0.40 V vs Ag/AgCl. The accumulated produced $CH_4$ amount, accumulated charges and accumulated COD removal were plotted together over time, as shown in **Figure 47**. The experiment was carried out for 92 days divided into three running cycles. The summarized results were presented in **Table 15**. The $CH_4$ production rate declined gradually from 90 $\mu mol \cdot day^{-1}$ in the first cycle to 80 and 70 $\mu mol \cdot day^{-1}$ in the second and third cycles, respectively. While the COD removal rates increased significantly from 55 $mg \cdot L^{-1} \cdot day^{-1}$ in the first cycle to 85 $mg \cdot L^{-1} \cdot day^{-1}$ in the second cycle and then decreased slightly to 80 $mg \cdot L^{-1} \cdot day^{-1}$ in the third cycle. Similarly, electrical charge consumption rate was found to be 110 $C \cdot day^{-1}$ in the first cycle, then increased to 150 $C \cdot day^{-1}$ in the second cycle and decreased to 140 $C \cdot day^{-1}$ in the last cycle. The COD removal efficiencies were found to be 52, 67 and 72% in cycle 1, 2 and 3, respectively, while the corresponding Faradaic efficiencies were of 66, 47 and 44%.

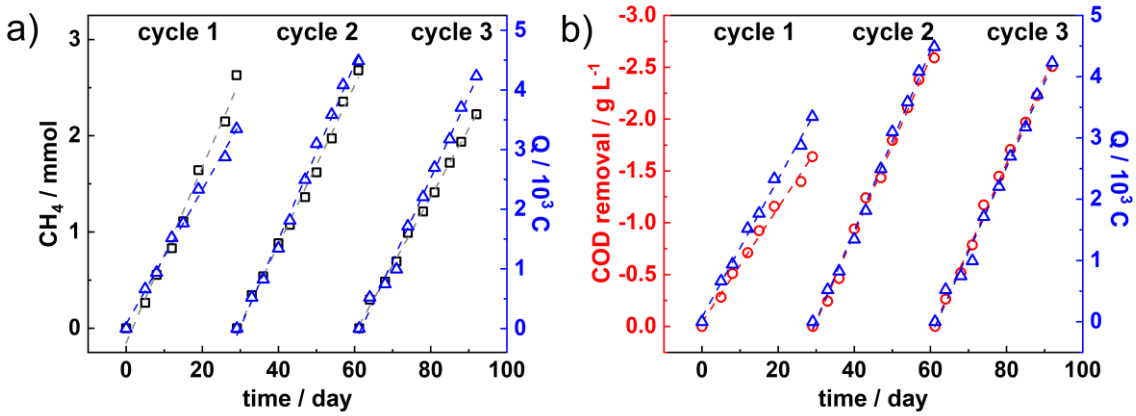


**Figure 47.** Plots of a) accumulated $CH_4$ production and b) accumulated COD removal together with accumulated charges passes through **BES 2** over running time.

| Parameter | Cycle 1 (29 days) | Cycle 2 (32 days) | Cycle 3 (31 days) | Overall (92 days) |
|---|---|---|---|---|
| $CH_4$ production / mmol | 2.6 | 2.7 | 2.2 | 7.5 |
| Q / C | 3350 | 4490 | 4230 | 12070 |
| COD removal / $g \cdot L^{-1}$ | 1.6 | 2.6 | 2.5 | 6.7 |
| $CH_4$ production rate / $\mu mol \cdot day^{-1}$ | 90 | 80 | 70 | 80 |
| Q rate / $C \cdot day^{-1}$ | 110 | 150 | 140 | 130 |
| COD removal rate / $mg \cdot L^{-1} \cdot day^{-1}$ | 55 | 85 | 80 | 70 |
| average %FE | 66% | 47% | 44% | 51% |
| Average %COD removal | 52% | 67% | 72% | 65% |

**Table 15.** Summarization of **BES 2**.

#### 3.1.4.3. BES 3

In **BES 3**, microbial electrodes were prepared using chitosan-modified carbon felt electrodes. While applying a constant potential of 0.40 V vs Ag/AgCl, the performance was monitored by COD removal and $CH_4$ production analysis. In **Figure 48**, accumulated $CH_4$ production, electrical charge consumption and COD degradation were plotted over time in three running cycles for 91 days. In each running cycle, linear curves present linearly data fitting, suggesting rates of those. The results were summarized in **Table 16**. The $CH_4$ production rate increased from 90 $\mu mol \cdot day^{-1}$ in the first cycle to 110 $\mu mol \cdot day^{-1}$ in the second cycle and then dropped significantly to 60 $\mu mol \cdot day^{-1}$ in the last cycle. While, the COD removal rate of the first cycle was of 65 $mg \cdot L^{-1} \cdot day^{-1}$. The removal rates raised up by 15 and 5 $mg \cdot L^{-1} \cdot day^{-1}$ in cycle 2 and 3, respectively. The charge consumption rates were found to be 130, 110 and 140 $C \cdot day^{-1}$ in cycle 1, 2 and 3, respectively. The average removal efficiencies were calculated to be 56, 73 and 71%, in cycle 1, 2 and 3, respectively, while those of Faradaic efficiencies were of 57, 72, 36%, respectively.

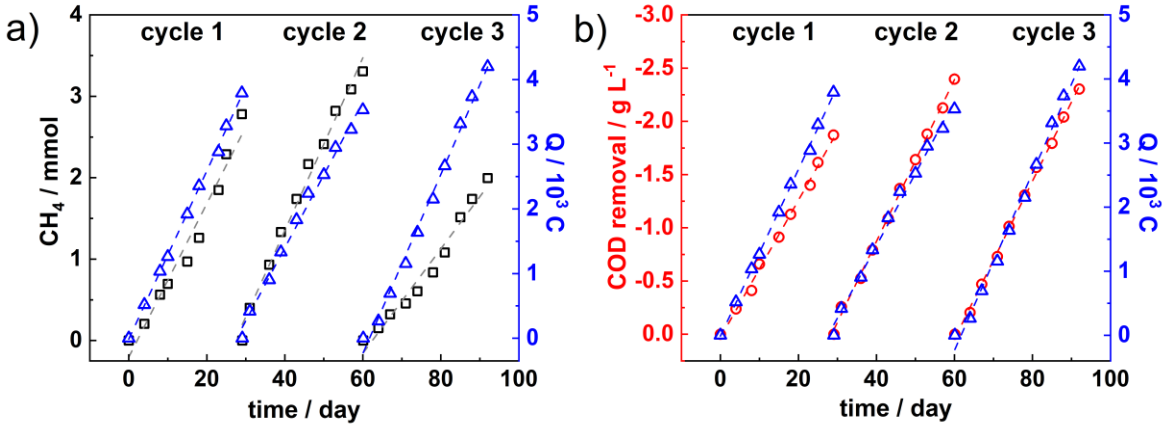


**Figure 48.** Plots of a) accumulated $CH_4$ production and b) accumulated COD removal together with accumulated charges passes through **BES 3** over running time.

| Parameter | Cycle 1 (29 days) | Cycle 2 (31 days) | Cycle 3 (32 days) | Overall (92 days) |
|---|---|---|---|---|
| $CH_4$ production / mmol | 2.8 | 3.3 | 2.0 | 8.1 |
| Q / C | 3790 | 3530 | 4200 | 11520 |
| COD removal / $g \cdot L^{-1}$ | 1.9 | 2.4 | 2.3 | 6.6 |
| $CH_4$ production rate / $\mu mol \cdot day^{-1}$ | 90 | 110 | 60 | 90 |
| Q rate / $C \cdot day^{-1}$ | 130 | 110 | 140 | 125 |
| COD removal rate / $mg \cdot L^{-1} \cdot day^{-1}$ | 65 | 80 | 70 | 70 |
| average %FE | 57% | 72% | 36% | 55% |
| Average %COD removal | 56% | 73% | 71% | 67% |

**Table 16.** Summarization of **BES 3**.

#### 3.1.4.4. Comparison of BES 1, 2 and 3

All parameters including $CH_4$ production, COD removal, charge consumption, production rate, degradation rate, removal efficiency and Faradaic efficiency observed from **BES 1**, **2** and **3** were summarized in **Table 17**. The total $CH_4$ production and overall production rates of modified-electrode-containing systems were around two times higher than those of non-modified system. While charge consumption and its rates in all cycles and whole period of **BES 2** and **3** were higher than those of **BES 1**. Additionally, improved total COD removal and removal rates were observed in **BES 2** and **3**. Accordingly, removal efficiencies and Faradaic efficiencies toward $CO_2$ reduction to $CH_4$ were enhanced. With the modification of carbon felt electrodes using poly(neutral red) and chitosan, the overall performance of microbial electrolysis systems improved. This might be the better adhesion of biofilm on the electrode (observed in **Figure 49** and**Figure 50**) or better electronic communications as suggested previously.[93]

| Parameter | BES 1 | | | | BES 2 | | | | BES 3 | | | |
|---|---|---|---|---|---|---|---|---|---|---|---|---|
| | 1 | 2 | 3 | all | 1 | 2 | 3 | all | 1 | 2 | 3 | all |
| $CH_4$ production / mmol | 0.8 | 1.2 | 1.8 | 3.8 | 2.6 | 2.7 | 2.2 | 7.5 | 2.8 | 3.3 | 2.0 | 8.1 |
| Q / $10^3$ C | 2.0 | 3.4 | 3.7 | 9.1 | 3.3 | 4.5 | 4.2 | 12 | 3.8 | 3.5 | 4.2 | 11.5 |
| COD removal / $g \cdot L^{-1}$ | 1.0 | 1.8 | 2.2 | 5.0 | 1.6 | 2.6 | 2.5 | 6.7 | 1.9 | 2.4 | 2.3 | 6.6 |
| $CH_4$ production rate / $\mu mol \cdot day^{-1}$ | 25 | 40 | 60 | 40 | 90 | 80 | 70 | 80 | 90 | 110 | 60 | 90 |
| Q rate / $C \cdot day^{-1}$ | 60 | 110 | 130 | 100 | 110 | 150 | 140 | 130 | 130 | 110 | 140 | 125 |
| COD removal rate/ $mg \cdot L^{-1} \cdot day^{-1}$ | 40 | 60 | 70 | 55 | 55 | 85 | 80 | 70 | 65 | 80 | 70 | 70 |
| average %FE | 39% | 29% | 38% | 36% | 66% | 47% | 44% | 51% | 57% | 72% | 36% | 55% |
| average %COD removal | 25% | 52% | 55% | 44% | 52% | 67% | 72% | 65% | 56% | 73% | 71% | 67% |

**Table 17.** Comparison of $CH_4$ production, electrical charges, COD removal, their corresponding rate, average Faradaic efficiencies and COD removal efficiency in each running cycle (cycle 1, 2 and 3) and in the whole period of **BES 1**, **2** and **3**.

#### 3.1.4.5. SEM measurements

SEM images of all bioelectrodes were taken as shown in **Figure 49** and **Figure 50**. The bioanodes obtained from modified carbon felts electrodes revealed better coverage and thicker biofilm, as compared to the bioanode developed from a non-modified carbon felt. Additionally, the observed microbial cells were of different shapes, indicating mixed microbial strains. While the SEM images of biocathodes were taken showing microbial colonization growth on the felt electrodes. The chitosan modified carbon felt showed greater biofilm coverage, as compared to the others. From the high magnified images, rod-shaped cells were mainly found coated on fibers, suggesting methanogens as dominant microorganisms.

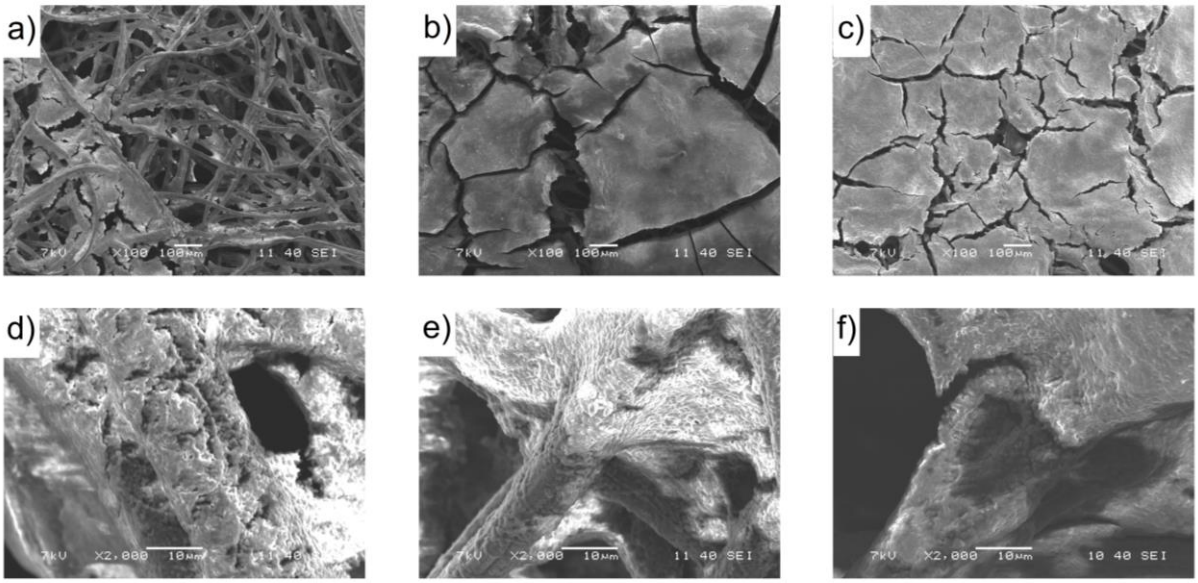


**Figure 49.** SEM images of bioanodes of **BES 1** (a and d), **BES 2** (b and e) and **BES 3** (c and f).

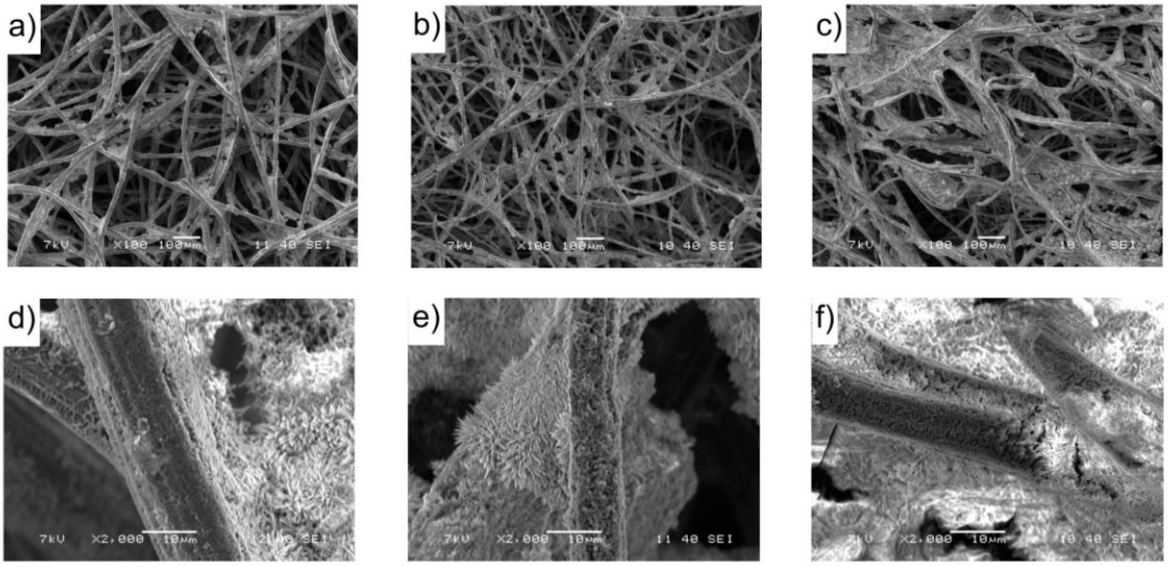


**Figure 50.** SEM images of biocathodes of **BES 1** (a and d), **BES 2** (b and e) and **BES 3** (c and f).

## 3.2. Enzymatic reductions

The results described in this section are published in: *ACS Applied Materials & Interfaces* **2020** *12* (1), 250-259.
DOI: 10.1021/acsami.9b17777
Authors: Hathaichanok Seelajaroen, Aristides Bakandritsos, Michal Otyepka, Radek Zbořil and Niyazi Serdar Sariciftci

In this section, synthesis of three dehydrogenases modified carboxylic acid graphene is being discussed and further their catalytic activities toward chemical and electrochemical reductions are going to be demonstrated.

### 3.2.1. Enzyme-graphene bio-nano catalyst

#### 3.2.1.1. Synthesis

The covalent functionalization of **G-COOH**, received from Dr. Aristides Bakandritsos (from Palacký University Olomouc) with dehydrogenases (DH) was performed through carbodiimide crosslinking chemistry by the conjugation of primary amine groups of enzymes (such as from lysine units). As shown in **Scheme 11**, the carboxylic acid groups were first activated through the coupling reaction of EDC-HCl and sulfo-NHS. In the first step, **G-COOH** reacted with EDC-HCl, yielding acylisourea derivative which is unstable under physiological conditions. Then, this intermediate reacted with water-dialog NHS (sulfo-NHS), forming more stable ester, **G-NHS**. For enzyme conjugation, **G-NHS** was incubated in buffer solution containing dehydrogenase under ambient condition, resulting dehydrogenase-modified graphene, **G-DH**.

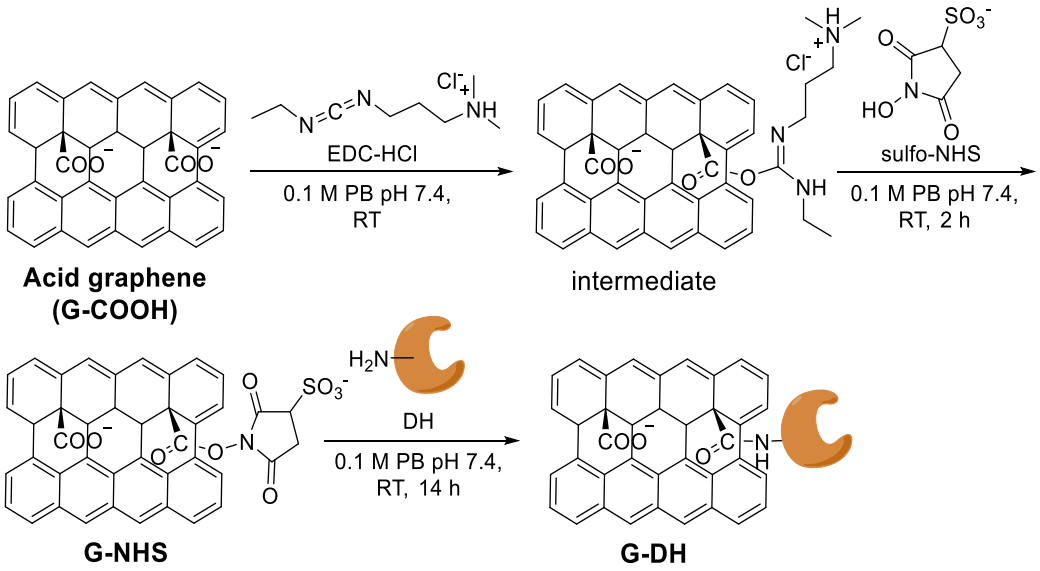


**Scheme 11.** Schematic synthesis of dehydrogenase (DH) functionalized graphene.

Among the three interested dehydrogenases, ADH was chosen for the first attempt due to its high protein contents (321 units·mg$^{-1}$), high Michaelis constant ($K_m$) and maximal reaction rate ($v_{max}$) towards the reduction of aldehydes. Since the covalent conjugation was carried out through primary amine groups (-$NH_2$) contained in proteins namely lysine units. Thus, the conjugation availability could be suggested from the amount and position of lysine units. From the reported study,[153] the yeast ADH (E.C. 1.1.1.1) consisted of 24 lysine units per molecule while the total amino acid units were of 347. Additionally, in the reported crystallography data deposited in the protein data bank, Debye–Waller factor or B-factor values of each atom (except hydrogen atom) were also provided. These values described the attenuation of X-ray or neutron scattering caused by thermal atomic motion, sometimes referred as temperature factor.[154] In protein analysis, these B-factor values were used to identify rigidity or flexibility of the proteins. The higher B-factor values were observed, the more flexible atoms/positions will be. The extracted B-factor values of nitrogen atom in the primary amine positions of lysine units in ADH were plotted over amino acid residue index, as shown in **Figure 51**. Comparing to average B-factor of all atoms (57 Å$^2$),[153] 18 lysine units have higher B-factor, revealing available reaction positions. Moreover, high flexible positions located at the beginning and the end of amino acid chains, which are not at their catalytic sites. Thus, the conjugation at such positions would barely affect to ADH catalytic mechanisms.

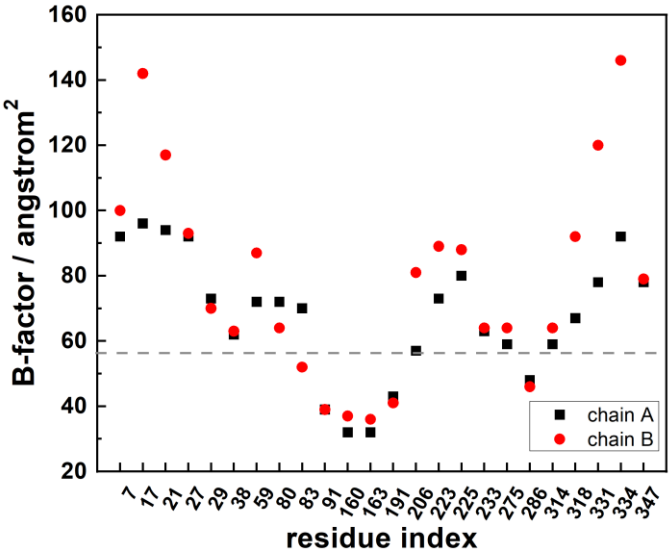


**Figure 51.** Plot of B-factor values over amino acid residue index observed in yeast-ADH.

#### 3.2.1.2. Characterization

After incubation of reactive graphene derivative in ADH solution, unbound ADH was washed off by centrifugal washing with buffer solution, yielding ADH modified **G-COOH**, **G-ADH**. The covalent attachment was confirmed by infrared spectroscopy as shown in **Figure 52a** and **b**. Comparing to the FTIR spectrum of pristine **G-COOH**, the dramatic drop in carboxyl band around 1700 $cm^{-1}$ (band 1) in **G-ADH** was observed. The graph of **G-ADH** also shows a new amide bond at 1660 $cm^{-1}$ (band 2). However, this identification is still complicated with the amide bonds observed in pristine ADH spectrum (band 3) and the bands in the region between 2000 and 1000 $cm^{-1}$ of ADH were not visible completely in spectrum of the **G-ADH**. These observations lead doubts about the successful functionalization. The high-resolution X-ray photoelectron spectroscopy (HR-XPS) analysis was performed by Martin Petr from Palacký University Olomouc with a PHI VersaProbe II (Physical Electronics) spectrometer using an Al Kα source (15 kV, 50 W). The obtained data were evaluated with the MultiPak (Ulvac-PHI, Inc.) software package. The HR-XPS results showed very clearly the characteristic fingerprint of pure ADH imprinted on C1s XPS envelope of the **G-ADH** hybrid (**Figure 52c**). In the C-H region, IR vibrations were observed in **G-ADH**, ascribing to the hydrocarbon chains of the enzyme. Further, the IR spectrum of **G-ADH** shows some characteristic peaks of ADH at 1520 and 1393 $cm^{-1}$ corresponding to the amide II vibration and the $COO^-$ stretching bands, respectively.[155] While observed bands at 1580 and 1210 $cm^{-1}$ (band 4 and 5) originated from aromatic ring stretchings of the graphene's backbone.[156,157]

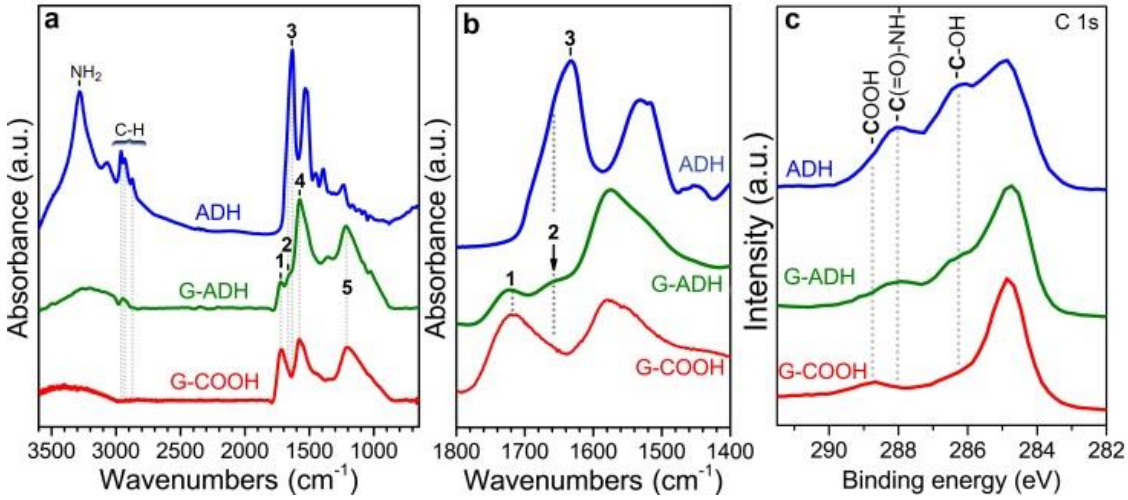


**Figure 52.** FTIR (a and b) and C1s HR-XPS (c) spectra of **G-COOH** (red solid line), **G-ADH** (green solid line) and pure ADH (blue solid line).

Further characterization was performed on thermogravimetric analysis (TGA) by Dr. Juri Ugolotti and Jana Havláková from Palacký University Olomouc with an STA 449 C Jupiter Netzsch Thermo-microbalance at a heating rate of 10°C·min$^{-1}$, under $N_2$ flow in the sample compartment. **Figure 53** shows TGA graphs of pristine **G-COOH** and **G-ADH**. The results revealed increased weight loss starting from around 200°C in **G-ADH** sample. The mass profile reflected the decomposition of protein at around 200-400°C.[158]

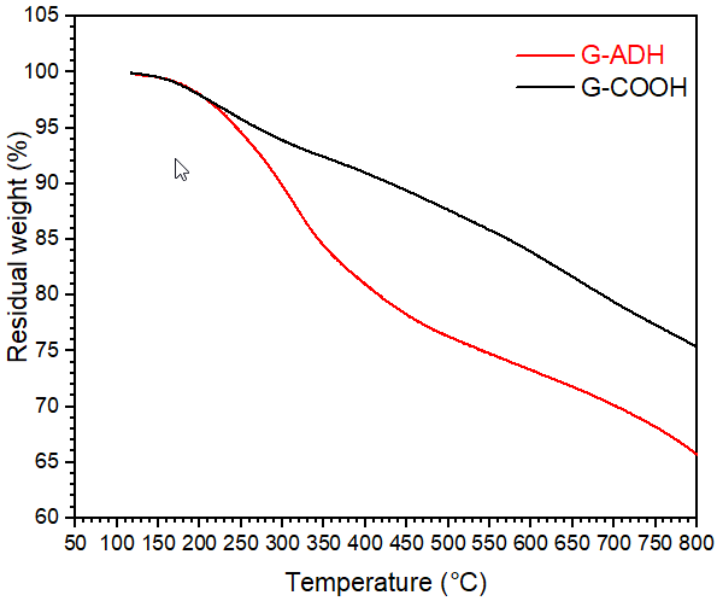


**Figure 53.** Thermogravimetric analysis of the pristine **G-COOH** (black solid line) and **G-ADH** (red solid line).

To investigate the morphology of enzyme-graphene material, transmission electron microscopy (TEM) was carried out with a JEOL-2100 electron microscope by evaporating a drop of the **G-ADH** dispersion in water on a holey carbon coated copper grid, performed by Jana Stráska and Dr. Klara Cepe from Palacký University Olomouc. **Figure 54** presents TEM images of **G-COOH** and **G-ADH**, showing that carboxylic acid graphene appeared to retain fully its morphological features after enzyme functionalization.

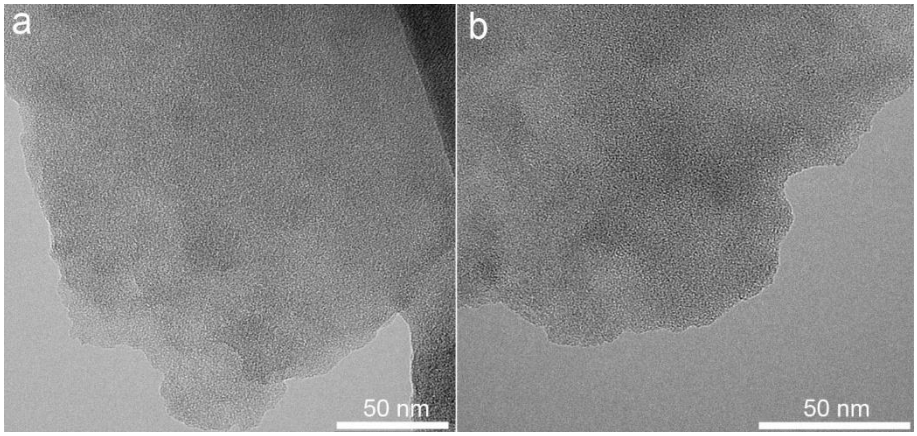


**Figure 54.** TEM images of pristine a) **G-COOH** and b) **G-ADH**.

The amount of ADH conjugated on graphene sheet was determined as protein contents using BCA assay by comparing with standard BSA protein. The amount of ADH was found to be 0.03 mg·mL$^{-1}$ with the graphene concentration of around 1 mg·mL$^{-1}$. The ADH enzymatic assay revealed that **G-ADH** contained 14.6 enzyme unit per mg protein while that of free ADH was found to be 76.2 unit per mg of protein. The results reflected the effect of covalent conjugation which might be because of changes in enzyme morphology/stereochemistry affecting the activity or due to the reduction of mass transfer of reactants to the active site.[159–161]

### 3.2.2. Enzymatic reductions

#### 3.2.2.1. Reduction of acetaldehyde to ethanol using G-ADH

##### 3.2.2.1.a Chemical reduction

**G-ADH** was tested its catalytic activity towards the reduction of acetaldehyde to ethanol using NADH as electrons and protons source. The experiments were carried out in the buffer solution containing prepared **G-ADH**, acetaldehyde and NADH, as catalyst, substrate and cofactor, respectively. **G-ADH** was first mixed with substrate. The reaction was initiated by adding NADH (1 µmol). After 2-h reaction, ethanol analysis using the gas chromatograph revealed the formation of ethanol (0.64 µmol), corresponding to 64% conversion efficiency (**Table 18**, entry 1). Control samples taken from reactions including the reaction without adding catalyst (no ADH or **G-ADH**) as a blank experiment (entry 2), with pristine **G-COOH** (entry 3) and with ADH-adsorbed **G-COOH** (entry 4) were analyzed. The blank and pristine **G-COOH** containing experiments displayed only 2 and 6% efficiency, respectively. The ADH-adsorbed **G-COOH** was prepared by incubation pristine **G-COOH** with ADH for 14 h and then washing non-adsorbed ADH out by centrifugal washing with buffer solution. The introduction of physically ADH-adsorbed **G-COOH** showed only 20% conversion efficiency, revealing that physical adsorption interactions are too weak to keep the enzyme fixed on the graphene surface. Since the immobilization of enzyme in alginate matrix could minimize loss of enzymatic activities from thermal and chemical denaturation/deactivation.[113,160,162,163] **G-ADH** was immobilized in the alginate matrix and further used in the reaction (as a heterogeneous catalysis) showing enhanced acetaldehyde conversion efficiency of 78% (entry 6) relative to **G-ADH** dispersed in the solution. Although the efficiency of **G-ADH** (in both free catalysts and immobilized in alginate beads) were lower than that of the free ADH (entry 5), the covalent conjugation and further hydrogel immobilization offer the advantages of stability and facile product separation.

| Entry | Sample | Ethanol / $\times 10^{-7}$ mol | Conversion efficiency |
|---|---|---|---|
| 1 | **G-ADH** (homogeneous) | 6.4 | 64% |
| 2 | blank | 0.2 | 2% |
| 3 | **G-COOH** (homogeneous) | 0.6 | 6% |
| 4 | **G-COOH**/ADH (homogeneous) | 2.0 | 20% |
| 5 | free ADH (homogeneous) | 9.2 | 92% |
| 6 | **G-ADH** immobilized in alginate beads (heterogeneous) | 7.8 | 78% |

**Table 18.** Chemical conversion efficiencies toward the reduction of acetaldehyde to ethanol using NADH as cofactor during 2-h reaction.

#### 3.2.2.1.b Electrochemical reduction

To proof the concept of electrochemical electron addressing from electrode to enzyme's active sites, **G-ADH** was immobilized in an alginate matrix coated on carbon felt electrode. The resulting carbon felt consisting of **G-ADH** was then used as a working electrode in an electrochemical setup. Cyclic voltammograms of **G-ADH** containing carbon felt electrode were carried out at the potentials between 0 and -1.20 V vs Ag/AgCl with the scan rate of 10 $mV \cdot s^{-1}$ under $N_2$-saturated conditions without acetaldehyde and with acetaldehyde (1 M), as shown in **Figure 55**. The graphs revealed increased reductive current at around -0.80 V in the presence of acetaldehyde, indicating the catalytic activity towards the reduction of acetaldehyde. Further, a comparison of cyclic voltammograms recorded under acetaldehyde containing $N_2$-saturated condition of a bare carbon felt, a carbon felt coated with alginate hydrogel matrix and **G-ADH** immobilized in alginate coated on carbon felt, are presented in **Figure 56**. The graphs displayed high catalytic activity reflected by remarkably enhanced reductive current starting around -0.80 V, as compared to those of bare carbon felt and alginate matrix-coated carbon felt electrodes.

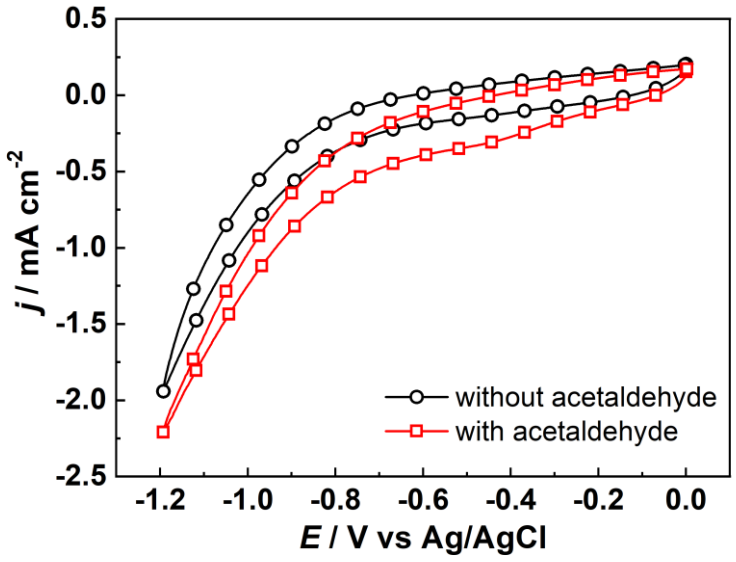


**Figure 55.** Cyclic voltammograms of a **G-ADH** immobilized in alginate coated on carbon felt were recorded in 0.1 M TRIS-HCl solution pH 7.4 in the absence of acetaldehyde (black line) and in the presence of acetaldehyde (1 M, red line) under $N_2$-saturated condition.

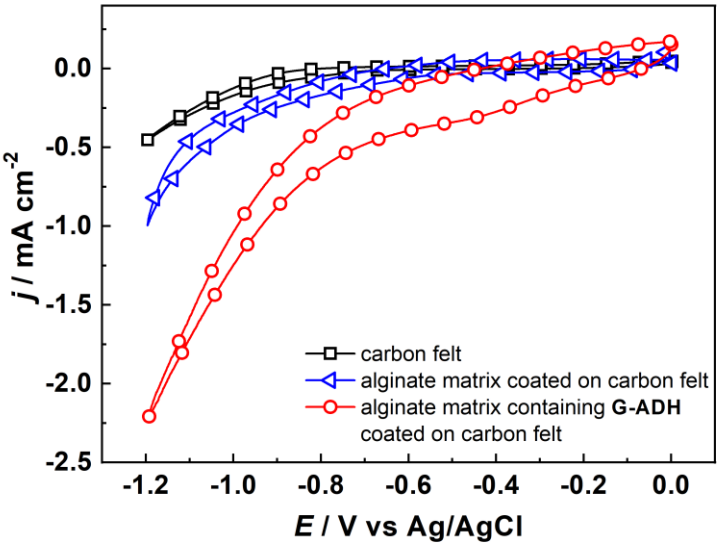


**Figure 56.** Cyclic voltammograms after adding acetaldehyde (1 M), of a bare carbon felt electrode, an alginate matrix coated on carbon felt electrode and a carbon felt electrode modified with alginate hydrogel containing **G-ADH** were recorded in 0.1 M TRIS-HCl buffer solution of pH 7.4 under $N_2$-saturated condition.

To further investigate on the electrochemical reduction of acetaldehyde to ethanol, a constant potential of -1.00 V vs Ag/AgCl was applied continuously for 20 h. The chronoamperogram of the electrolysis was plotted and presented with the plot of accumulated electrical charge over electrolysis time, as shown in **Figure 57**. The reductive current increased from around -0.24 mA at the beginning to around -0.29 mA at around 4 h of reaction and then gradually decreased. At 5 h, the huge drop of current was observed which resulted from mechanical process of sampling and smaller electroactive surface area due to lower amount of working solution. Regardless the huge drop, the reductive current tended to decrease continuously to -0.20 mA at 20 h, as suggested dashed line in **Figure 57**. From the early to 4 h of electrolysis, the slope of the curve was observed to be highest and then decreased gradually over the time. The decline trend showed instability of the system which might due to electrode stability (such as degradation of alginate matrix, enzyme or enzyme-graphene nanohybrid) or limiting of substrate concentration at the electrode surface due to slow diffusion process.

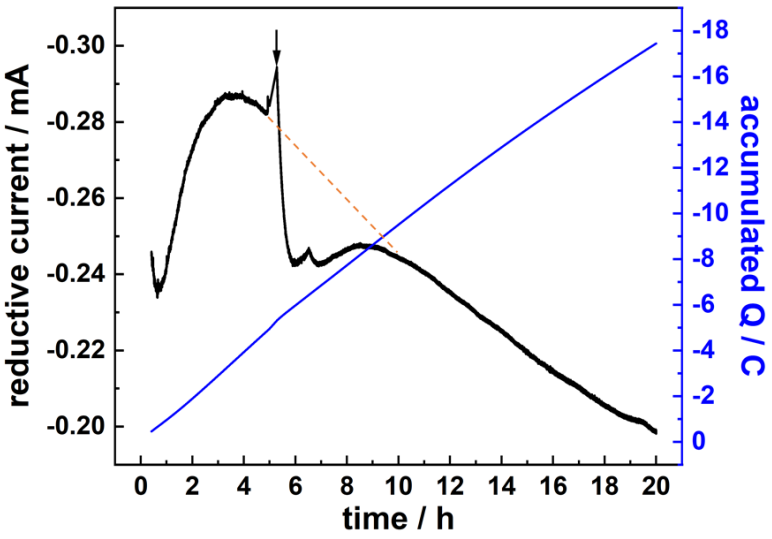


**Figure 57.** Transient curve of a constant-potential electrolysis of **G-ADH** immobilized in alginate coated on carbon felt at -1.00 V vs Ag/AgCl in 0.1 M TRIS-HCl buffer solution pH 7.4 containing 1 M acetaldehyde under $N_2$-saturated condition. Arrow indicates liquid solution sampling.

Liquid samples were taken from cathodic electrolyte solution before and after 5-h and 20-h electrolysis. Ethanol analysis of those samples were presented in **Figure 58**. The chromatographic results exhibited an ethanol peak at the retention time of 5.1 min observed in the samples collected after electrolysis. After 5-h electrolysis, the formation of 5.5 µmol of ethanol was detected, corresponding to a Faradaic efficiency for the conversion of acetaldehyde to ethanol of 21%. While, 19.9 µmol of ethanol was detected in the samples collected after 20-h electrolysis of which the ethanol formation corresponded to a Faradaic efficiency of 22%. The results revealed continuous ethanol formation at around 20% efficiency showing the stability of this electrochemical system for at least 20 h electrolysis. Furthermore, the results supported the electrochemical addressing of electrons from electrode directly to enzyme and subsequent electrochemical reduction of acetaldehyde to ethanol.

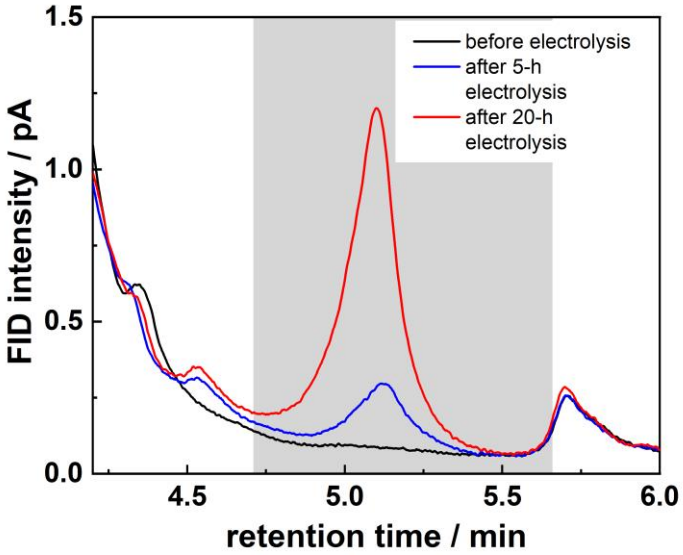


**Figure 58.** Ethanol analysis of liquid samples collected before electrolysis (black line) and after 5-h (blue line) and 20-h (red line) electrolysis in the presence of acetaldehyde under $N_2$-saturated condition using **G-ADH** immobilized in alginate coated on carbon felt.

Further, the stability test was performed by applying a constant potential at -1.00 V vs Ag/AgCl for 132 h. The current was recorded continuously as presented in **Figure 59**. The reductive current increased significantly from -0.1 at the beginning to -0.4 mA at around 1-day electrolysis. The slowly increase in current was observed until around after 2 day of electrolysis. The current stated declining gradually to -0.3 mA at the end of the experiment. This observation confirmed the system instability according to long-term electrochemical reaction. These results of which the applied potential corresponded to **-**0.36 V vs reversible hydrogen electrode (RHE), show comparable efficiency to a reported non-enzymatic system, an oxide-derived copper electrode (Faradaic efficiency of about 30% at **-**0.33 V vs RHE).[164] The study reflected enzymatic electrochemical process as a promising approach and opens rooms for the development of many other biotechnological applications.

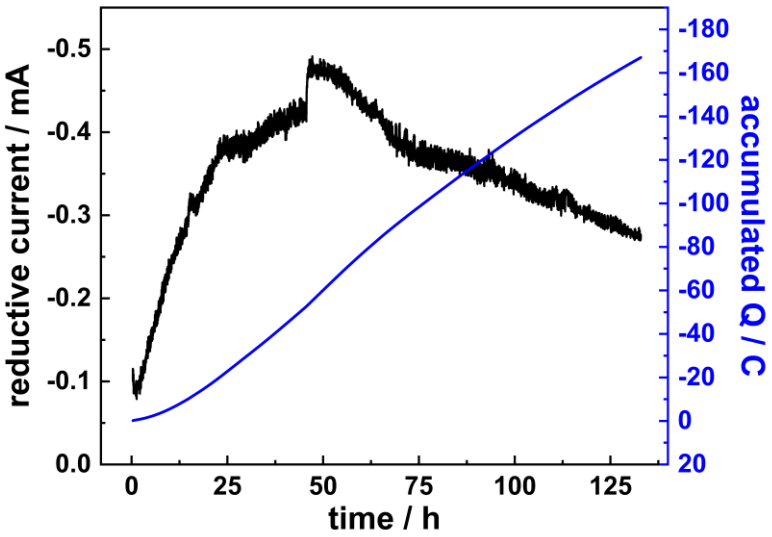


**Figure 59.** Transient curve and plot of accumulated charge of a constant-potential electrolysis of **G-ADH** immobilized in alginate coated on carbon felt at -1.00 V vs Ag/AgCl in 0.1 M TRIS-HCl buffer solution pH 7.4 containing 1 M acetaldehyde under $N_2$-saturated condition for 132 h.

### 3.2.2.2. Reduction of $CO_2$ to $CH_3OH$ using three G-DHs combined

#### 3.2.2.2.a Chemical reduction

Encouraged by the results of single enzyme reaction, the concept on three cascade reactions catalyzed by three dehydrogenases namely $F_{ate}$DH, $F_{ald}$DH and ADH for the conversion of $CO_2$ to methanol, a value-added chemical. The three-step reaction is shown in **Scheme 2**. The three dehydrogenases modified graphenes were synthesized through amidation separately for each enzyme as previously described for **G-ADH**, resulting **G-$F_{ate}$DH**, **G-$F_{ald}$DH** and **G-ADH**. The protein determination of **G-$F_{ate}$DH** and **G-$F_{ald}$DH** was conducted using the BCA assay. The results revealed amount of $F_{ate}$DH and $F_{ald}$DH covalently bound on carboxylate graphene of 0.3 and 0.1 mg·mL$^{-1}$ in **G- $F_{ate}$DH** and **G-$F_{ald}$DH** solution (with the concentration of graphene ~1 mg·mL$^{-1}$), respectively. The enzymatic activity of $F_{ate}$DH bound **G-$F_{ate}$DH** was found to be 0.1 enzyme unit per milligram of protein which was defined from catalytic activity for the conversion of formate in the presence of $NAD^+$ to $CO_2$ and NADH. While enzymatic activity of $F_{ald}$DH in **G-$F_{ald}$DH** was of 1.0 enzyme unit per milligram of protein which was defined from the conversion of formaldehyde and $NAD^+$ to formate and NADH.

In these three reductions namely the reduction of $CO_2$ to formate, the reduction of formate to formaldehyde and the reduction of formaldehyde to methanol, the first step, the conversion of $CO_2$ occurs very slowly. However, the second step where formate is transformed to formaldehyde is suggested to be the real bottleneck among these three reactions. Because the formaldehyde that was generated from this step under aqueous condition, quickly converted to its hydrated form, methanediol, which is relatively more stable.[108,165,166] Therefore, to further perform the last reduction; the dehydration of methanediol back to formaldehyde is needed. This back reaction is known as the slowest reaction, so the second step in the cascade reaction is considered as the rate-limiting step. As these reactions are in the equilibrium of forward and reverse reactions. Co-immobilization of three catalysts in one matrix is suggested to be able to improve the overall efficiency since the generated intermediates will be consumed immediately *in situ* by the enzymes catalyzed the next step.[167] Therefore three dehydrogenases modified graphenes, **G-DHs**, were

mixed and immobilized in alginate hydrogel beads. The chemical reduction of $CO_2$ to methanol was performed using **G-DHs** immobilized in alginate beads. The reaction was initiated by adding NADH as electrons and protons donor. The liquid solution was taken for methanol analysis at after 5 h and 14 h of the reaction. **Figure 60** presents gas chromatograms of methanol analysis. The chromatographic results revealed methanol formation after 5 and 14 h. During this cascade reaction, 2.26 µmol of methanol was formed after 14 h, corresponding to 50% conversion efficiency relative to added NADH.

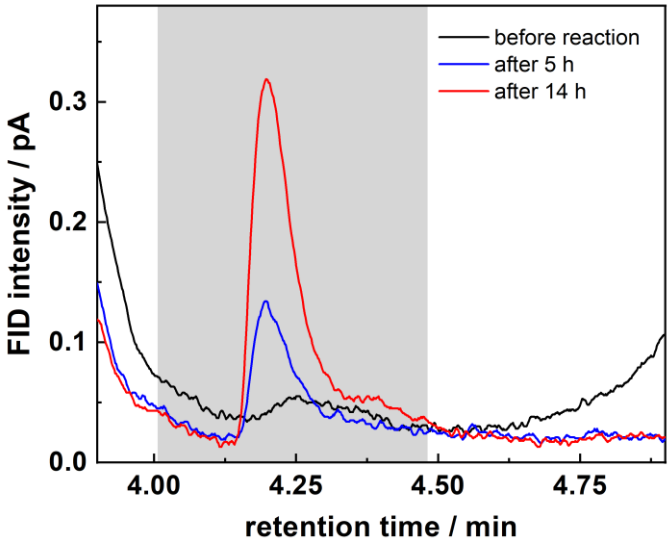


**Figure 60.** Methanol analysis of liquid samples collected before (black line) and after 5-h (blue line) and 14-h (red line) chemical reaction using NADH as cofactor under $CO_2$-saturated condition using **G-DHs** immobilized in alginate beads.

#### 3.2.2.2.b Electrochemical reduction

The electrochemical investigation of three dehydrogenases modified graphene was further investigated in this section. The electrochemical features of each **G-DH** to its substrate was characterized by means of cyclic voltammetry. The cyclic voltammograms were recorded in TRIS-HCl buffer solution pH 7.0 using carbon felt electrodes coated with alginate hydrogel matrix containing each **G-DH**. **Figure 61** reveals cyclic voltammograms of **G-F$_{ate}$DH** recorded with a scan rate of 10 mV·s$^{-1}$ under $N_2$- and $CO_2$-satuarated conditions. In the presence of $CO_2$ as a substrate of F$_{ate}$DH, reductive current at around -1.20 V increased slightly from -1.00 to -1.20 mA·cm$^{-2}$, revealing catalytic response towards the reduction of $CO_2$.

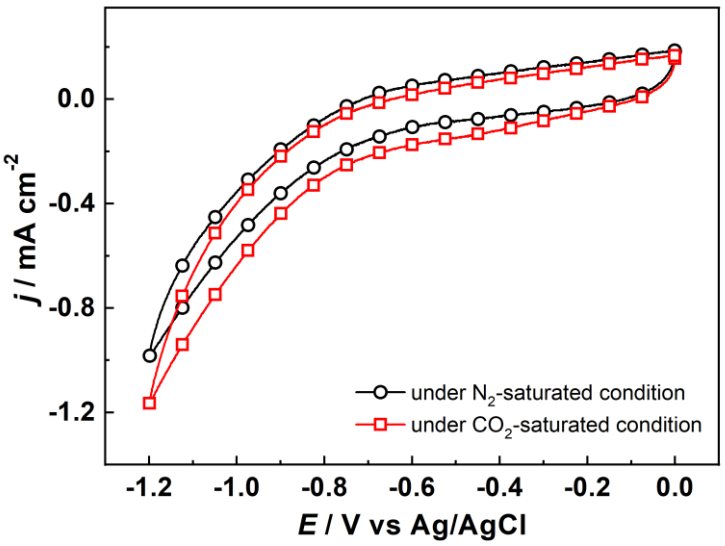


**Figure 61.** Cyclic voltammograms of a **G-F$_{ate}$DH** immobilized in alginate coated on carbon felt were recorded in 0.1 M TRIS-HCl solution pH 7.0 under $N_2$- (black line) and $CO_2$- (red line) saturated conditions.

**Figure 62** exhibits cyclic voltammograms of **G-F$_{ald}$DH** modified carbon felt electrode recorded in two conditions: without and with formate, a substrate of F$_{ald}$DH. Comparing to the inert condition, the reductive current recorded under formate-containing condition started increasing at around -0.50 V and current enhanced significantly at around -1.10 V. Moreover, at the potential of -1.20 V, the current density increased by around 0.3 mA·cm$^{-2}$, as compared to formate-free condition. The graphs suggested the catalytic activity towards the reduction of formate to formaldehyde.

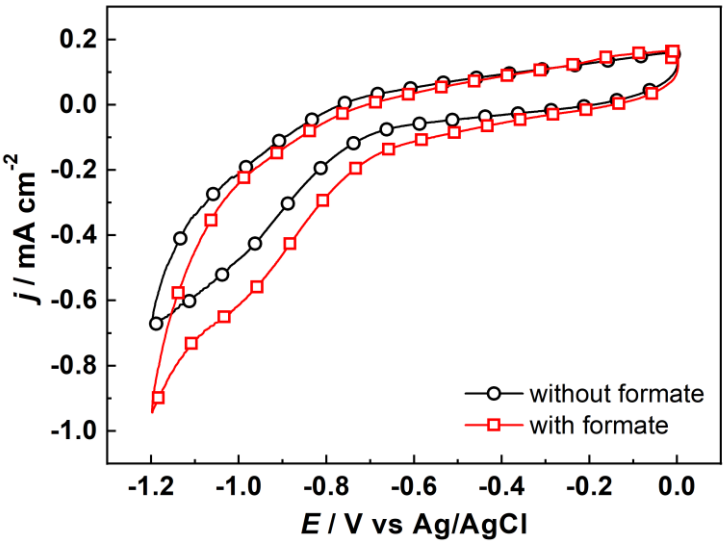


**Figure 62.** Cyclic voltammograms of a **G-F$_{ald}$DH** immobilized in alginate coated on carbon felt were recorded in 0.1 M TRIS-HCl solution pH 7.0 in the absence of formate (black line) and in the presence of formate (0.1 M, red line) under $N_2$-saturated condition.

Characterization of **G-ADH** immobilized in alginate matrix coated on carbon felt electrode was conducted by performing cyclic voltammetry under formaldehyde-free and formaldehyde

containing $N_2$-saturated conditions with the scan rate of 10 mV·s$^{-1}$. As shown in **Figure 63**, cyclic voltammograms are presented. Comparing to the formaldehyde-free condition, the increase in reductive current was detected in the presence of formaldehyde starting at around –1.00 V vs Ag/AgCl. And at the potential of -1.20 V, the current increased from -1.50 to -2.10 mA·cm$^{-2}$, relative to the inert condition. The results suggested the catalytic activity towards the conversion of formaldehyde. Among all three dehydrogenases modified electrodes, **G-ADH** modified electrode showed the highest current improvement of around 0.6 mA·cm$^{-2}$ at -1.20 V. While the **G-F$_{ate}$DH** modified electrode exhibited less current enhancement due to its natural slow process. Additionally, in all three dehydrogenases, enhanced reductive currents recorded in the presence of substrate were observed at -1.20 V vs Ag/AgCl.

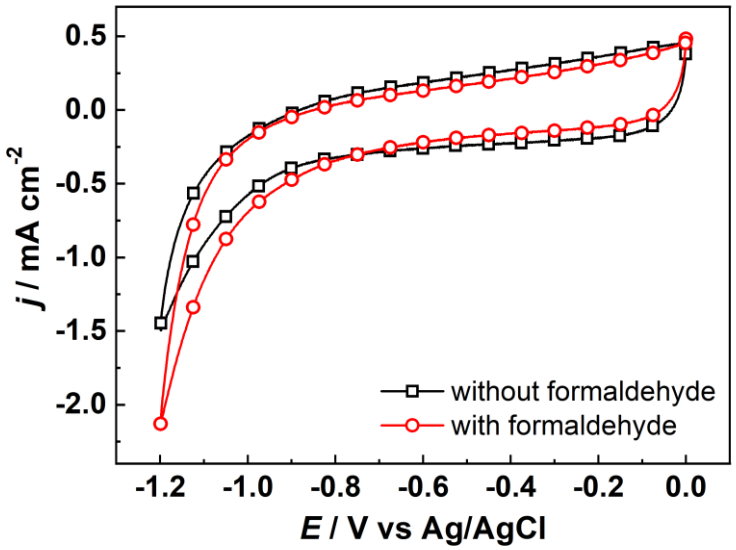


**Figure 63.** Cyclic voltammograms of a **G-ADH** immobilized in alginate coated on carbon felt were recorded in 0.1 M TRIS-HCl solution pH 7.0 in the absence of formaldehyde (black line) and in the presence of formaldehyde (0.1 M, red line) under $N_2$-saturated condition.

The investigation of co-immobilized three dehydrogenases-modified graphene (**G-F$_{ate}$DH**, **G-F$_{ald}$DH** and **G-ADH)** in alginate matrix coated on carbon felt electrode was prepared and utilized as a working electrode. Characterization of **G-DHs** modified carbon felt was conducted by cycling potentials between 0 and -1.20 V with a scan rate of 10 mV·s$^{-1}$ under $N_2$- and $CO_2$-saturated conditions. Recorded cyclic voltammograms are shown in **Figure 64**. The graphs showed slight increase in reductive current at -1.20 V vs Ag/AgCl, as compared to that of $N_2$-saturated condition. Further investigation was done by comparing cyclic voltammograms of a bare carbon felt, a carbon felt coated with alginate matrix and a carbon felt coated with alginate matrix containing three **G-DH**s, as depicted in **Figure 65**. The capacitive currents were observed to be higher in the case of alginate coated carbon felt due to low conductive alginate matrix. While the capacitive currents were found to be even higher in case of **G-DH**s modified electrode which related to the insulator properties of the three dehydrogenases immobilized in the matrix. Moreover, steep reductive response at -1.00 V was observed only in case of the **G-DHs** modified electrode, reflecting catalytic response towards $CO_2$ reduction.

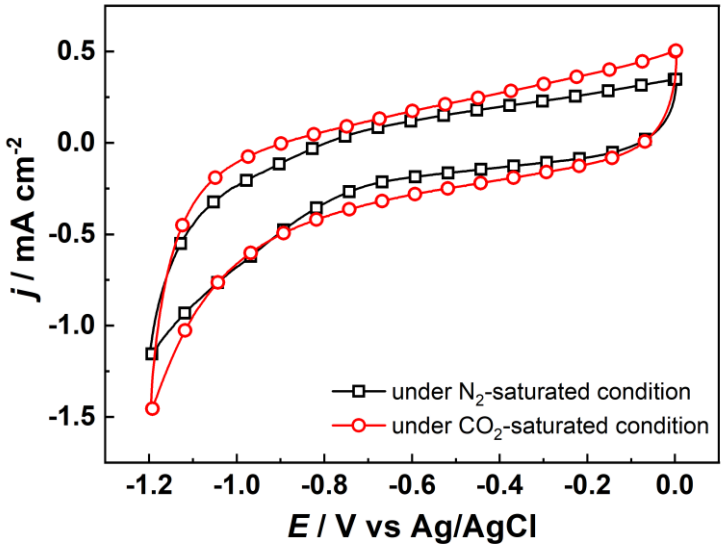


**Figure 64**. Cyclic voltammograms of a **G-DHs** immobilized in alginate coated on carbon felt were recorded in 0.1 M TRIS-HCl solution pH 7.0 under $N_2$- (black) and $CO_2$-saturated conditions (red line).

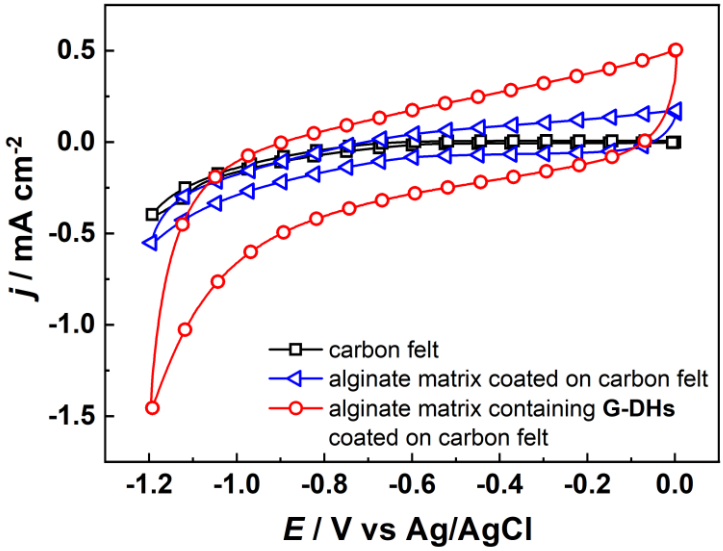


**Figure 65**. Cyclic voltammograms of a bare carbon felt electrode, an alginate matrix coated on carbon felt electrode and carbon felt electrode coated with alginate matrix containing three **G-DHs** were recorded in 0.1 M TRIS-HCl buffer solution of pH 7.0 under $CO_2$-saturated condition.

Determination of electrochemical catalytic activity was performed by applying a constant potential at -1.20 V vs Ag/AgCl. The current passed through the system was collected and was depicted in **Figure 66**. The recorded current was calculated with the running time, giving accumulated charges information, reported as a blue curve in **Figure 66**. The chronoamperogram showed remarkable increase in reductive current by 0.3 mA in the first hour and then slowly increased from -0.7 to -0.8 mA at 5 h of the electrolysis. The jump in reductive current was observed due to mechanical process from electrolyte sampling. After that, the current reached to a stable current at around -0.9 mA and remained the same until the end of the reaction, without any signs of dropping. The trends were clearly shown in the accumulated charge plot. The slope of the curve in period of

5-20 h was observed to be higher than that was observed in the early state (0-5 h), corresponding to the higher charge consumption rate.

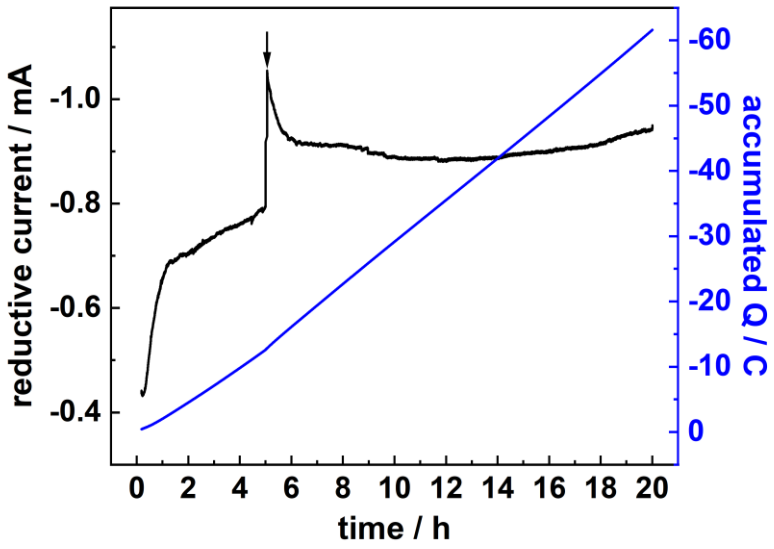


**Figure 66.** Transient curve and plot of accumulated charge of a constant-potential electrolysis of **G-DHs** immobilized in alginate coated on carbon felt at **-**1.20 V vs Ag/AgCl in 0.1 M TRIS-HCl buffer solution pH 7.0 under $CO_2$-saturated condition for 20 h. Arrow indicates liquid solution sampling.

Determination of products was conducted on three liquid samples taken from cathodic electrolyte solution including before electrolysis, after 5 h and after 20 h of the electrolysis. Liquid-injection gas chromatograms of those samples were depicted in **Figure 67**. The chromatographic results showed methanol formation observed as a peak in the retention time range of 4.00-4.50 min only in the sample collected after 20-h electrolysis. The methanol amount was found to be 12.4 µmol which corresponds to a Faradaic efficiency of 12% for the reduction of $CO_2$ to methanol (a 6-electron process).

Since the three-step enzymatic reductions involves the formation of formate and formaldehyde as intermediates in the cascade reaction. The analysis of those products was carried out using ion chromatography and high-performance liquid chromatography, respectively. The analysis showed non-detectable amounts. In the literature, several gases products were reported in the electrochemical $CO_2$ reduction systems such as CO and $CH_4$. Therefore, the headspace samples from cathodic chamber were taken and analyzed using a gas-injection gas chromatograph. The headspace analysis revealed no CO and $CH_4$ observed in the experiment. Additionally, $H_2$ generation was often reported as a side-reaction of the electrochemical reduction of $CO_2$ in aqueous solution which might involve significantly in electrons consumption. According to headspace analysis, $H_2$ formation was observed, corresponding to a Faradaic efficiency of 40%. This observation revealed the major loss of applied electrons.

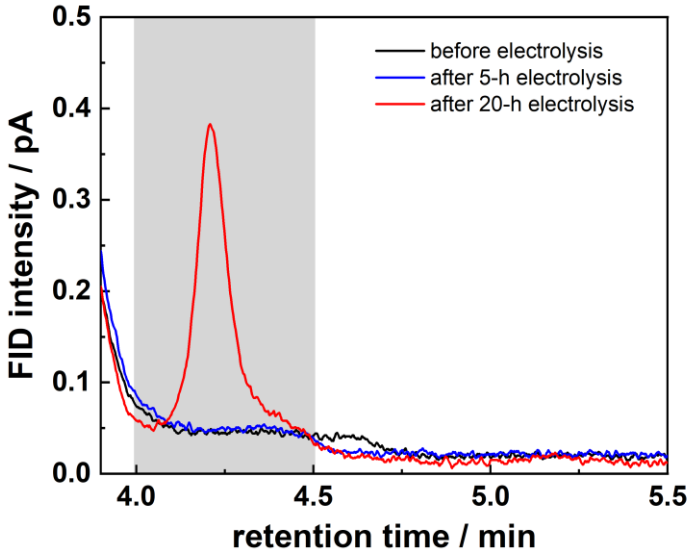


**Figure 67.** Methanol analysis of liquid samples collected before electrolysis (black line) and after 5-h (blue line) and 20-h (red line) electrolysis under $CO_2$-saturated condition using **G-DHs** immobilized in alginate coated on carbon felt.

The morphology of modified carbon felt was investigated by scanning electron microscopy. The SEM images of a bare carbon felt and dried samples of the **G-DHs** immobilized in alginate matrix coated on carbon felt electrode before using and after using as a working electrode for the electrochemical $CO_2$ reduction, were taken and are presented in **Figure 68**. Comparing to a bare carbon felt (**Figure 68**a), it was observed that alginate matrix covered the felts and voids homogeneously while parts of the felts could be seen so they could be exposed to the electrolyte solution. Additionally, this alginate morphology was preserved nicely after using in the 20-h electrolysis, suggesting high stability of the modified electrode.

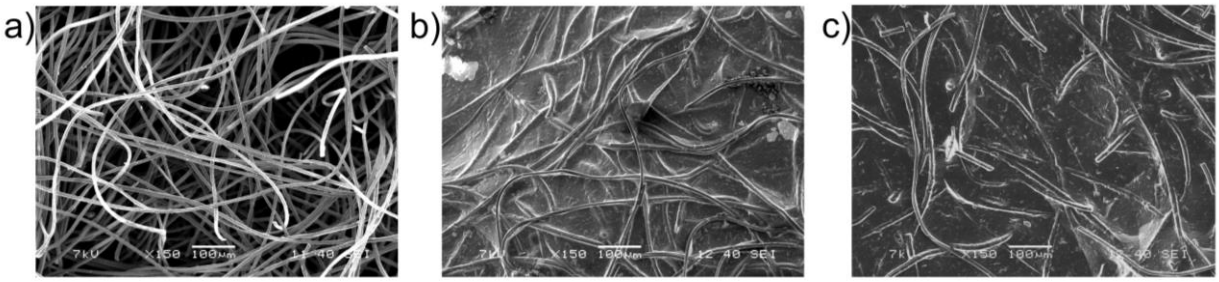


**Figure 68.** SEM images of a) bare carbon felt, **G-DHs** immobilized in alginate matrix coated on carbon felt b) before electrolysis and c) after 20-h electrolysis.

As a control experiment, electrolysis of **G-DHs** immobilized in alginate matrix coated on carbon felt electrode under $N_2$-satuarated inert condition was performed by applying a constant potential of -1.20 V vs Ag/AgCl. The current recorded during the reaction as well as the corresponding accumulated charges were presented in **Figure 69**. The transient curve showed reductive current drop from -0.4 mA at the beginning to -0.2 mA at after 5 h of electrolysis. The current jump was observed after sampling and then became stable at around -0.2 mA until at least for 20 h. The observed reductive current was much lower, as compared to the electrolysis under $CO_2$-saturated condition, reflecting that $CO_2$ reduction was a major reaction. With a similar manner to electrolysis under $CO_2$-saturated condition, liquid samples were taken before and after 20 h of electrolysis and

were analyzed using a gas chromatograph. As shown in **Figure 70**, the gas chromatographic analysis revealed no methanol formation observed from the electrolysis under $N_2$-saturated condition, confirming the electrochemical conversion of $CO_2$ to methanol. As mentioned in the electrochemical reduction of $CO_2$, $H_2$ was found to be a major side-product. Therefore, headspace analysis of the electrochemical reduction under $N_2$-saturated condition was also performed. The analysis revealed $H_2$ formation observed at a Faradaic efficiency of 41%. The $H_2$ generation efficiencies of both conditions were found to be in the similar range, suggesting that the $H_2$ formation was not related to any $CO_2$ reduction processes.

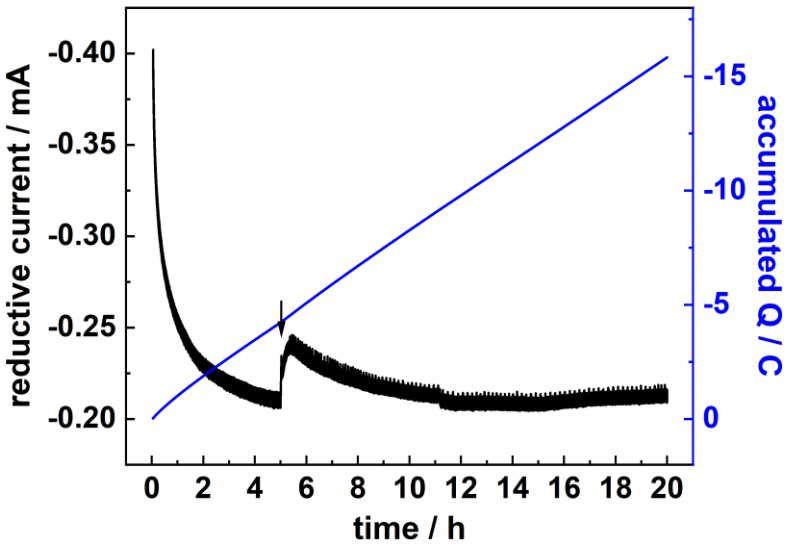


**Figure 69.** Transient curve and plot of accumulated charge of a constant-potential electrolysis of **G-DHs** immobilized in alginate coated on carbon felt at **-**1.20 V vs Ag/AgCl in 0.1 M TRIS-HCl buffer solution pH 7.0 under $N_2$-saturated condition for 20 h. Arrow indicates liquid solution sampling.

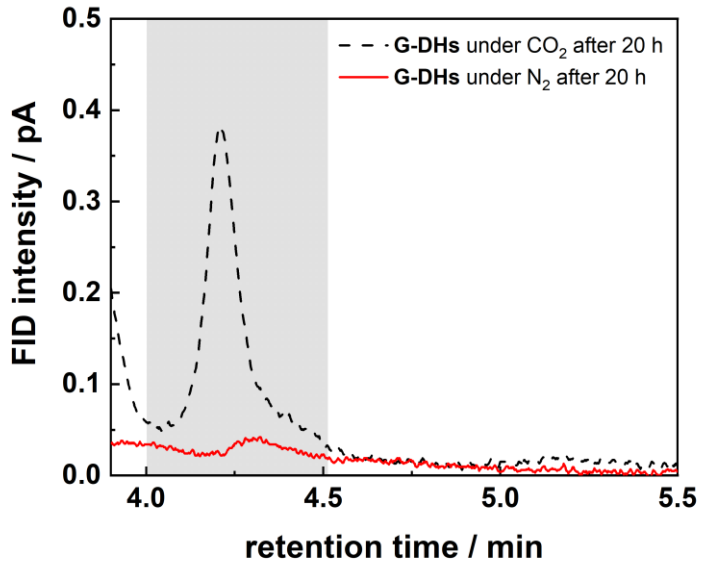


**Figure 70.** Methanol analysis of liquid samples collected after 20-h electrolysis under $N_2$-saturated (red solid line) and $CO_2$-saturated (black dashed line, extracted from **Figure 67**) conditions using **G-DHs** immobilized in alginate coated on carbon felt.

Another concern on using graphene as a support for electrochemical reduction is trace metal impurities from the synthesis which often found left over in graphene.[168] As reported in the previous work of Dr. Aristides Bakandritsos,[169] an inductively coupled plasma mass spectrometry (ICP-MS) analysis of **G-COOH** was performed in order to investigate metal contents in the sample. **Table 19** showed metal contents found in **G-COOH**. The results revealed the highest metal contents were found for Fe and Zn at the concentration around 70 ppm. These two metals were observed as rather inert catalysts for $CO_2$ reduction. However, the control experiment of bare **G-COOH** immobilized in alginate matrix coated on carbon felt was carried out by means of cyclic voltammetry and controlled potential electrolysis. As shown in **Figure 71**, cyclic voltammograms of both $N_2$- and $CO_2$-saturated conditions showed no enhanced reductive current. Moreover, by applying a constant potential of -1.20 V vs Ag/AgCl, reductive current passed through the system was recorded (**Figure 72**). The transient curve revealed that high reductive current was observed. The current increased remarkably in the early period up to 5**Figure 73**Based on this observation, we could claim that metal impurities in **G-COOH** could hardly affect the electrocatalytic process

| Metal | Cr | Mn | Fe | Co | Ni | Cu | Zn | Pd | Pt |
|---|---|---|---|---|---|---|---|---|---|
| Content (µg/g) | 4.4 | 2.7 | 76.3 | LTQL | 30.4 | 54.6 | 69.9 | LTQL | LTQL |

**Table 19.** Inductively coupled plasma mass spectrometry (ICP-MS) trace metal analysis of the **G-COOH** sample (LTQL stands for: lower than the quantitation limit).[169]

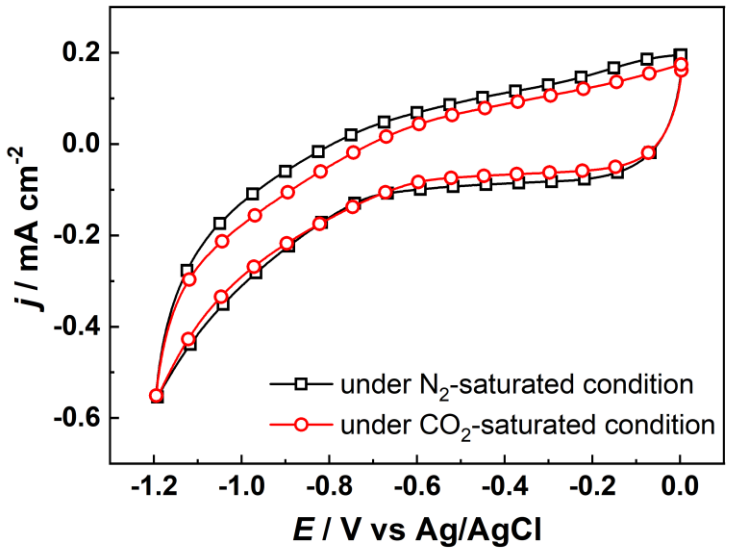


**Figure 71.** Cyclic voltammograms of a **G-COOH** immobilized in alginate coated on carbon felt were recorded in 0.1 M TRIS-HCl solution pH 7.0 under $N_2$- (black) and $CO_2$-saturated conditions (red line).

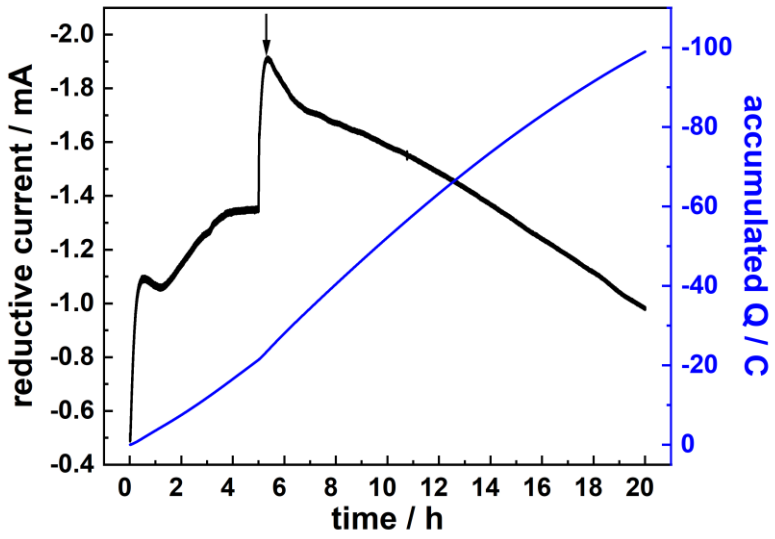


**Figure 72.** Transient curve and plot of accumulated charge of a constant-potential electrolysis of **G-COOH** immobilized in alginate coated on carbon felt at **-**1.20 V vs Ag/AgCl in 0.1 M TRIS-HCl buffer solution pH 7.0 under $CO_2$-saturated condition for 20 h. Arrow indicates liquid solution sampling.

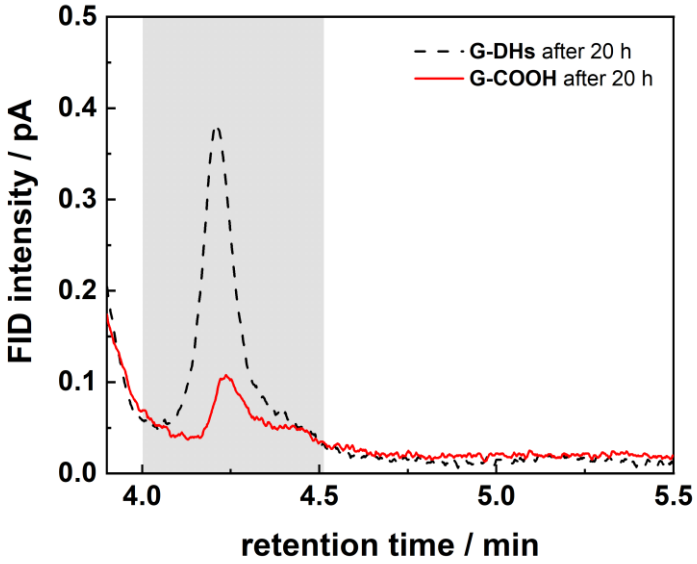


**Figure 73.** Methanol analysis of liquid samples collected after 20-h electrolysis under $CO_2$-saturated condition using **G-COOH** (red solid line) and **G-DHs**(black dashed line, extracted from **Figure 67**) immobilized in alginate coated on carbon felt electrodes.

The electrochemical reduction of $CO_2$ *via* the direct electron addressing to dehydrogenases was reported previously be Schlager *et al.*.[109] The reported system was developed with the same alginate matrix immobilization technique without any further modifications (same carbon felt (2×0.6×0.6 $cm^3$) was used as a working electrode). Methanol was detected after 4-h electrolysis in phosphate buffer solution pH 7.6 at a controlled potential of -1.20 V vs Ag/AgCl with a concentration of 0.1 ppm and reductive current was observed as around -0.08 mA, corresponding to a Faradaic efficiency of around 10%. Comparing to this work, the three dehydrogenases modified graphene system reflected one order of magnitude higher absolute reductive currents

suggesting a far more efficient electron transport from the electrode to the enzymes' active sites, *via* the conductive graphene support with a higher methanol production rate of 0.6 μmol·$h^{-1}$. Furthermore, while the reductive current profile in the presented case of the covalent immobilization was preserved for at least 20 h. Another advantage of this approach is much lower enzyme added. These observations reflected the advantage of using the conductive carboxylic graphene acid as a platform for covalent enzyme immobilization. Comparing to the state-of-the-art electrocatalysts as summarized in **Table 20** for the $CO_2$ to methanol conversion, this enzyme-graphene based system offers high selectivity towards methanol production under neutral aqueous solution and moderate overpotential of 0.61 V. Moreover, the bio-origin materials have a great advantage of large material availability over rare metal-based systems.

| Catalysts | Electrolyte | Electrode | Applied potential | η[a]/V | *j*/mA cm$^{-2}$ | %FE | Other product(s) |
|---|---|---|---|---|---|---|---|
| $Cu_2O/Zn_2O$[170] | 0.5 M $KHCO_3$ | GDE[b] | -1.16 V vs Ag/AgCl | 0.54 | 10 | 27.5 (17.7[c]) | $C_2H_6O$ |
| $Pd/SnO_2$ nanosheet[171] | 0.1 M $NaHCO_3$ | Carbon paper | -0.24 V vs RHE | 0.27 | 1.45 | 54.8 | formate |
| Copper selenide ($Cu_{1.63}Se$) nanoparticle[172] | [Bmim]$PF_6$[d] (30wt%) /$CH_3CN$/$H_2O$ (5wt%) | Carbon paper | -2.1 V vs $Ag/Ag^+$ (-1.175 V vs RHE) | 1.2 | 41.5 | 77.6 | formate, CO |
| PYD[e]@Cu-Pt alloy[173] | 0.5 M KCl | Free standing electrode | -0.6 V vs SCE | 0.07 | 22 | 37 | formate |
| $Cu_2O$-MWCNTs[h,174] | 0.5 M $KHCO_3$ | Cu foil | -0.8 V vs Ag/AgCl | -[f] | 6 | 38 | not reported |
| Cu nanocluster/ZnO[175] | 0.1 M $KHCO_3$ | Single crystal ZnO | -1.4 V vs Ag/AgCl | 0.83 | 12 | 2.8 | CO, $CH_4$, $C_2H_4$, $C_2H_6O$, methyl formate |
| Ni | 0.1 M $KHCO_3$ | Ni foil | -1.0 V vs RHE | 1.03 | 5 | 2.3 | $CH_4$, $C_2H_4$, formate |
| BDD[176] | 1 M $NH_3$ | Si wafer | -1.3 V vs Ag/AgCl | 0.67 | -[f] | 24.3 | CO, $CH_4$ |
| Dehydrogenases[109] | 0.05 M phosphate buffer pH 7.6 | Carbon felt | -1.2 V vs Ag/AgCl | 0.58 | 0.08 | 10 | not observed |

**Table 20.** State-of-the-art electrochemical reduction of $CO_2$ to methanol.

[a]Overpotential (η) is compared with the thermodynamic potential for the conversion of $CO_2$ to methanol of 0.03 V vs RHE[176] where *E* (V vs RHE) is calculated form *E* (V vs Ag/AgCl) + 0.205 V + 0.0591*pH or *E* (V vs SCE) + 0.244 V + 0.0591*pH.
[b]GDE stands for Gas diffusion electrode.
[c]The experiment was performed without supplying $CO_2$ to GDE.
[d][Bmim]$PF_6$: 1-butyl-3-methylimidazolium hexafluorophosphate
[e]PYD: 4-(3-phenoxy-2,2-bis(phenoxymethyl)propoxy)pyridine
[f]The information was not given.
[g]Multi wall carbon nanotubes (MWCNTs) impregnated with $Cu_2O$.
[h]BDD stands for boron-doped diamond electrode.

# 4. Summary and Outlook

## 4.1. Summary

In this thesis, carbon dioxide capture and utilization approach was investigated by converting $CO_2$, a source of carbon, to value-added fuels (such as formate and $CH_4$) as a new-generation of renewable and sustainable source of energy. These non-fossil fuels offer a feasible alternative as they are easy to storage and transportable. This idea became a candidate approach and therefore has been extremely investigated. From chemistry point-of-view, $CO_2$ is highly stable molecule, so high energy input is required to overcome energy barrier of the $CO_2$ conversion. To avoid additional overpotential, catalysts are introduced into systems. Furthermore, a combination of the $CO_2$ reductions ideas with energy supplied from renewable sources (i.e. electricity or temperature) is of promise. In order to pursue the desired reductions, appropriate catalyst is of critical. Some reported catalysts are, for examples, metal-based catalysts and synthetic compounds including organometallic compounds. However, the systems containing such catalysts often suffered from harsh reaction conditions, low selectivity towards desired product and sometimes, low availability of catalyst (i.e. rare-earth metals). Bio-origin catalysts are proposed due to high availability from biosphere and high selectivity under mild conditions.

Herein, the bio-origin materials were employed in electrochemical $CO_2$ reductions. Two biological materials including microorganisms and enzymes were utilized. Microorganisms are living organisms offering self-regeneration; therefore, they are candidate catalysts in term of sustainability. Since there are various strains of microorganisms, serving different metabolisms, products/reactions could be tuned accordingly. An acetogen, *Methylobacterium extorquens*, was introduced into the microbial electrolysis cells. The results showed that *M. extroquens* is capable for electrochemical reduction of $CO_2$ as sole carbon source to formate *via* the Wood-Ljungdahl pathway. The long-term experiment was performed showing formate production corresponding to average Faradaic efficiency of around 2%. To enhance the performance of the system, one would consider improving electron transfer process from the electrode to microorganisms. Although the mechanisms were still not clear, addition of artificial redox mediators could enhance the processes. The systems containing neutral red as homogeneous redox mediator, showed higher formate formation as well as electrical charge consumption which corresponded to average Faradaic efficiency of 4% for overall experiment. Nonetheless, this approach showed main drawbacks of redox mediator cost and product separation issue since redox mediator is dissolved in the solution. The proposed idea is to heterogenized mediator directly onto the electrode aiming to reduce diffusions and simplify product separation. Neutral red was then electropolymerized through its primary amine units, resulting poly(neutral red) modified electrode for being a support for biofilm growth. An average Faradaic efficiency of 4% was also observed in long-term electrochemical experiment of biocathode from poly(neutral red), revealing enhanced electron transfer process relative to biocathode from a bare carbon felt. Although introduction of neutral red in both approaches improved catalytic performance, the efficiency is still too low and it clearly showed that after the second running cycle (around 57 days), current and formate production started declining. A possible reason might be due to the loss of biofilm and limited growth rate, as the experiments were only performed in $CO_2$-saturated phosphate buffer solution without any other vitamin, trace elements or other carbon sources.

The investigation on mixed culture microorganisms was presented. The biocathode was developed from the sewage sludge containing different strains. The adaptation was performed

under anaerobic condition saturated with $CO_2$ and the suitable substances were included. The biocathode was examined its long-term electrocatalytic activity (63 day) towards the reduction of $CO_2$ to $CH_4$ with methane production rate of 4 µmol·day$^{-1}$ corresponding Faradaic efficiency of 8%. These reflected electromethanogenesis process. Encouraged by the results, bio-electrochemical systems containing bioanode and biocathode were exhibited for dual applications including organic substances oxidation giving electrons back to the circuit and conversion of $CO_2$ to $CH_4$ by using electrons delivered from the biocathode. Both bioelectrodes were developed from the same sewage sludge having mix cultured microorganisms but under different substrates conditions. These dual-chamber dual-application systems were monitored their performance through COD value and $CH_4$ amount, for anode and cathode, respectively. The average $CH_4$ production and COD degradation rate were observed as 40 µmol·day$^{-1}$ and 55 mg·L$^{-1}$·day$^{-1}$, respectively, and average Faradaic efficiency was of 36%. Further attempts on electrode modifications were also employed in this two-bioelectrode system. Poly(neutral red) and chitosan modifications were presented, revealing remarkable enhanced overall system performance. These might be because of improved biofilm quality (suggested from SEM images) and/or enhanced electron transfer.

Even though microbial systems exhibited sustainable systems. But part of applied energy is used for their growth. Moreover, microbial systems are highly complicated due to several metabolic pathways involved in. Due to these reasons, enzymes were extracted and investigated for fundamental studies. In $CO_2$ reduction and fixation metabolic pathways, dehydrogenase redox enzymes play important role. However, they require costly and sacrificial cofactors as source of protons and electrons. To avoid this limitation, electrochemical addressing of electrons could be promising approach. Immobilization technique is critical for efficient electron transfer. Schlager *et al.* reported direct electron injection of dehydrogenases immobilized in alginate matrix. Although alginate matrix could keep enzymes close to electrode and could also prevent enzymes from denaturation, low current delivered during controlled potential electrolysis was observed which is due to low conductivity. Improving the electron transfer is suggested by introduction of graphene, a nanoplatform. Conjugated dehydrogenases onto graphene support was presented and characterized by means of spectroscopic methods. Both single and three dehydrogenases graphene hybrids were further immobilized in alginate matrix and by applying a constant potential, enhanced production rate as well as electron consumption were observed, as compared to previous study. The results reveal highly selectivity and the $CO_2$ reduction to methanol could be performed at neutral condition with a moderate overpotential of 0.61 V which is comparable with state-of-the-art metal-based materials.

## 4.2. Outlook

The results received in this thesis strongly suggested and confidently supported the utilization of bio-origin materials for electrochemical of $CO_2$ and many other electrochemical systems. There are rooms to further investigate variety of the biosphere such as different microorganisms, different enzymes (*i.e.* from different sources). In microbial systems, more fundamental investigations including electrochemical parameters (i.e. applied potential), feeding conditions and extracellular electron transfer mechanism, are needed in order to develop for large-scale production. One limitation of two-chamber systems is limited current flow and high operation cost due to the introduction of membrane. In order to achieve high performance, membrane-less systems and continuous operation mode (to ensure enough substrate) should be investigated. Comparing to two different **MECs** (pure strain and mixed cultures), mixed-culture containing biofilm showed

higher stability with higher system efficiency, suggesting an appropriate system for microorganisms. Encouraged by dual-bioelectrode systems, combination of both bioelectrodes showed promising results which should be further tested in as a microbial fuel cell device where no external applied voltage. In case of enzymatic system, since active sites of dehydrogenases are varied according to their living sources. The exploring and comparing dehydrogenases from different sources (such as from yeast, algae or bacteria) could be very interesting. Moreover, other immobilization techniques using linkers as either electron relay units or redox mediators could be an option to further optimize the system.

## 5. References


(1) Baede, A. P. M.; Linden, P. van der; Verbruggen, A. *Annex II to IPCC Fourth Assessment Report*; 2007.

(2) Forster, P.; Ramaswamy, V.; Artaxo, P.; Berntsen, T.; Betts, R.; Fahey, D. W.; Haywood, J.; Lean, J.; Lowe, D. C.; Myhre, G.; et al. *Changes in Atmospheric Constituents and in Radiative Forcing Chapter 2*; Cambridge University Press: United Kingdom, 2007.

(3) Arrhenius, S. XXXI. On the Influence of Carbonic Acid in the Air upon the Temperature of the Ground. *Philos. Mag. Ser. 5* **1896**, *41* (251), 237–276.

(4) US Department of Commerce, NOAA, E. S. R. L. ESRL Global Monitoring Division - Global Greenhouse Gas Reference Network https://www.esrl.noaa.gov/gmd/ccgg/trends/global.html (accessed Dec 24, 2019).

(5) Hashimoto, K. Global Temperature and Atmospheric Carbon Dioxide Concentration; 2019; pp 5–17.

(6) Lüthi, D.; Le Floch, M.; Bereiter, B.; Blunier, T.; Barnola, J.-M.; Siegenthaler, U.; Raynaud, D.; Jouzel, J.; Fischer, H.; Kawamura, K.; et al. High-Resolution Carbon Dioxide Concentration Record 650,000–800,000 Years before Present. *Nature* **2008**, *453* (7193), 379–382.

(7) Lewis, N. S.; Nocera, D. G. Powering the Planet: Chemical Challenges in Solar Energy Utilization. *Proc. Natl. Acad. Sci. U. S. A.* **2006**, *103* (43), 15729–15735.

(8) Aresta, M.; Dibenedetto, A. Utilisation of $CO_2$ as a Chemical Feedstock: Opportunities and Challenges. *Dalt. Trans.* **2007**, No. 28, 2975–2992.

(9) Kondratenko, E. V.; Mul, G.; Baltrusaitis, J.; Larrazábal, G. O.; Pérez-Ramírez, J. Status and Perspectives of $CO_2$ Conversion into Fuels and Chemicals by Catalytic, Photocatalytic and Electrocatalytic Processes. *Energy Environ. Sci.* **2013**, *6* (11), 3112–3135.

(10) Li, H.; Opgenorth, P. H.; Wernick, D. G.; Rogers, S.; Wu, T.-Y.; Higashide, W.; Malati, P.; Huo, Y.-X.; Cho, K. M.; Liao, J. C. Integrated Electromicrobial Conversion of $CO_2$ to Higher Alcohols. *Science* **2012**, *335* (6076), 1596.

(11) Aresta, M.; Dibenedetto, A. Key Issues in Carbon Dioxide Utilization as a Building Block for Molecular Organic Compounds in the Chemical Industry. In *ACS Symposium Series*; American Chemical Society, 2002; Vol. 809, pp 54–70.

(12) Olah, G. A. Beyond Oil and Gas: The Methanol Economy. *Angew. Chemie Int. Ed.* **2005**, *44* (18), 2636–2639.

(13) Olah, G. A.; Goeppert, A.; Prakash, G. K. S. Chemical Recycling of Carbon Dioxide to Methanol and Dimethyl Ether: From Greenhouse Gas to Renewable, Environmentally Carbon Neutral Fuels and Synthetic Hydrocarbons. *J. Org. Chem.* **2009**, *74* (2), 487–498.

(14) Cuéllar-Franca, R. M.; Azapagic, A. Carbon Capture, Storage and Utilisation Technologies: A Critical Analysis and Comparison of Their Life Cycle Environmental Impacts. *J. CO2 Util.* **2015**, *9*, 82–102.

(15) Cotel, A. J. A Trigger Mechanism for the Lake Nyos Disaster. *J. Volcanol. Geotherm. Res.* **1999**, *88* (4), 343–347.

(16) ICEF Innovation for Cool Earth Forum https://www.icef-forum.org/platform/thematic_discussion_topic13_session2.php (accessed Dec 24, 2019).

(17) Müller, K.; Mokrushina, L.; Arlt, W. Thermodynamic Constraints for the Utilization of $CO_2$. *Chemie Ing. Tech.* **2014**, *86* (4), 497–503.

(18) Appel, A. M.; Bercaw, J. E.; Bocarsly, A. B.; Dobbek, H.; DuBois, D. L.; Dupuis, M.; Ferry, J. G.; Fujita, E.; Hille, R.; Kenis, P. J. A.; et al. Frontiers, Opportunities, and Challenges in Biochemical and Chemical Catalysis of $CO_2$ Fixation. *Chem. Rev.* **2013**, *113* (8), 6621–6658.

(19) Whipple, D. T.; Kenis, P. J. A. Prospects of $CO_2$ Utilization via Direct Heterogeneous Electrochemical Reduction. *J. Phys. Chem. Lett.* **2010**, *1* (24), 3451–3458.

(20) Peterson, A. A.; Nørskov, J. K. Activity Descriptors for $CO_2$ Electroreduction to Methane on Transition-Metal Catalysts. *J. Phys. Chem. Lett.* **2012**, *3* (2), 251–258.

(21) Hori, Y.; Kikuchi, K.; Suzuki, S. Production of CO and $CH_4$ in Electrochemical Reduction of $CO_2$ at Metal Electrodes in Aqueous Hydrogencarbonate Solution. *Chem. Lett.* **1985**, *14* (11), 1695–1698.

(22) Kuhl, K. P.; Cave, E. R.; Abram, D. N.; Jaramillo, T. F. New Insights into the Electrochemical Reduction of Carbon Dioxide on Metallic Copper Surfaces. *Energy Environ. Sci.* **2012**, *5* (5), 7050.

(23) Inoue, T.; Fujishima, A.; Konishi, S.; Honda, K. Photoelectrocatalytic Reduction of Carbon Dioxide in Aqueous Suspensions of Semiconductor Powders. *Nature* **1979**, *277* (5698), 637–638.
(24) Wang, C.; Xie, Z.; deKrafft, K. E.; Lin, W. Doping Metal–Organic Frameworks for Water Oxidation, Carbon Dioxide Reduction, and Organic Photocatalysis. *J. Am. Chem. Soc.* **2011**, *133* (34), 13445–13454.
(25) Kumar, B.; Llorente, M.; Froehlich, J.; Dang, T.; Sathrum, A.; Kubiak, C. P. Photochemical and Photoelectrochemical Reduction of $CO_2$. *Annu. Rev. Phys. Chem.* **2012**, *63* (1), 541–569.
(26) Hawecker, J.; Lehn, J.-M.; Ziessel, R. Photochemical and Electrochemical Reduction of Carbon Dioxide to Carbon Monoxide Mediated by (2,2'-Bipyridine) Tricarbonylchlororhenium(I) and Related Complexes as Homogeneous Catalysts. *Helv. Chim. Acta* **1986**, *69* (8), 1990–2012.
(27) Lehn, J. M.; Ziessel, R. Photochemical Generation of Carbon Monoxide and Hydrogen by Reduction of Carbon Dioxide and Water under Visible Light Irradiation. *Proc. Natl. Acad. Sci. U. S. A.* **1982**, *79* (2), 701–704.
(28) Hansen, H. A.; Varley, J. B.; Peterson, A. A.; Nørskov, J. K. Understanding Trends in the Electrocatalytic Activity of Metals and Enzymes for $CO_2$ Reduction to CO. *J. Phys. Chem. Lett.* **2013**, *4* (3), 388–392.
(29) Shen, J.; Kortlever, R.; Kas, R.; Birdja, Y. Y.; Diaz-Morales, O.; Kwon, Y.; Ledezma-Yanez, I.; Schouten, K. J. P.; Mul, G.; Koper, M. T. M. Electrocatalytic Reduction of Carbon Dioxide to Carbon Monoxide and Methane at an Immobilized Cobalt Protoporphyrin. *Nat. Commun.* **2015**, *6* (1), 8177.
(30) Costentin, C.; Drouet, S.; Robert, M.; Savéant, J.-M. A Local Proton Source Enhances $CO_2$ Electroreduction to CO by a Molecular Fe Catalyst. *Science* **2012**, *338* (6103), 90–94.
(31) Asadi, M.; Kumar, B.; Behranginia, A.; Rosen, B. A.; Baskin, A.; Repnin, N.; Pisasale, D.; Phillips, P.; Zhu, W.; Haasch, R.; et al. Robust Carbon Dioxide Reduction on Molybdenum Disulphide Edges. *Nat. Commun.* **2014**, *5* (1), 4470.
(32) Lin, S.; Diercks, C. S.; Zhang, Y.-B.; Kornienko, N.; Nichols, E. M.; Zhao, Y.; Paris, A. R.; Kim, D.; Yang, P.; Yaghi, O. M.; et al. Covalent Organic Frameworks Comprising Cobalt Porphyrins for Catalytic $CO_2$ Reduction in Water. *Science* **2015**, *349* (6253), 1208–1213.
(33) Kortlever, R.; Peters, I.; Koper, S.; Koper, M. T. M. Electrochemical $CO_2$ Reduction to Formic Acid at Low Overpotential and with High Faradaic Efficiency on Carbon-Supported Bimetallic Pd–Pt Nanoparticles. *ACS Catal.* **2015**, *5* (7), 3916–3923.
(34) Chen, Y.; Li, C. W.; Kanan, M. W. Aqueous $CO_2$ Reduction at Very Low Overpotential on Oxide-Derived Au Nanoparticles. *J. Am. Chem. Soc.* **2012**, *134* (49), 19969–19972.
(35) Li, C. W.; Kanan, M. W. $CO_2$ Reduction at Low Overpotential on Cu Electrodes Resulting from the Reduction of Thick $Cu_2O$ Films. *J. Am. Chem. Soc.* **2012**, *134* (17), 7231–7234.
(36) Hori, Y.; Wakebe, H.; Tsukamoto, T.; Koga, O. Electrocatalytic Process of CO Selectivity in Electrochemical Reduction of $CO_2$ at Metal Electrodes in Aqueous Media. *Electrochim. Acta* **1994**, *39* (11–12), 1833–1839.
(37) Hori, Y. Electrochemical $CO_2$ Reduction on Metal Electrodes. In *Modern Aspects of Electrochemistry*; Springer New York: New York, 2008; pp 89–189.
(38) Rakowski Dubois, M.; Dubois, D. L.; Rakowski, M.; And, D.; Dubois, D. L. Development of Molecular Electrocatalysts for $CO_2$ Reduction and $H_2$ Production/Oxidation. *Acc. Chem. Res.* **2009**, *42* (12), 1974–1982.
(39) Schuchmann, K.; Müller, V. Direct and Reversible Hydrogenation of $CO_2$ to Formate by a Bacterial Carbon Dioxide Reductase. *Science* **2013**, *342* (6164), 1382–1385.
(40) Chiu, S.-Y.; Kao, C.-Y.; Chen, C.-H.; Kuan, T.-C.; Ong, S.-C.; Lin, C.-S. Reduction of $CO_2$ by a High-Density Culture of *Chlorella Sp.* in a Semicontinuous Photobioreactor. *Bioresour. Technol.* **2008**, *99* (9), 3389–3396.
(41) Aresta, M.; Dibenedetto, A.; Pastore, C. Biotechnology to Develop Innovative Syntheses Using $CO_2$. *Environ. Chem. Lett.* **2005**, *3* (3), 113–117.
(42) Schlager, S.; Fuchsbauer, A.; Haberbauer, M.; Neugebauer, H.; Sariciftci, N. S. Carbon Dioxide Conversion to Synthetic Fuels Using Biocatalytic Electrodes. *J. Mater. Chem. A* **2017**, *5* (6), 2429–2443.
(43) Logan, B. E.; Rabaey, K. Conversion of Wastes into Bioelectricity and Chemicals by Using Microbial Electrochemical Technologies. *Science* **2012**, *337* (6095), 686–690.
(44) Rabaey, K.; Rozendal, R. A. Microbial Electrosynthesis — Revisiting the Electrical Route

for Microbial Production. *Nat. Rev. Microbiol.* **2010**, *8* (10), 706–716.
(45) Rabaey, K.; Read, S. T.; Clauwaert, P.; Freguia, S.; Bond, P. L.; Blackall, L. L.; Keller, J. Cathodic Oxygen Reduction Catalyzed by Bacteria in Microbial Fuel Cells. *ISME J.* **2008**, *2* (5), 519–527.
(46) Lowy, D. A.; Tender, L. M.; Zeikus, J. G.; Park, D. H.; Lovley, D. R. Harvesting Energy from the Marine Sediment-Water Interface II. Kinetic Activity of Anode Materials. *Biosens. Bioelectron.* **2006**, *21* (11), 2058–2063.
(47) Logan, B. E.; Call, D.; Cheng, S.; Hamelers, H. V. M.; Sleutels, T. H. J. A.; Jeremiasse, A. W.; Rozendal, R. A. Microbial Electrolysis Cells for High Yield Hydrogen Gas Production from Organic Matter. *Environ. Sci. Technol.* **2008**, *42* (23), 8630–8640.
(48) Butler, C. S.; Clauwaert, P.; Green, S. J.; Verstraete, W.; Nerenberg, R. Bioelectrochemical Perchlorate Reduction in a Microbial Fuel Cell. *Environ. Sci. Technol.* **2010**, *44* (12), 4685–4691.
(49) Gregory, K. B.; Bond, D. R.; Lovley, D. R. Graphite Electrodes as Electron Donors for Anaerobic Respiration. *Environ. Microbiol.* **2004**, *6* (6), 596–604.
(50) Clauwaert, P.; Rabaey, K.; Aelterman, P.; De Schamphelaire, L.; Pham, T. H.; Boeckx, P.; Boon, N.; Verstraete, W. Biological Denitrification in Microbial Fuel Cells. *Environ. Sci. Technol.* **2007**, *41* (9), 3354–3360.
(51) Strycharz, S. M.; Woodard, T. L.; Johnson, J. P.; Nevin, K. P.; Sanford, R. A.; Löffler, F. E.; Lovley, D. R. Graphite Electrode as a Sole Electron Donor for Reductive Dechlorination of Tetrachlorethene by *Geobacter Lovleyi*. *Appl. Environ. Microbiol.* **2008**, *74* (19), 5943–5947.
(52) Aulenta, F.; Reale, P.; Canosa, A.; Rossetti, S.; Panero, S.; Majone, M. Characterization of an Electro-Active Biocathode Capable of Dechlorinating Trichloroethene and Cis-Dichloroethene to Ethene. *Biosens. Bioelectron.* **2010**, *25* (7), 1796–1802.
(53) Aulenta, F.; Catervi, A.; Majone, M.; Panero, S.; Reale, P.; Rossetti, S. Electron Transfer from a Solid-State Electrode Assisted by Methyl Viologen Sustains Efficient Microbial Reductive Dechlorination of TCE. *Environ. Sci. Technol.* **2007**, *41* (7), 2554–2559.
(54) Gregory, K. B.; Lovley, D. R. Remediation and Recovery of Uranium from Contaminated Subsurface Environments with Electrodes. *Environ. Sci. Technol.* **2005**, *39* (22), 8943–8947.
(55) Saint-Amans, S.; Girbal, L.; Andrade, J.; Ahrens, K.; Soucaille, P. Regulation of Carbon and Electron Flow in Clostridium Butyricum VPI 3266 Grown on Glucose-Glycerol Mixtures. *J. Bacteriol.* **2001**, *183* (5), 1748–1754.
(56) Kim, T. S.; Kim, B. H. Electron Flow Shift in Clostridiumacetobutylicum Fermentation by Electrochemically Introduced Reducing Equivalent. *Biotechnol. Lett.* **1988**, *10* (2), 123–128.
(57) Clauwaert, P.; Tolêdo, R.; van der Ha, D.; Crab, R.; Verstraete, W.; Hu, H.; Udert, K. M.; Rabaey, K. Combining Biocatalyzed Electrolysis with Anaerobic Digestion. *Water Sci. Technol.* **2008**, *57* (4), 575–579.
(58) Peters, V.; Janssen, P. H.; Conrad, R. Transient Production of Formate during Chemolithotrophic Growth of Anaerobic Microorganisms on Hydrogen. *Curr. Microbiol.* **1999**, *38* (5), 285–289.
(59) Gottschalk, G.; Braun, M. Revival of the Name Clostridium Aceticum. *Int. J. Syst. Bacteriol.* **1981**, *31* (4), 476.
(60) Slate, A. J.; Whitehead, K. A.; Brownson, D. A. C.; Banks, C. E. Microbial Fuel Cells: An Overview of Current Technology. *Renew. Sustain. Energy Rev.* **2019**, *101*, 60–81.
(61) Thrash, J. C.; Van Trump, J. I.; Weber, K. A.; Miller, E.; Achenbach, L. A.; Coates, J. D. Electrochemical Stimulation of Microbial Perchlorate Reduction. *Environ. Sci. Technol.* **2007**, *41* (5), 1740–1746.
(62) Hongo, M.; Iwahara, M. Application of Electro-Energizing Method to l-Glutamic Acid Fermentation. *Agric. Biol. Chem.* **1979**, *43* (10), 2075–2081.
(63) Park, D. H.; Laivenieks, M.; Guettler, M. V.; Jain, M. K.; Zeikus, J. G. Microbial Utilization of Electrically Reduced Neutral Red as the Sole Electron Donor for Growth and Metabolite Production. *Appl. Environ. Microbiol.* **1999**, *65* (7), 2912–2917.
(64) Park, D. H.; Zeikus, J. G. Utilization of Electrically Reduced Neutral Red by Actinobacillus Succinogenes: Physiological Function of Neutral Red in Membrane-Driven Fumarate Reduction and Energy Conservation. *J. Bacteriol.* **1999**, *181* (8), 2403–2410.
(65) Park, D. H.; Zeikus, J. G. Electricity Generation in Microbial Fuel Cells Using Neutral Red as an Electronophore. *Appl. Environ. Microbiol.* **2000**, *66* (4), 1292–1297.

(66) Peguin, S.; Goma, G.; Delorme, P.; Soucaille, P. Metabolic Flexibility of Clostridium Acetobutylicum in Response to Methyl Viologen Addition. *Appl. Microbiol. Biotechnol.* **1994**, *42* (4), 611–616.
(67) Dinh, H. T.; Kuever, J.; Mußmann, M.; Hassel, A. W.; Stratmann, M.; Widdel, F. Iron Corrosion by Novel Anaerobic Microorganisms. *Nature* **2004**, *427* (6977), 829–832.
(68) Daniels, L.; Belay, N.; Rajagopal, B. S.; Weimer, P. J. Bacterial Methanogenesis and Growth from $CO_2$ with Elemental Iron as the Sole Source of Electrons. *Science* **1987**, *237* (4814), 509–511.
(69) Virdis, B.; Rabaey, K.; Yuan, Z.; Rozendal, R. A.; Keller, J. Electron Fluxes in a Microbial Fuel Cell Performing Carbon and Nitrogen Removal. *Environ. Sci. Technol.* **2009**, *43* (13), 5144–5149.
(70) Virdis, B.; Rabaey, K.; Yuan, Z.; Keller, J. Microbial Fuel Cells for Simultaneous Carbon and Nitrogen Removal. *Water Res.* **2008**, *42* (12), 3013–3024.
(71) Cheng, S.; Xing, D.; Call, D. F.; Logan, B. E. Direct Biological Conversion of Electrical Current into Methane by Electromethanogenesis. *Environ. Sci. Technol.* **2009**, *43* (10), 3953–3958.
(72) Van Eerten-Jansen, M. C. A. A.; Heijne, A. Ter; Buisman, C. J. N.; Hamelers, H. V. M. Microbial Electrolysis Cells for Production of Methane from $CO_2$: Long-Term Performance and Perspectives. *Int. J. Energy Res.* **2012**, *36* (6), 809–819.
(73) Villano, M.; Aulenta, F.; Ciucci, C.; Ferri, T.; Giuliano, A.; Majone, M. Bioelectrochemical Reduction of $CO_2$ to $CH_4$ via Direct and Indirect Extracellular Electron Transfer by a Hydrogenophilic Methanogenic Culture. *Bioresour. Technol.* **2010**, *101* (9), 3085–3090.
(74) Ljungdhal, L. G. The Autotrophic Pathway of Acetate Synthesis in Acetogenic Bacteria. *Annu. Rev. Microbiol.* **1986**, *40* (1), 415–450.
(75) Wieringa, K. T. Over Het Verdwijnen van Waterstof En Koolzuur Onder Anaerobe Voorwaarden. *Antonie Van Leeuwenhoek* **1936**, *3* (1–4), 263–273.
(76) Wieringa, K. T. The Formation of Acetic Acid from Carbon Dioxide and Hydrogen by Anaerobic Spore-Forming Bacteria. *Antonie Van Leeuwenhoek* **1939**, *6* (1), 251–262.
(77) Ragsdale, S. W.; Pierce, E. Acetogenesis and the Wood–Ljungdahl Pathway of $CO_2$ Fixation. *Biochim. Biophys. Acta - Proteins Proteomics* **2008**, *1784* (12), 1873–1898.
(78) Jones, W. J.; Donnelly, M. I.; Wolfe, R. S. Evidence of a Common Pathway of Carbon Dioxide Reduction to Methane in Methanogens. *J. Bacteriol.* **1985**, *163* (1), 126–131.
(79) Clauwaert, P.; Verstraete, W. Methanogenesis in Membraneless Microbial Electrolysis Cells. *Appl. Microbiol. Biotechnol.* **2009**, *82* (5), 829–836.
(80) Schlager, S.; Haberbauer, M.; Fuchsbauer, A.; Hemmelmair, C.; Dumitru, L. M.; Hinterberger, G.; Neugebauer, H.; Sariciftci, N. S. Bio-Electrocatalytic Application of Microorganisms for Carbon Dioxide Reduction to Methane. *ChemSusChem* **2017**, *10* (1), 226–233.
(81) Belkhelfa, S.; Labadie, K.; Cruaud, C.; Aury, J.-M.; Roche, D.; Bouzon, M.; Salanoubat, M.; Döring, V. Complete Genome Sequence of the Facultative Methylotroph *Methylobacterium extorquens* TK 0001 Isolated from Soil in Poland. *Genome Announc.* **2018**, *6* (8).
(82) Hwang, H.; Yeon, Y. J.; Lee, S.; Choe, H.; Jang, M. G.; Cho, D. H.; Park, S.; Kim, Y. H. Electro-Biocatalytic Production of Formate from Carbon Dioxide Using an Oxygen-Stable Whole Cell Biocatalyst. *Bioresour. Technol.* **2015**, *185*, 35–39.
(83) Schrader, J.; Schilling, M.; Holtmann, D.; Sell, D.; Filho, M. V.; Marx, A.; Vorholt, J. A. Methanol-Based Industrial Biotechnology: Current Status and Future Perspectives of Methylotrophic Bacteria. *Trends Biotechnol.* **2009**, *27* (2), 107–115.
(84) Debabov, V. G. Electricity from Microorganisms. *Microbiology*. April 2008, pp 123–131.
(85) Lovley, D. R.; Nevin, K. P. Electricity Production with Electricigens. In *Bioenergy*; American Society of Microbiology, 2014; pp 295–306.
(86) Bond, D. R.; Holmes, D. E.; Tender, L. M.; Lovley, D. R. Electrode-Reducing Microorganisms that Harvest Energy from Marine Sediments. *Science* **2002**, *295* (5554), 483–485.
(87) Lovley, D. R. The Microbe Electric: Conversion of Organic Matter to Electricity. *Curr. Opin. Biotechnol.* **2008**, *19* (6), 564–571.
(88) Villano, M.; Monaco, G.; Aulenta, F.; Majone, M. Electrochemically Assisted Methane Production in a Biofilm Reactor. *J. Power Sources* **2011**, *196* (22), 9467–9472.
(89) Kalathil, S.; Patil, S. A.; Pant, D. *Microbial Fuel Cells: Electrode Materials*; Elsevier Inc., 2018.

(90) Huang, L.; Jiang, L.; Wang, Q.; Quan, X.; Yang, J.; Chen, L. Cobalt Recovery with Simultaneous Methane and Acetate Production in Biocathode Microbial Electrolysis Cells. *Chem. Eng. J.* **2014**, *253*, 281–290.
(91) Hindatu, Y.; Annuar, M. S. M.; Gumel, A. M. Mini-Review: Anode Modification for Improved Performance of Microbial Fuel Cell. *Renew. Sustain. Energy Rev.* **2017**, *73*, 236–248.
(92) Santoro, C.; Arbizzani, C.; Erable, B.; Ieropoulos, I. Microbial Fuel Cells: From Fundamentals to Applications. A Review. *J. Power Sources* **2017**, *356*, 225–244.
(93) Zhang, T.; Nie, H.; Bain, T. S.; Lu, H.; Cui, M.; Snoeyenbos-West, O. L.; Franks, A. E.; Nevin, K. P.; Russell, T. P.; Lovley, D. R. Improved Cathode Materials for Microbial Electrosynthesis. *Energy Environ. Sci.* **2013**, *6* (1), 217–224.
(94) Cheng, S.; Logan, B. E. Ammonia Treatment of Carbon Cloth Anodes to Enhance Power Generation of Microbial Fuel Cells. *Electrochem. commun.* **2007**, *9* (3), 492–496.
(95) Higgins, S. R.; Foerster, D.; Cheung, A.; Lau, C.; Bretschger, O.; Minteer, S. D.; Nealson, K.; Atanassov, P.; Cooney, M. J. Fabrication of Macroporous Chitosan Scaffolds Doped with Carbon Nanotubes and Their Characterization in Microbial Fuel Cell Operation. *Enzyme Microb. Technol.* **2011**, *48* (6–7), 458–465.
(96) Lai, B.; Tang, X.; Li, H.; Du, Z.; Liu, X.; Zhang, Q. Power Production Enhancement with a Polyaniline Modified Anode in Microbial Fuel Cells. *Biosens. Bioelectron.* **2011**, *28* (1), 373–377.
(97) Krajewska, B. Application of Chitin- and Chitosan-Based Materials for Enzyme Immobilizations: A Review. *Enzyme Microb. Technol.* **2004**, *35* (2–3), 126–139.
(98) Schlager, S.; Dibenedetto, A.; Aresta, M.; Apaydin, D. H.; Dumitru, L. M.; Neugebauer, H.; Sariciftci, N. S. Biocatalytic and Bioelectrocatalytic Approaches for the Reduction of Carbon Dioxide Using Enzymes. *Energy Technol.* **2017**, *5* (6), 812–821.
(99) Rocchitta, G.; Spanu, A.; Babudieri, S.; Latte, G.; Madeddu, G.; Galleri, G.; Nuvoli, S.; Bagella, P.; Demartis, M. I.; Fiore, V.; et al. Enzyme Biosensors for Biomedical Applications: Strategies for Safeguarding Analytical Performances in Biological Fluids. *Sensors* **2016**, *16* (6), 780.
(100) De Poulpiquet, A.; Ciaccafava, A.; Lojou, E. New Trends in Enzyme Immobilization at Nanostructured Interfaces for Efficient Electrocatalysis in Biofuel Cells. *Electrochim. Acta* **2014**, *126*, 104–114.
(101) Ghindilis, A. L.; Atanasov, P.; Wilkins, E. Enzyme-Catalyzed Direct Electron Transfer: Fundamentals and Analytical Applications. *Electroanalysis* **1997**, *9* (9), 661–674.
(102) Shi, J.; Jiang, Y.; Jiang, Z.; Wang, X.; Wang, X.; Zhang, S.; Han, P.; Yang, C. Enzymatic Conversion of Carbon Dioxide. *Chem. Soc. Rev.* **2015**, *44* (17), 5981–6000.
(103) Mandler, D.; Willner, I. Photochemical Fixation of Carbon Dioxide: Enzymic Photosynthesis of Malic, Aspartic, Isocitric, and Formic Acids in Artificial Media. *J. Chem. Soc., Perkin Trans. 2* **1988**, No. 6, 997.
(104) Parkinson, B. A.; Weaver, P. F. Photoelectrochemical Pumping of Enzymatic $CO_2$ Reduction. *Nature* **1984**, *309* (5964), 148–149.
(105) Li, L. F.; Ljungdahl, L.; Wood, H. G. Properties of Nicotinamide Adenine Dinucleotide Phosphate-Dependent Formate Dehydrogenase from Clostridium Thermoaceticum. *J. Bacteriol.* **1966**, *92* (2), 405–412.
(106) Seelbach, K.; Riebel, B.; Hummel, W.; Kula, M.-R.; Tishkov, V. I.; Egorov, A. M.; Wandrey, C.; Kragl, U. A Novel, Efficient Regenerating Method of NADPH Using a New Formate Dehydrogenase. *Tetrahedron Lett.* **1996**, *37* (9), 1377–1380.
(107) Obert, R.; Dave, B. C. Enzymatic Conversion of Carbon Dioxide to Methanol: Enhanced Methanol Production in Silica Sol-Gel Matrices. *J. Am. Chem. Soc.* **1999**, *121*, 12192–12193.
(108) Singh, R. K. R.; Singh, R. K. R.; Sivakumar, D.; Kondaveeti, S.; Kim, T.; Li, J.; Sung, B. H.; Cho, B.-K.; Kim, D. R.; Kim, S. C.; et al. Insights into Cell-Free Conversion of $CO_2$ to Chemicals by a Multienzyme Cascade Reaction. *ACS Catal.* **2018**, *8* (12), 11085–11093.
(109) Schlager, S.; Dumitru, L. M.; Haberbauer, M.; Fuchsbauer, A.; Neugebauer, H.; Hiemetsberger, D.; Wagner, A.; Portenkirchner, E.; Sariciftci, N. S. Electrochemical Reduction of Carbon Dioxide to Methanol by Direct Injection of Electrons into Immobilized Enzymes on a Modified Electrode. *ChemSusChem* **2016**, *9* (6), 631–635.
(110) Schlager, S.; Neugebauer, H.; Haberbauer, M.; Hinterberger, G.; Sariciftci, N. S. Direct Electrochemical Addressing of Immobilized Alcohol Dehydrogenase for the Heterogeneous Bioelectrocatalytic Reduction of Butyraldehyde to Butanol. *ChemCatChem* **2015**, *7* (6),

967–971.
(111) Karyakin, A. A.; Bobrova, O. A.; Karyakina, E. E. Electroreduction of $NAD^+$ to Enzymatically Active NADH at Poly(Neutral Red) Modified Electrodes. *J. Electroanal. Chem.* **1995**, *399* (1–2), 179–184.
(112) El-Zahab, B.; Donnelly, D.; Wang, P. Particle-Tethered NADH for Production of Methanol from $CO_2$ Catalyzed by Coimmobilized Enzymes. *Biotechnol. Bioeng.* **2008**, *99* (3), 508–514.
(113) Dibenedetto, A.; Stufano, P.; Macyk, W.; Baran, T.; Fragale, C.; Costa, M.; Aresta, M. Hybrid Technologies for an Enhanced Carbon Recycling Based on the Enzymatic Reduction of $CO_2$ to Methanol in Water: Chemical and Photochemical NADH Regeneration. *ChemSusChem* **2012**, *5* (2), 373–378.
(114) Oppelt, K. T.; Gasiorowski, J.; Egbe, D. A. M.; Kollender, J. P.; Himmelsbach, M.; Hassel, A. W.; Sariciftci, N. S.; Knör, G. Rhodium-Coordinated Poly(Arylene-Ethynylene)-*alt*-Poly(Arylene-Vinylene) Copolymer Acting as Photocatalyst for Visible-Light-Powered $NAD^+$/NADH Reduction. *J. Am. Chem. Soc.* **2014**, *136* (36), 12721–12729.
(115) Reda, T.; Plugge, C. M.; Abram, N. J.; Hirst, J. Reversible Interconversion of Carbon Dioxide and Formate by an Electroactive Enzyme. *Proc. Natl. Acad. Sci. U. S. A.* **2008**, *105* (31), 10654–10658.
(116) Amao, Y.; Shuto, N. Formate Dehydrogenase-Viologen-Immobilized Electrode for $CO_2$ Conversion, for Development of an Artificial Photosynthesis System. *Res. Chem. Intermed.* **2014**, *40* (9), 3267–3276.
(117) Lima, F.; Maia, G. Direct Electron Transfer from Alcohol Dehydrogenase. *RSC Adv.* **2014**, *4* (43), 22575–22588.
(118) Logan, B. E.; Regan, J. M. Electricity-Producing Bacterial Communities in Microbial Fuel Cells. *Trends Microbiol.* **2006**, *14* (12), 512–518.
(119) Zhao, X.; Mai, Z.; Kang, X.; Zou, X. Direct Electrochemistry and Electrocatalysis of Horseradish Peroxidase Based on Clay-Chitosan-Gold Nanoparticle Nanocomposite. *Biosens. Bioelectron.* **2008**, *23*, 1032–1038.
(120) Zhou, Y.; Yang, H.; Chen, H.-Y. Direct Electrochemistry and Reagentless Biosensing of Glucose Oxidase Immobilized on Chitosan Wrapped Single-Walled Carbon Nanotubes. *Talanta* **2008**, *76*, 419–423.
(121) Shan, D.; Wang, S.; Xue, H.; Cosnier, S. Direct Electrochemistry and Electrocatalysis of Hemoglobin Entrapped in Composite Matrix Based on Chitosan and $CaCO_3$ Nanoparticles. *Electrochem. Commun.* **2006**, *9* (4), 529–534.
(122) Liu, J.; Guo, C.; Li, C. M.; Li, Y.; Chi, Q.; Huang, X.; Liao, L.; Yu, T. Carbon-Decorated ZnO Nanowire Array: A Novel Platform for Direct Electrochemistry of Enzymes and Biosensing Applications. *Electrochem. Commun.* **2008**, *11*, 202–205.
(123) Zang, J.; Li, C. M.; Cui, X.; Wang, J.; Sun, X.; Dong, H.; Sun, C. Q. Tailoring Zinc Oxide Nanowires for High Performance Amperometric Glucose Sensor. *Electroanalysis* **2007**, *19* (9), 1008–1014.
(124) Zhang, Q.; Zhang, L.; Liu, B.; Lu, X.; Li, J. Assembly of Quantum Dots-Mesoporous Silicate Hybrid Material for Protein Immobilization and Direct Electrochemistry. *Biosens. Bioelectron.* **2007**, *23*, 695–700.
(125) Nadzhafova, O.; Etienne, M.; Walcarius, A. Direct Electrochemistry of Hemoglobin and Glucose Oxidase in Electrodeposited Sol-Gel Silica Thin Films on Glassy Carbon. *Electrochem. Commun.* **2007**, *9* (5), 1189–1195.
(126) Luckarift, H. R.; Spain, J. C.; Naik, R. R.; Stone, M. O. Enzyme Immobilization in a Biomimetic Silica Support. *Nat. Biotechnol.* **2004**, *22* (2), 211–213.
(127) Avnir, D.; Braun, S.; Lev, O.; Ottolenghi, M. Enzymes and Other Proteins Entrapped in Sol-Gel Materials. *Chem. Mater.* **1994**, *6* (10), 1605–1614.
(128) Zhang, J. J.; Zhang, F.; Yang, H.; Huang, X.; Liu, H.; Zhang, J. J.; Guo, S. Graphene Oxide as a Matrix for Enzyme Immobilization. *Langmuir* **2010**, *26* (9), 6083–6085.
(129) Zuo, X.; He, S.; Li, D.; Peng, C.; Huang, Q.; Song, S.; Fan, C. Graphene Oxide-Facilitated Electron Transfer of Metalloproteins at Electrode Surfaces. *Langmuir* **2010**, *26* (3), 1936–1939.
(130) Park, J.; Yan, M. Covalent Functionalization of Graphene with Reactive Intermediates. *Acc. Chem. Res.* **2013**, *46* (1), 181–189.
(131) Liao, L.; Peng, H.; Liu, Z. Chemistry Makes Graphene beyond Graphene. *J. Am. Chem. Soc. 2014,* **2014**, *136*, 12194−12200.

(132) Prasad, K. P.; Chen, Y.; Chen, P. Three-Dimensional Graphene-Carbon Nanotube Hybrid for High-Performance Enzymatic Biofuel Cells. *ACS Appl. Mater. Interfaces* **2014**, *6* (5), 3387–3393.
(133) Guo, K.; Qian, K.; Zhang, S.; Kong, J.; Yu, C.; Liu, B. Bio-Electrocatalysis of NADH and Ethanol Based on Graphene Sheets Modified Electrodes. *Talanta* **2011**, *85* (2), 1174–1179.
(134) Liu, Y.; Yu, D.; Zeng, C.; Miao, Z.; Dai, L. Biocompatible Graphene Oxide-Based Glucose Biosensors. *Langmuir* **2010**, *26* (9), 6158–6160.
(135) Shao, Y.; Wang, J.; Wu, H.; Liu, J.; Aksay, I. A. A.; Lin, Y. Graphene Based Electrochemical Sensors and Biosensors: A Review. *Electroanalysis* **2010**, *22* (10), 1027–1036.
(136) Urbanová, V.; Holá, K.; Bourlinos, A. B.; Čépe, K.; Ambrosi, A.; Loo, A. H.; Pumera, M.; Karlický, F.; Otyepka, M.; Zbořil, R. Thiofluorographene-Hydrophilic Graphene Derivative with Semiconducting and Genosensing Properties. *Adv. Mater.* **2015**, *27* (14), 2305–2310.
(137) Liu, C.; Alwarappan, S.; Chen, Z.; Kong, X.; Li, C.-Z. Membraneless Enzymatic Biofuel Cells Based on Graphene Nanosheets. **2010**, *25* (7), 1829–1833.
(138) Pavlidis, I. V; Patila, M.; Bornscheuer, U. T.; Gournis, D.; Stamatis, H. Graphene-Based Nanobiocatalytic Systems: Recent Advances and Future Prospects. *Trends Biotechnol.* **2014**, *32*, 312–320.
(139) Yong, A.; Eng, S.; Kiang Chua, C.; Pumera, M. Refinements to the Structure of Graphite Oxide: Absolute Quantification of Functional Groups via Selective Labelling. *Nanoscale* **2015**, *7*, 20256–20266.
(140) Marcano, D. C.; Kosynkin, D. V.; Berlin, J. M.; Sinitskii, A.; Sun, Z.; Slesarev, A.; Alemany, L. B.; Lu, W.; Tour, J. M. Improved Synthesis of Graphene Oxide. *ACS Nano* **2010**, *4* (8), 4806–4814.
(141) Lerf, A.; He, H.; Forster, M.; Klinowski, J. Structure of Graphite Oxide Revisitedǁ. *J. Phys. Chem. B* **1998**, *102* (23), 4477–4482.
(142) Bakandritsos, A.; Pykal, M.; Błoński, P. B.; Jakubec, P.; Chronopoulos, D. D.; Bourlinos, A. B.; Zbořil, R.; Otyepka, M. Cyanographene and Graphene Acid: Emerging Derivatives Enabling High-Yield and Selective Functionalization of Graphene. *ACS Nano* **2017**, *11*, 2982−2991.
(143) Pauliukaite, R.; Ghica, M. E.; Barsan, M.; Brett, C. M. A. Characterisation of Poly(Neutral Red) Modified Carbon Film Electrodes; Application as a Redox Mediator for Biosensors. *J. Solid State Electrochem.* **2007**, *11* (7), 899–908.
(144) Zeppilli, M.; Villano, M.; Aulenta, F.; Lampis, S.; Vallini, G.; Majone, M. Effect of the Anode Feeding Composition on the Performance of a Continuous-Flow Methane-Producing Microbial Electrolysis Cell. *Environ. Sci. Pollut. Res.* **2015**, *22* (10), 7349–7360.
(145) Smith, P. K.; Krohn, R. I.; Hermanson, G. T.; Mallia, A. K.; Gartner, F. H.; Provenzano, M. D.; Fujimoto, E. K.; Goeke, N. M.; Olson, B. J.; Klenk, D. C. Measurement of Protein Using Bicinchoninic Acid. *Anal. Biochem.* **1985**, *150* (1), 76–85.
(146) Harrington, T. D.; Tran, V. N.; Mohamed, A.; Renslow, R.; Biria, S.; Orfe, L.; Call, D. R.; Beyenal, H. The Mechanism of Neutral Red-Mediated Microbial Electrosynthesis in Escherichia Coli: Menaquinone Reduction.
(147) Harewood, A. J. T.; Popuri, S. R.; Cadogan, E. I.; Lee, C. H.; Wang, C. C. Bioelectricity Generation from Brewery Wastewater in a Microbial Fuel Cell Using Chitosan/Biodegradable Copolymer Membrane. *Int. J. Environ. Sci. Technol.* **2017**, *14* (7), 1535–1550.
(148) Srinophakun, P.; Thanapimmetha, A.; Plangsri, S.; Vetchayakunchai, S.; Saisriyoot, M. Application of Modified Chitosan Membrane for Microbial Fuel Cell: Roles of Proton Carrier Site and Positive Charge. *J. Clean. Prod.* **2017**, *142*, 1274–1282.
(149) Barsan, M. M.; Pinto, E. M.; Brett, C. M. A. Electrosynthesis and Electrochemical Characterisation of Phenazine Polymers for Application in Biosensors. *Electrochim. Acta* **2008**, *53* (11), 3973–3982.
(150) Müller, V. Energy Conservation in Acetogenic Bacteria. *Appl. Environ. Microbiol.* **2003**, *69* (11), 6345–6353.
(151) Terada, A.; Yuasa, A.; Kushimoto, T.; Tsuneda, S.; Katakai, A.; Tamada, M. Bacterial Adhesion to and Viability on Positively Charged Polymer Surfaces. *Microbiology* **2006**, *152* (12), 3575–3583.
(152) Saito, T.; Mehanna, M.; Wang, X.; Cusick, R. D.; Feng, Y.; Hickner, M. A. Effect of Nitrogen Addition on the Performance of Microbial Fuel Cell Anodes. *Bioresour. Technol.* **2011**, *102* (1), 395–398.

(153) Plapp, B. V.; Charlier, H. A.; Ramaswamy, S. Mechanistic Implications from Structures of Yeast Alcohol Dehydrogenase Complexed with Coenzyme and an Alcohol. *Arch. Biochem. Biophys.* **2016**, *591*, 35–42.
(154) Sun, Z.; Liu, Q.; Qu, G.; Feng, Y.; Reetz, M. T. Utility of B-Factors in Protein Science: Interpreting Rigidity, Flexibility, and Internal Motion and Engineering Thermostability. *Chem. Rev.* **2019**, *119* (3), 1626–1665.
(155) Hall, W. H.; Jagodzinski, P. W. Raman and Fourier Transform Infrared Study of Yeast Alcohol Dehydrogenase. *J. Raman Spectrosc.* **1987**, *18* (2), 119–122.
(156) Szabó, T.; Berkesi, O.; Forgó, P.; Josepovits, K.; Sanakis, Y.; Petridis, D.; Dékány, I. Evolution of Surface Functional Groups in a Series of Progressively Oxidized Graphite Oxides. *Chem. Mater.* **2006**, *18* (11), 2740–2749.
(157) Mayo, D. W. Characteristic Frequencies of Aromatic Compounds (Group Frequencies of Arenes). In *Course Notes on the Interpretation of Infrared and Raman Spectra*; Dana W., M., Foil A., M., Robert W., H., Eds.; John Wiley & Sons, Inc., 2004; pp 101–140.
(158) Csach, K.; Juríková, A.; Miškuf, J.; Koneracká, M.; Závišová, V.; Kubovčíková, M.; Kopčanský, P. Thermogravimetric Study of the Decomposition of BSA-Coated Magnetic Nanoparticles. *Acta Phys. Pol. A* **2012**, *121* (5–6), 1293–1295.
(159) Hanefeld, U.; Gardossi, L.; Magner, E. Understanding Enzyme Immobilisation. *Chem. Soc. Rev.* **2009**, *38* (2), 453–468.
(160) Mohamad, N. R.; Marzuki, N. H. C.; Buang, N. A.; Huyop, F.; Wahab, R. A. An Overview of Technologies for Immobilization of Enzymes and Surface Analysis Techniques for Immobilized Enzymes. *Biotechnol. Biotechnol. Equip.* **2015**, *29* (2), 205–220.
(161) Trevan, M. D. Enzyme Immobilization by Covalent Bonding. In *New Protein Techniques*; Humana Press: New Jersey, 1988; pp 495–510.
(162) Zhao, F.; Li, H.; Wang, X.; Wu, L.; Hou, T.; Guan, J.; Jiang, Y.; Xu, H.; Mu, X. CRGO/Alginate Microbeads: An Enzyme Immobilization System and Its Potential Application for a Continuous Enzymatic Reaction. *J. Mater. Chem. B* **2015**, *3* (48), 9315–9322.
(163) Won, K.; Kim, S.; Kim, K. J.; Park, H. W.; Moon, S. J. Optimization of Lipase Entrapment in Ca-Alginate Gel Beads. *Process Biochem.* **2005**, *40* (6), 2149–2154.
(164) Bertheussen, E.; Verdaguer-Casadevall, A.; Ravasio, D.; Montoya, J. H.; Trimarco, D. B.; Roy, C.; Meier, S.; Wendland, J.; Nørskov, J. K.; Stephens, I. E. L.; et al. Acetaldehyde as an Intermediate in the Electroreduction of Carbon Monoxide to Ethanol on Oxide-Derived Copper. *Angew. Chem., Int. Ed.* **2016**, *55*, 1450–1454.
(165) Winkelman, J. G. M.; Voorwinde, O. K.; Ottens, M.; Beenackers, A. A. C. M.; Janssen, L. P. B. M. Kinetics and Chemical Equilibrium of the Hydration of Formaldehyde. *Chem. Eng. Sci.* **2002**, *57* (19), 4067–4076.
(166) Ma, K.; Yehezkeli, O.; Park, E.; Cha, J. N. Enzyme Mediated Increase in Methanol Production from Photoelectrochemical Cells and $CO_2$. *ACS Catal.* **2016**, *6* (10), 6982–6986.
(167) Luo, J.; Meyer, A. S.; Mateiu, R. V.; Pinelo, M. Cascade Catalysis in Membranes with Enzyme Immobilization for Multi-Enzymatic Conversion of $CO_2$ to Methanol. *N. Biotechnol.* **2015**, *32* (3), 319–327.
(168) Mazánek, V.; Luxa, J.; Matějková, S.; Kučera, J.; Sedmidubský, D.; Pumera, M.; Sofer, Z. Ultrapure Graphene Is a Poor Electrocatalyst: Definitive Proof of the Key Role of Metallic Impurities in Graphene-Based Electrocatalysis. *ACS Nano* **2019**, *13* (2), 1574–1582.
(169) Blanco, M.; Mosconi, D.; Otyepka, M.; Medveď, M.; Bakandritsos, A.; Agnoli, S.; Granozzi, G. Combined High Degree of Carboxylation and Electronic Conduction in Graphene Acid Sets New Limits for Metal Free Catalysis in Alcohol Oxidation. *Chem. Sci.* **2019**, *10* (41), 9438–9445.
(170) Albo, J.; Irabien, A. $Cu_2O$-Loaded Gas Diffusion Electrodes for the Continuous Electrochemical Reduction of $CO_2$ to Methanol. *J. Catal.* **2016**, *343*, 232–239.
(171) Zhang, W.; Qin, Q.; Dai, L.; Qin, R.; Zhao, X.; Chen, X.; Ou, D.; Chen, J.; Chuong, T. T.; Wu, B.; et al. Electrochemical Reduction of Carbon Dioxide to Methanol on Hierarchical Pd/$SnO_2$ Nanosheets with Abundant Pd-O-Sn Interfaces. *Angew. Chemie Int. Ed.* **2018**, *57* (30), 9475–9479.
(172) Yang, D.; Zhu, Q.; Chen, C.; Liu, H.; Liu, Z.; Zhao, Z.; Zhang, X.; Liu, S.; Han, B. Selective Electroreduction of Carbon Dioxide to Methanol on Copper Selenide Nanocatalysts. *Nat. Commun.* **2019**, *10* (1), 677.
(173) Yang, H. P.; Yue, Y. N.; Qin, S.; Wang, H.; Lu, J. X. Selective Electrochemical Reduction

of $CO_2$ to Different Alcohol Products by an Organically Doped Alloy Catalyst. *Green Chem.* **2016**, *18* (11), 3216–3220.

(174) Irfan Malik, M.; Malaibari, Z. O.; Atieh, M.; Abussaud, B. Electrochemical Reduction of $CO_2$ to Methanol over MWCNTs Impregnated with $Cu_2O$. *Chem. Eng. Sci.* **2016**, *152*, 468–477.

(175) Andrews, E.; Ren, M.; Wang, F.; Zhang, Z.; Sprunger, P.; Kurtz, R.; Flake, J. Electrochemical Reduction of $CO_2$ at Cu Nanocluster/(1010) ZnO Electrodes. *J. Electrochem. Soc.* **2013**, *160* (11).

(176) Kuhl, K. P.; Hatsukade, T.; Cave, E. R.; Abram, D. N.; Kibsgaard, J.; Jaramillo, T. F. Electrocatalytic Conversion of Carbon Dioxide to Methane and Methanol on Transition Metal Surfaces. *J. Am. Chem. Soc.* **2014**, *136* (40), 14107–14113.